UNIVERSITÀ DEGLI STUDI DI PARMA

Dipartimento di Chimica Organica ed Industriale

Ph.D. in Science and Technology of Innovative Materials XXI° Cycle

MULTIDENTATE CAVITAND LIGANDS IN SELF-ASSEMBLY AND ANION RECOGNITION

Francesca Gruppi

Coordinator: **Prof. Anna Painelli**

Supervisor: **Prof. Enrico Dalcanale**

Author: **Francesca Gruppi**

TABLE OF CONTENTS

CHAPTER 3

SELF-ASSEMBLY OF A CAVITAND BASED COORDINATION CAGE

CHAPTER 4

RHENIUM BASED COORDINATION CAGES

CHAPTER 5

HETERONUCLEAR DIMERIC CAGES

CHAPTER 6

FLUORESCENT PROBES FOR INTRACELLULAR MANGANESE (II)

General introduction 1

1.1 Supramolecular chemistry

Supramolecular chemistry was defined by Jean-Marie Lehn: "..the chemistry beyond the molecule..".[1] Supramolecular chemistry defines the chemistry of non-covalent bonding whereas molecular chemistry is characterized by covalent bonding. The aim of this branch is to create systems that are designed to form selective self-assembling, self-recognizing and self-learning compounds. Supramolecular chemistry is an interdisciplinary endeavor involving inorganic and organic chemistry as well as biology, physics and materials science.[2-3]

The host-guest interactions can be considered the simplest form of supramolecular chemistry [4-5]. In fact, a host molecule binds non-covalently a guest molecule forming a host-guest complex. Usually the host is a molecule possessing a cavity which can be preorganized for the appropriate guest utilizing multivalent and cooperative interactions[6,12]. In complexation and self-assembly there are several non-covalent interactions involved, such as hydrogen interactions, hydrophobic effect, π- π interactions [2].

1.2 Self-assembly

An intriguing definition of self-assembly was given by Whitesides[7]: "self-assembly is one of the few practical strategies for making ensembles of nanostructures". The advantage of the self-assembly is the fact that is a reversible process allowing the system to self-repair possible structural defects. H-bonding and netal coordination are the work horses of interactions employed for self-assembly. The focus here will be on the second type.

1.2.1 Metal-direct Self assembly

Metal-direct self-assembly is one of the most exploited and appealing protocols utilized so far. The reason lies in the directionality of the metal-ligand interaction and their versatility due to different transition-metal complexes and multidentate ligands available as building blocks. In metal direct self-assembly two are the major approaches: Stang's and Raymond's. In Stang's approach there are two factors to be considered in design of coordination-based discrete supramolecular entities: the symmetry and the overall shape of the resulting macrocyclic assembly. This is determined by the type and properties of the multidentate building units used in the construction of the assembly. They proposed the synthesis of two and three dimensional nanoscopic, high symmetry ensembles formed by mixing together complementary building blocks with the appropriate, predefined geometries in a stoichiometric ratio. [8, 9] In Raymond's approach the symmetry elements of the components determine the nature and the symmetry of the final thermodynamic product. For instance, to design a cluster with *D*3 symmetry, an M_2L_3 triple helicate, both the *C*2 and *C*3 axes of the point group must be taken into account.[10].

A wide range of compound have been synthesized via metal direct self-assembly such as boxes, cages, catenanes, dendrimers, grids, helicates, rotaxanes, and others. [11-12]. Fujiita *et al.* reported several examples of metal-directed self assembly of discrete two and three dimensional structures. Calixarene and resorcinarene –based cavitands with their inherent bowl-shaped structure represents the suitable building blocks for the self assembly of supramolecular architectures and in particular of coordination cages. In fact these are rigid molecular scaffold suitable as highly preorganized and multidentate ligands. The large internal cavities of these architectures is available and useful for different application such as catalysis and inclusion of molecules, biomolecules and nanosize particles.[13, 14]

Part of this thesis will focus on the self-assembly of cavitand-based coordination cages using Stang's approach; in particular on the design of suitable building blocks; several different assembly strategy will be presented with the final aim to obtain cage networks.

1.3 Host-guest interactions in the gas phase.

Host guest interaction usually take place between a large and concave surface and smaller organic or inorganic ions or molecules. Most of the time the interactions are weak but multiple. A particularly appealing technique to analyze host-guest interactions is the mass spectrometry; it allows the study of host-guest interactions in two different ways. The first one is the characterization of the interaction products formed in solution (ESI MS), whereas in the second case, the interactions occur in the gas phase inside the mass spectrometer (FTICRMS). The advantage of the second approach is that it avoids the presence of solvent that could affect the one-to-one interaction between the host and the guest. Experiments conducted in the gas phase let host-guest chemistry to be investigated as the result of pure biomolecular interactions, in the absence of interfering species. The use of this MS spectrometry in host-.guest interactions is particularly indicated when one of the two is a charged species, because the ionization does not influence the interaction mode. Several studies has been performed using cavitands as hosts for cationic species.[15, 16] Anion recognition in the gas phase is by far less traveled and totally unexplored using cavitands. Chapter 2 of this thesis will focus on the anion complexation with cavitands in the gas phase.

1.4 References

1. J.-M. Lehn, *Angew. Chem.-Int. Edit.*, 1988, **27**, 89-112.
2. L. R. MacGillivray and J. L. Atwood, *Supramol. Chem.*, 2000, **11**, 293-299.
3. H.-J. Schneider and A. Yatsimirski, in *Principles and Methods in Supramolecular Chemistry* Wiley 2000.
4. D. J. Cram, *Science*, 1988, **240**, 760-767.
5. D. A. Rudkevich, *Bull. Chem. Soc. Jpn.*, 2002, **75**, 393-413.
6. J. D. Badjic, A. Nelson, S. J. Cantrill, W. B. Turnbull and J. F. Stoddart, *Acc. Chem. Res.*, 2005, **38**, 723-732.
7. G. M. Whitesides and B. Grzybowski, *Science*, 2002, **295**, 2418-2421.
8. P. J. Stang and B. Olenyuk, *Acc. Chem. Res.*, 1997, **30**, 502-518.

9. B. H. Northrop, H. B. Yang and P. J. Stang, *Chem. Commun.*, 2008, 5896-5908.
10. D. L. Caulder and K. N. Raymond, *Acc. Chem. Res.*, 1999, **32**, 975-982.
11. J.-M. Lehn, in *Supramolecular Chemistry: Concepts and Perspectives.*, VCH:Weinheim,, 1995.
12. S. Leininger, B. Olenyuk and P. J. Stang, *Chem. Rev.*, 2000, **100**, 853-907.
13. L. Pirondini, F. Bertolini, B. Cantadori, F. Ugozzoli, C. Massera and E. Dalcanale, *Proc. Natl. Acad. Sci. U. S. A.,*, 2002, **99**, 4911-4915.
14. L. Pirondini, D. Bonifazi, B. Cantadori, P. Braiuca, M. Campagnolo, R. De Zorzi, S. Geremia, F. Diederich and E. Dalcanale, *Tetrahedron*, 2006, **62**, 2008-2015.
15. E. Ventola, P. Vainiotalo, M. Suman and E. Dalcanale, *Journal of the American Society for Mass Spectrometry*, 2006, **17**, 213-221.
16. M. Melegari, M. Suman, L. Pirondini, D. Moiani, C. Massera, F. Ugozzoli, E. Kalenius, P. Vainiotalo, J. C. Mulatier, J. P. Dutasta and E. Dalcanale, *Chem.-Eur. J.*, 2008, **14**, 5772-5779.

Anion Binding to Resorcinarene-Cavitands: The Importance of C_H···Anion Interactions *

2

2.1 Introduction

As one of the traditional work horses in supramolecular chemistry, resorcinarenes[1] represent a highly interesting multipurpose scaffold for numerous applications ranging from the assembly of capsules[2] such as the resorcinarene hexamers,[3] coordination cages,[4] and molecular loops,[5] to applications in supramolecular sensors[6] and phase-transfer catalysts.[7]

The simplest resorcinarenes such as **1** (Scheme 1) are held in a cone conformation through O–H···O hydrogen bonding along the upper rim and are well known to accommodate guest cations inside their cavities, for example, quaternary ammonium ions.[8] For anion binding,[9] more elaborate cavitand receptors have been developed,[10] in which the resorcinarene merely provides the scaffold, while the (thio)-urea, N-heterocyclic, or quaternary ammonium binding sites are located in the apical positions on the edge of the cavity. In quite a number of anion receptors, anion binding is supported by additional weaker interactions of the anion with aromatic C–H bonds.[11] However, reports on interactions between anions and nonaromatic CH groups as hydrogen-bond donors are rare,[12] and only two recent NMR spectroscopic and crystallographic studies[13] reported C–H···X hydrogen bonding involving the inwards oriented acetal hydrogen atoms of methylene-bridged cavitands comparable to **2** (Scheme 1). Gas-phase experiments are a powerful tool to examine the anion-binding capabilities of cavitands such as **2–11**.
Unexpected effects of solvent or counterions can be ruled out, and it is possible to study the intrinsic properties of the anion– cavitand complexes.[14]

Part of this chapter has been published on *Angew. Chem.-Int. Edit.*, 2008, **47**, 788-792

Consequently, electrospray ionization Fourier-transform ion-cyclotron resonance mass spectrometric (ESI-FTICR-MS) experiments were used to

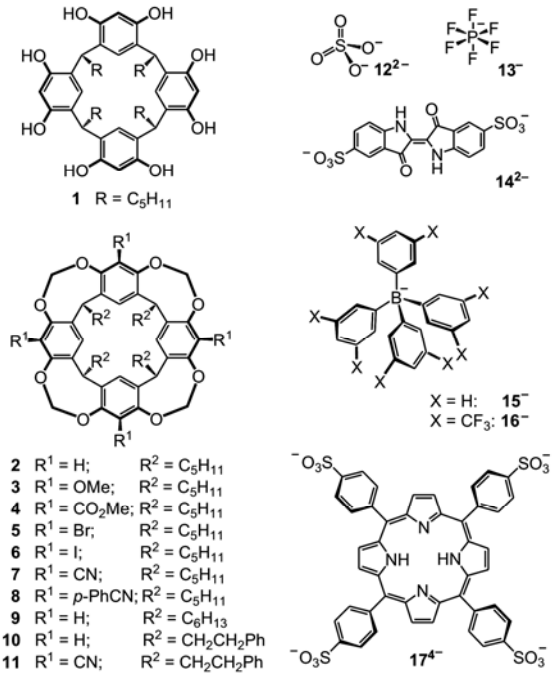

Scheme 1 Resorcinarene-based hosts **1–11** and anions **12**^{2}**_–17**^{4}**_** used in this study.

assess the anion-binding behavior of hosts **1–11**.[15]

2.2 Result and Discussion

When an acetone solution of Me_4N^+**13**$^-$ with **1** was sprayed in the positive-ion mode, intense signals for cation–host complexes were observed, while with **2** no signals for complexes with the same guest cation were evident. In marked contrast, **1** did not give intense anion–host complexes [**13@1**$^-$ in the negativeion mode (Figure 1a), while a surprisingly clean mass spectrum (Figure 1b) was obtained with **2**. The host–guest complex [**13@2**]$^-$ is the predominant complex formed in the ion source. Thus, nonbridged resorcinarene **1** forms complexes with cations, even though it could bind anions through O–H···anion hydrogen bonds. In contrast, methylene-bridged cavitands have a significant preference for suitable anions, even when cations are present that could compete for binding. Experiments with other anions such as chloride, bromide,

iodide, and nitrate also provided strong signals for the formation of anion–cavitand complexes. Encouraged by these results, we extended the study to sulfate as an example of a small dianion. Isolated sulfate di–anions are calculated to be roughly 1.3–1.6eV (≈130–160 kJmol^{-1})higher in energy than the corresponding anions and thus would spontaneously undergo electron autodetachment when generated under gas phase conditions.[16]

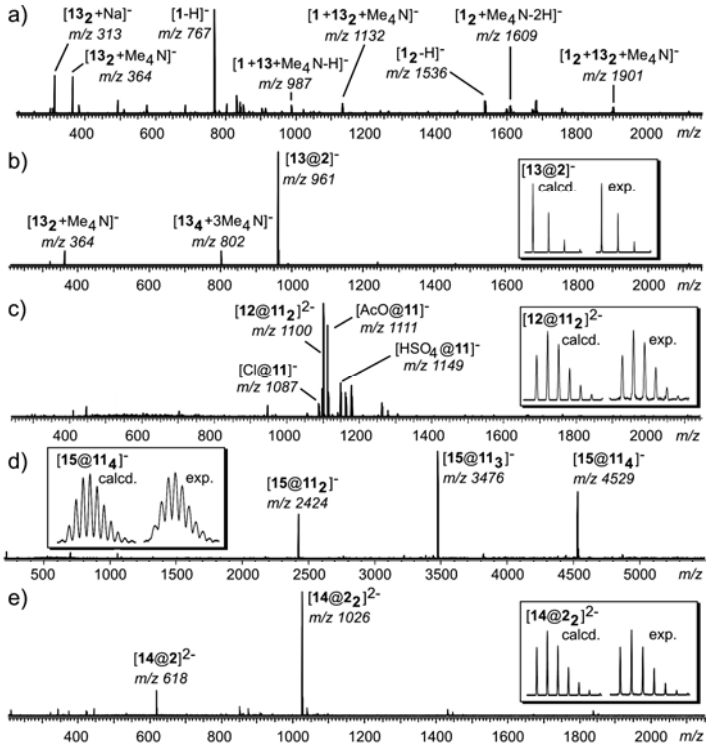

Figure 1 ESI-FTICR mass spectra of solutions of a) 1 + 1 equiv Me4N+13_ (200 mm), b) 2 + 1 equiv $Me_4N^+13^-$ (200 mm), c) 11 + 10 equiv $(Me_4N^+)_2 12^{2-}$ (680 mm), d) 11 + 0.25 equiv Na^+15^- (250 mm), e) 2 + 0.5 equiv $Na^+{}_2 14^{2-}$ (780 mm) in acetone (a–b,d) or acetone/MeOH (40:7 (c), and 40:1 (e)). AcO=acetate.

Therefore, sulfate can be observed in the gas phase only if solvated, for example, by at least three water molecules.[17] Despite the inherent instability of sulfate, the ESI-FTICR mass spectrum (Figure 1c) obtained from spraying an acetone/methanol solution of **11** and $(Me_4N^+)_2$**12**$^{2-}$ reveals the abundant formation of the 2:1 complexes [**12@ 11$_2$**]$^{2-}$. With cavitand **2**, formation of [**12@2$_2$**]$^{2-}$ was likewise observed.

To gain further insight, we conducted tandem MS experiments with mass-selected $[\mathbf{12@2_2}]^{2-}$ and $[\mathbf{12@11_2}]^{2-}$ ions (for experimental details, see the Supporting Information). In a collision-induced-decomposition (CID) experiment using argon as the collision gas, $[\mathbf{12@2}]^{2-}$ cleanly fragments through the loss of one cavitand (Figure 2a, process A). The formation of the 1:1 complex $[\mathbf{12@2}]^{2-}$ provides evidence for the sufficient stabilization of sulfate against electron autodetachment even through binding to only one cavitand. Even if theory[16] overestimates the energy gain from electron autodetachment (130–160 $kJmol^{-1}$) to some extent, the cavitand–anion binding energy must be higher than that and is thus substantial.

When the same experiment is performed with cyano-substituted $[\mathbf{12@11_2}]^{2-}$ (Figure 2b), three fragmentation pathways are populated: A) loss of one neutral cavitand, B) a charge-separating loss of $[HSO_4@\mathbf{11}]^-$ involving the formation of a deprotonated cavitand, and C) loss of CH_2O and SO_3 through nucleophilic substitution and fragmentation. Two subsequent 1,2-elimination reactions of styrene and/or CO follow the primary reaction in pathway B; pathway C (Scheme 2) can lead to the subsequent loss of a neutral cavitand. The results are remarkable in that deprotonation of an acetal proton can compete not only with electron autodetachment but also with breaking covalent interactions for $[\mathbf{12@11_2}]^{2-}$, while this is not true for $[\mathbf{12@2_2}]^{2-}$.

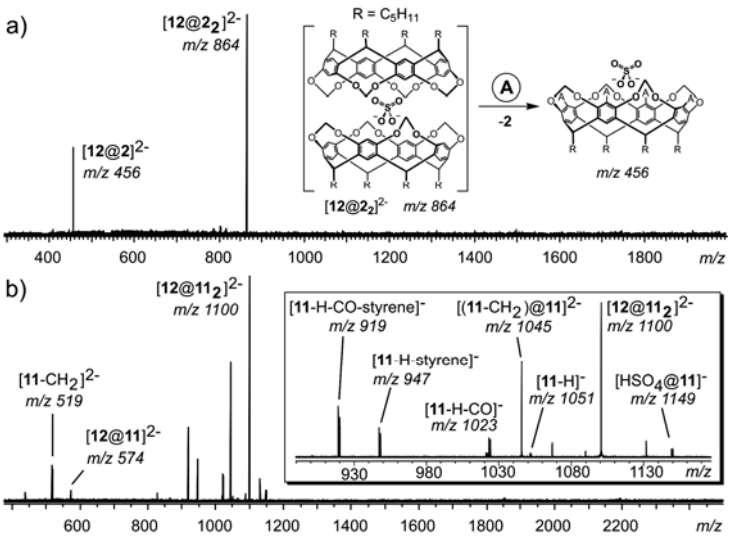

Figure 2 CID mass spectra with mass-selected a) $[\mathbf{12@2_2}]_2$ and b) $[\mathbf{12@11_2}]_2$

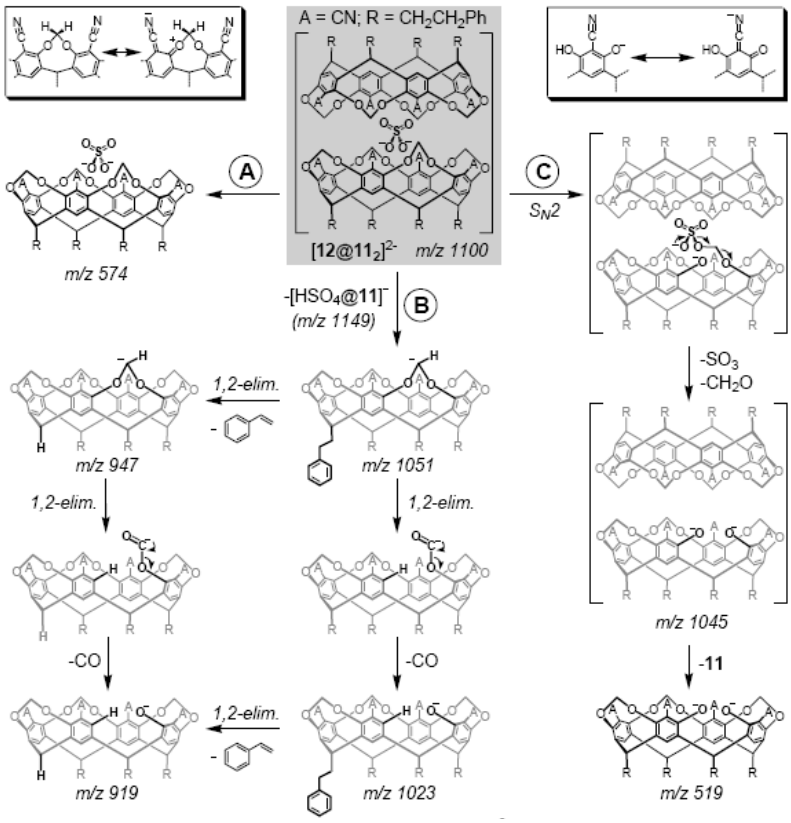

Scheme 2 Fragmentation pathways (**A**, **B**, **C**) of $[\mathbf{12@11_2}]^{2-}$ as observed in the CID mass spectra. The insets show the effect of electron-withdrawing substituents such as nitrile on theacetal C-H polarization and the phenolate leaving group properties

Scheme 2 shows the gas-phase fragmentations of $[\mathbf{12@11_2}]^{2-}$ as observed in the corresponding CID mass spectra (Figure 2b). In these MS/MS experiments, ions corresponding to the second peak from the isotope pattern were mass-selected, which contain one ^{13}C atom. Charge-separating fragmentations preferentially lead to fragments approximately half the size of the parent ion (e.g. monomer loss from a dimer). Consequently, the ^{13}C atom can be incorporated either in the neutral or in the ionic fragment so that two product signals are observed with a peak spacing of 1 amu. Fragmentation into a product di-anion and small neutral fragment (e.g. loss of SO3 and CH2=O)

leaves almost all carbons within the ionic product, which then only appears as one, non-split signal. This approach permits to directly determine whether a fragment is singly or doubly charged and thus facilitates interpretation of the MS/MS experiments.

Consequently, the binding energy of **11** to sulfate must even be significantly higher than that of **2**. A rationalization for this feature is the direct conjugation of the acetal oxygen with the nitrile group. An electron-withdrawing substituent such as the nitrile group thus increases the positive partial charge on the acetal hydrogens and increases the strength of their interactions with anionsSize-selectivity experiments with large monoanions such as tetraphenylborates $\mathbf{15}^-$ and $\mathbf{16}^-$ may provide insight into the binding mode. Upon addition of 0.25 equiv $Na^+\mathbf{15}^-$ to asolution of **11**, dimeric, trimeric, and tetrameric complexes ($[\mathbf{15@11_2}]^-$, $[\mathbf{15@11_3}]^-$, $[\mathbf{15@11_4}]^-$ were observed in the mass spectrum (Figure 1d). Similar results were also obtained with cavitands **2**, **9**, and **10**. In marked contrast, cavitand **8** with its extended cavity, gave rise exclusively to the 1:1 complex $[\mathbf{15@\ 8}]^-$. Apparently, this is a result of the steric congestion caused by the longer and quite rigid side chains on the upper rim of **8** and points to anion binding in the cavitand's cavity. In control experiments with the sterically more demanding guest $Na^+\mathbf{16}^-$, no complex formation occurred with cavitands **9** and **11**, and free $\mathbf{16}^-$ was the only ion observed. Each phenyl group of tetraphenylborate ($\mathbf{15}^-$) can dive into one cavitand cavity to form complexes with compositions of up to 4:1. This binding mode is unavailable when the size of the phenyl groups is increased by the attachment of two CF_3 groups in the **3**- and **5**-positions. Anion $\mathbf{16}^-$ is thus incongruent with the cavity in size and shape. Finally, larger dianions such as $\mathbf{14}^{2-}$ and $\mathbf{17}^{4-}$ were studied. The mass spectrum (Figure 1e) obtained from a solution of **2** and $Na^+{}_2\mathbf{14}^{2-}$ clearly shows the predominant presence of the dimer–guest complex $[\mathbf{14@2_2}]^{2-}$ accompanied by the corresponding monomer–guest complex $[\mathbf{14@2}]^{2-}$ With the tetrasulfonated porphyrin $\mathbf{17}^{4-}$, 4:1 complexes $[\mathbf{17@2_4}]^{4-}$ of cavitand and tetra-anion were observed as the base peak in the ESI mass spectrum. With guest $\mathbf{14}^{2-}$ and a 1:1 mixture of two different cavitands, it is possible to generate heterodimeric host–guest complexes. Upon addition of 14^{2-} to a mixture of two cavitands such as **2** and **3**, which have the same overall structure but carry different substituents, heterodimeric cavitand–dianion complexes such as $[\mathbf{14@2_1 3_1}]^{2-}$ were observed in the gas phase. After mass-selection of the heterodimeric complexes, CID experiments were performed. A qualitative ranking of the relative intrinsic strengths of the cavitand–sulfonate interactions can be easily determined by

comparing the intensities of fragment ions such as $[\mathbf{14@2}]^{2-}$ and $[\mathbf{14@3}]^{2-}$ for three reasons:[18]

1) Fragmentation occurs exclusively through the loss of one neutral cavitand, which is not significantly influenced by the other because of the distance between the two anionic sites on the guest.

2) The ratio of two fragment ions in the CID spectra is independent of ionization processes and spectrometer settings, because a true gas-phase experiment is performed.

3) The number of vibrational degrees of freedom into which the internal energy can be distributed in either fragment is not significantly different.

Consequently, it is possible to examine how the electronic nature of electron-withdrawing or electron-donating substituents on the cavitands's upper rims influences complex stabilities. Following this protocol, CID experiments were conducted with mass-selected $[\mathbf{14@5_17_1}]^{2-}$, $[\mathbf{14@5_16_1}]^{2-}$, $[\mathbf{14@4_16_1}]^{2-}$, $[\mathbf{14@2_14_1}]^{2-}$, and $[\mathbf{14@2_13_1}]^{2-}$ ions (Figure 3a–e). These CID spectra clearly show that the strengths of cavitand– sulfonate interactions increase as follows: 3≤2«4«5≈6« 7. In terms of the substituents electronic nature, the order is: OMe≤H«CO_2Me«Br≈I«CN. The experimentally obtained tendency is in good agreement with the electron withdrawing or -donating ability of the aromatic substituents.

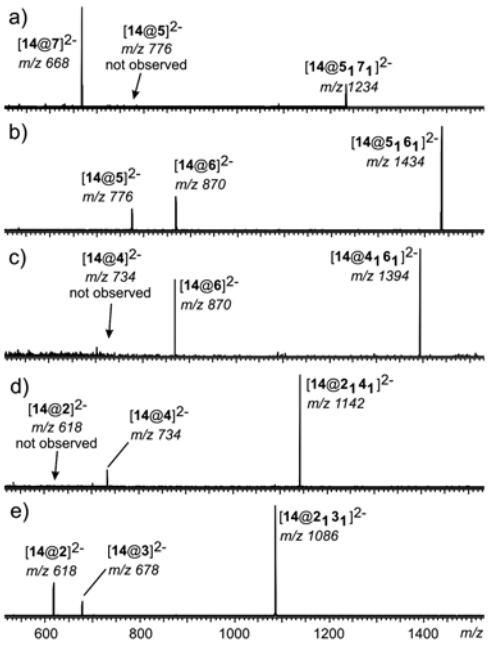

Figure 3 CID experiments with mass-selected, doubly charged heterodimer indigo carmine complexes: a) $[14@5_17_1]^{2-}$, b) $[14@5_16_1]^{2-}$, c) $[14@4_16_1]^{2-}$, d) $[14@2_14_1]^{2-}$, e) $[14@2_13_1]2^{-}$

The only exception is the CO_2Me group, which apparently affects the complexation through its conformationally flexible methoxy arms which extend to the vicinity of the binding sites. Nevertheless, this effect is not too prominent since **4** still binds sulfonate far better than **2** and **3** do. These experiments provide evidence for a cavitand–anion interaction mediated by C–H···anion hydrogen bonds that involve the acetal protons pointing into the cavitand bowl. The following points support this conclusion: 1) Anion–p interactions[19] do not play a significant role, since otherwise, **1** would be expected to be an equally good host for anions. 2) The substantial stability of the cavitand—anion complexes, particularly that of $[\mathbf{12@11_2}]^{2-}$, indicates that complexation is mediated by multiple interactions and thus likely occurs inside the cavitand bowl.

Cavitand **8** has the same alkyl feet as **2–7** but displays a significantly different complexation behavior with $\mathbf{14}^{2-}$and $\mathbf{15}^{-}$. This excludes binding of the anions at the bottom rim, since then no such effects would be expectedto occur. Steric effects attributed to the longer cyanophenyl substituents can easily be understood, however, if anion binding inside the cavity is assumed.4) The fragmentation of $[\mathbf{12@11_2}]^{2-}$ includes the deprotonation of one of the acetal positions, suggesting sulfate binding to occur close to the methylene inner protons. 5) Substituent effects revealed by the CID spectra of heterodimeric host–guest complexes with $\mathbf{14}^{2-}$ provide evidence for the binding sites to be located in the "influence region" of substituents at the upper rim. This applies in particular to the acetal protons which carry a higher positive partial charge when electron-withdrawing substituents are present. For more detailed insight into the thermodynamic forces driving anion binding to the cavitands through C–H···anion interactions, we performed a series of quantum chemical calculations on a C_{4v}-symmetric model system for [**13@2**]$^-$ in which the C_5H_{11} moieties where replaced simply by H, and which is designated [**13@2'**]$^-$ (Figure 4). Geometry optimizations and energy second-derivative calculations were conducted with the hybrid density functional B3LYP[20] with a split valence double-zeta basis set augmented with one set of polarization functions and diffuse functions on all atoms (6-31++G(d,p)) as implemented in Gaussian03.[21] Adopting the rigid-rotor harmonic-oscillator approximation, the free energy of association at room temperature ($\Delta G°_{298}$) for [**13@ 2'**]$^-$ is calculated to be –24.2 $kJmol^{-1}$, which is quite substantial in view of the assumed weak individual enthalpic contributions and the entropic cost of any associative mechanism. In a second step, generalized compliance constants[22] were calculated in order to quantify the individual contributions and, if possible, to discriminate between C–H···anion and possible anion–p interactions. To the best of our knowledge this is the first direct quantification of this type of weak, non-covalent C–H···ion

interaction. The anion–p contacts measured as displacements of the internal coordinates between the fluorine atoms of the PF_6^- anion and aromatic carbons in the resorcinarenes are very soft, with compliance constants between 30 and 40 Mmdyne^{-1}. Note that a higher compliance constant is connected with a softer interaction. Anion_p contacts can thus indeed be excluded as the enthalpic driving force during the association. On the other hand, the compliance constant for the **2'**C–H···F–PF_5- interactions point to a hydrogen bond in the range between a strong N–H···O (≈5 Mmdyne⁻1) and a C–H···O hydrogen bond (≈20 Mmdyne^{-1}). The strength of the 2'C–H···F–PF_5^- interaction measured by generalized compliance constants is computed to be 15.2 Mmdyne^{-1}. The four individual C–H···F contacts in [**13@2'**]$^-$, which are intensified through the negative charge on the guest molecule, are therefore mainly responsible for the stability of the adduct. In conclusion, mass spectrometric experiments together with theory indicate that suitably positioned C–H bonds can complex anions, if they are polarized by neighboring electronegative heteroatoms.

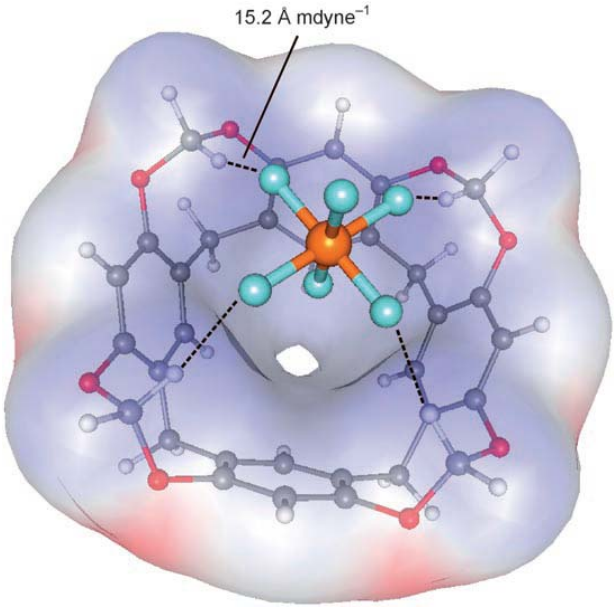

Figure 4 The B3LYP/6-31++G(d,p)-optimized structure of the model complex [13@2']$^-$ mapped with the electrostatic potential on the host surface. C_H···F hydrogen bonds are depicted.

The easy-to-access methylene-bridged resorcinarene cavitands provide exactly the right geometric arrangement of such groups to support anion binding through multiple interactions with up to four converging C_H groups. Particularly remarkable is the fact that even one cavitand is able to solvate a sulfate dianion well enough to prevent electron autodetachment.
This experiment shows that the interaction strength between host and guest anion can amount to substantial values. From a fundamental point of view, this study provides new insight into the nature and importance of C–H···anion interactions. This mode of hydrogen bonding, that is, hydrogen bonds between an anion and a nonaromatic C–H bond, is very rare and not well studied so far. To the best of our knowledge, the phenomenon that neutral cavitands complex different anions exclusively through this type of weak interaction has not been described previously.

2.3 Experimental section

Experimental Details for the Mass Spectrometric Experiments

High resolution ESI mass spectra and MS/MS spectra were recorded on a Bruker APEX IV Fourier-transform ion-cyclotron-resonance (FT-ICR) mass spectrometer with an Apollo electrospray ion source equipped with an off-axis 70° spray needle. Typically, acetone or a mixture of acetone and methanol (e.g. 40:7 or 40:1) served as the spray solvent. The solutions were 200 to 780 µM with respect to the concentration of the hosts. In case of anionic guests (sulfate, indigo carmine) which are insoluble in pure acetone, high concentration solutions (160 mM for sulfate, 16 mM for indigo carmine) were prepared in pure methanol and then added in very small amounts to the acetone solutions of hosts. Analyte solutions were introduced into the ion source with a syringe pump (Cole-Parmers Instruments, Series 74900) at flow rates of ca. 3 - 7 µL/min. Ion transfer into the first of three differential pumpingstages in the ion source occurred through a glass capillary with 0.5 mm inner diameter and nickel coatings at both ends. Ionization parameters were adjusted as follows: capillary voltage: 4.5 kV; endplate voltage: 4.0 kV; capexit voltage: -30 to -400 V; skimmer voltages: -10 to -20 V; temperature of drying gas: 150-200 °C. The flows of the drying (ca. 15 psi) and nebulizer gases (ca. 30 psi) were kept in a medium range. Depending on the achievable abundances of ions produced in the ion source, the ions were accumulated in the instrument's hexapole for 0.7 – 10.0 s. The ions are then introduced into the FT-ICR cell, which was operated at pressures below 10-10 mbar, and finally

detected by a standard excitation and detection sequence. For each measurement 4 to 120 scans were averaged to improve the signal-to-noise ratio.
For MS/MS experiments, the whole isotope patterns of the ion of interest were isolated by applying correlated sweeps, followed by high resolution isolation shots to remove the higher isotopes (in case of [**14**@**5161**]2-: higher isotopes were not removed by isolation shots; in case of [**14**@**5171**]2-: all isotopes were removed except for *m/z* 1234.3 and *m/z* 1234.8). After isolation, argon was introduced into the ICR cell as the collision gas through a pulsed valve at a pressure of ca. 10-8 mbar. The ions were accelerated by a standard excitation protocol and detected after a 2 s pumping delay. A sequence of several different spectra was recorded at different excitation pulse attenuations in order to get at least a rough and qualitative idea of the effects of different collision energies on the fragmentation patterns. Typical parameter settings for the CID experiments with heterodimer complexes are: Parameters of the

Apollo ESI source: nebulizing gas: 30 psi, drying gas: 15 psi, drying gas temperature: 200°C, vacuum lens voltages: capillary 4.5 kV, end plate 4 kV, capexit -340 V, 1st skimmer -20 V, 2nd skimmer - 10 V, offset -1.5 V, RF amplitude 500 V, trap -15 V, extract 15 V

Ion transfer and cell parameters of APEX IV FTICR mass spectrometer beam steering parameter XDFL: -20 V, beam steering parameter YDFL: 0 V, voltage gradient at the cell entrance (DEV2): -3.02 V, attenuation level of excitation (excite / PL3): 3.6 dB

MSMS parameters of APEX IV FTICR mass spectrometer attenuation level of correlated sweep (CorrSweep / PL4): 17.3 dB, attenuation level of correlated shots (CorrShot / PL7): 45.3 dB, attenuation level of ion activation (activation / PL9): 60.8 dB, collision gas: Argon 4.6, pulsed valve opening duration: 0.02 sec, pumping delay: 2 sec.

2.4 Synthesis of cavitands

General. Chemicals and dry DMF were purchased from Sigma-Aldrich, Fluka, Merck and used as received. The solvents (except DMF) were dried using standard techniques. Thinlayer chromatography (TLC) was carried out on TLC plates pre-coated with silica gel 60 F254 from Merck. Melting points were

determined on hot stage (Mikroskop Heiztisch) SM-Luxfrom Leitz. Mass spectra were recorded using Bruker APEX IV Fourier-transform ioncyclotron-resonance (FT-ICR) mass spectrometer with an Apollo electrospray ion source equipped with an off-axis 70° spray needle. 1H NMR and 13C NMR spectra were recorded using 300, 400, and 500 MHz Bruker instrument.

a)7,11,17,23-Tetramethoxy-1,21,23,25-tetrapentyl-2,20:3,19-di-metheno-1H,21H,23H,25H bis[1,3]dioxocino[5,4-i:5´,4´-i´]benzo[1,2-d:5,4d´]bis[1,3] benzodioxocine (3):

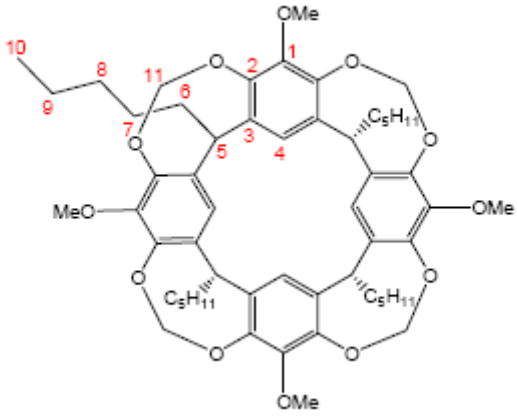

500 mg (0.61 mmol) unfunctionalized cavitand **2** was dissolved in 10 mL dry THF under argon. The solvent was then removed in vacuo. This procedure was repeated once more. **2** was again dissolved in 5 mL dry THF and cooled down to -78 °C. At this temperature, 4.08 mL (6.12 mmol, 10 eq.) *s*-BuLi was slowly added through a syringe and stirred for 30 min at - 78 °C. 0.69 ml (6.12 mmol, 10 eq.) trimethylborate was then added, the reaction mixture was allowed to warm up to RT and stirred for 1 h. Upon addition of a 1:1-mixture of 4 ml 3 N sodium hydroxide solution and 4 ml hydrogen peroxide solution (35%), the mixture was stirred for 18 h at RT. Sodium sulfite solution (10%) was added, the organic layer was separated and the aqueous layer was extracted using ethyl acetate. The combined organic layers were washed with sodium bicarbonate solution, water and brine, dried over magnesium sulfate and concentrated in vacuo. 520 mg (3.66 mmol, 6 eq.) iodomethane and 674 mg (4.88 mmol, 8 eq.) potassium carbonate was added to the crude. Upon

addition of 15 mL acetone, the mixture was refluxed and concentrated in vacuo after the reaction was complete. The residue was taken up in ethyl acetate, washed with water (several times) and brine (1x), dried over sodium sulfate and concentrated in vacuo. After purification by column chromatography on silica gel (eluent: *n*-hexane/ethyl acetate = 5:1), the product was obtained as a colourless solid in 52% yield (298 mg); m. p. > 300°C; *Rf* = 0.26 (*n*-hexane/ethyl acetate = 5:1); **^{1}H NMR** (500.1 MHz, CDCl3, 25°C): δ = 0.91 (t, 3*J* (H-9,H-10) = 7.1 Hz, 12H; H-10); 1.32-1.43 (m, 24H; H-7 to H-9), 2.13-2.19 (m, 8H; H-6), 3.76 (s, 12H; -OCH3), 4.36 (d, 2*J* (H-11inside,H-11outside) = -7.1 Hz, 4H; H-11inside), 4.70 (t, 3*J* (H-5,H-6) = 8.1 Hz, 4H; H-5), 5.84 (d, 2*J* (H- 11inside,H-11outside) = -7.1 Hz, 4H; H-11outside), 6.78 (s, 4H; H-4); **^{13}C NMR** (125.8 MHz, CDCl3, 25°C): δ = 14.2 (C-10), 22.7 (C-9), 27.6 (C-8), 29.9 (C-6), 32.1 (C-7), 37.0 (C-5), 61.1 (-OCH3), 99.7 (C-11), 114.1 (C-4), 139.0 C-3), 145.3 (C-1), 148.2 (C-2); **ESI-FTICRMS** (negative mode, sprayed from acetone, 1 eq. Bu4NCl added): *m/z* = 971 ([M+Cl]-, 100%).

b)7,11,17,23-Tetraiodo-1,21,23,25-tetrapentyl-2,20:3,19-dimetheno-1H,21H,23H,25Hbis[1,3]dioxocino[5,4-i:5´,4´i´]benzo[1,2-d:5,4d´]bis[1,3]-benzodioxocine.(6)

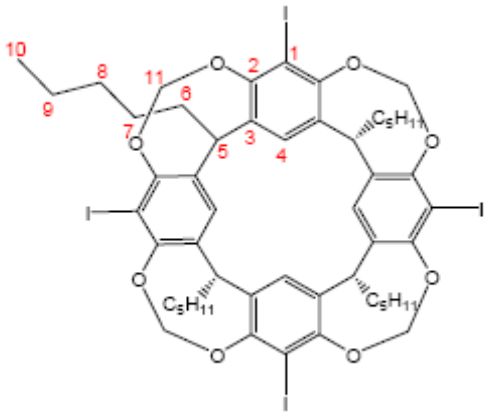

400 mg (0.35 mmol) tetrabromocavitand **5** were dissolved in 5 mL dry THF under argon. The solvent was then removed in vacuo. This procedure was repeated once more. **5** was again dissolved in in 5 mL dry THF and cooled down to -78 °C. 1.41 mL (2.12 mmol, 6 eq.) *n*-BuLi (1.5 M in *n*-hexane) was added, and the mixture was stirred for 0.5 h at this temperature. 717 mg (2.83 mmol, 8 eq.) iodine were dissolved in 5 mL dry THF and slowly dropped into the reaction mixture at -78 °C. The cooling bath was removed, and the mixture

was stirred for 1 h at RT. 20 mL dichloromethane was then added. The organic layer was washed with saturated aqueous sodium thiosulfate solution, water (2x), brine (1x), dried over sodium sulfate and concentrated in vacuo. After purification by column chromatography on silica gel (eluent: *n* hexane/ethyl acetate = 5:1), the product was obtained as a colourless solid in 42% yield (194 mg); m. p. > 300°C; *Rf* = 0.93 (*n*-hexane/ethyl acetate = 5:1); 1H NMR (300.1 MHz, CDCl3, 25°C): δ = 0.90 (t, 3*J* (H-9,H-10) = 7.1 Hz, 12H; H-10); 1.27-1.46 (m, 24H; H-7 to H-9), 2.15- 2.22 (m, 8H; H-6), 4.31 (d, 2*J* (H-11inside,H-11outside) = -7.1 Hz, 4H; H-11inside), 4.84 (t, 3*J* (H- 5,H-6) = 8.1 Hz, 4H; H-5), 5.96 (d, 2*J* (H 11inside,H-11outside) = -7.1 Hz, 4H; H-11outside), 7.05 (s, 4H; H-4); 13C NMR (75.5 MHz, CDCl3, 25°C): δ = 14.1 (C-10), 22.7 (C-9), 27.5 (C-8), 30.1 (C-6), 31.9 (C-7), 38.0 (C-5), 93.1 (C-1), 98.8 (C-11), 120.7 (C-4), 138.8 (C-3), 154.9 (C-2); ESI-FTICR-MS (negative mode, sprayed from acetone, 1 eq. Bu4NCl added): *m/z* = 1355 ([M+Cl]-, 100%).

c)7,11,17,23-Tetracyano-1,21,23,25-tetrapentyl-2,20:3,19-di-metheno-1H,21H,23H,25Hbis[1,3]dioxocino[5,4-i:5´,4´-i´] (7)

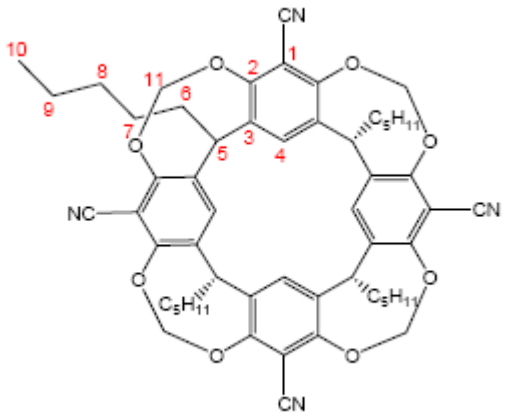

150 mg (0.11 mmol) tetraiodocavitand **6**, 96 mg (0.82 mmol, 7.2 eq.) zinc(II)cyanide, 2.4 mg (0.036 mmol, 32 mol%) zinc and 12 mg (0.023 mmol, 20 mol%) [Pd(P*t*Bu3)2] were put in a Schlenk flask which was then evacuated and flushed with argon. After dissolving the solid in 5 mL dry DMF, the reaction mixture was stirred at 100°C over night. After cooling down, DMF was removed in vacuo, 5 mL dichloromethane and 5 mL water were added. The mixture was stirred briefly, and the organic layer was separated. The aqueous layer was washed with dichloromethane, the combined organic layers were dried over

sodium sulfate and concentrated. After purification by column chromatography on silica gel (eluent: *n*hexane/ ethyl acetate = 5:1), the product was obtained as a colourless solid in 71% yield (72 mg); m. p. > 300°C; *Rf* = 0.57 (*n*-hexane/ethyl acetate = 5:1); **^{1}H NMR** (400.1 MHz, CDCl3, 25°C): δ = 0.90 (t, 3*J* (H-9,H-10) = 7.1 Hz, 12H; H-10); 1.31-1.41 (m, 24H; H-7 to H-9), 2.19-2.24 (m, 8H; H-6), 4.58 (d, 2*J* (H-11inside,H-11outside) = -7.4 Hz, 4H; H-11inside), 4.80 (t, 3*J* (H- 5,H-6) = 8.1 Hz, 4H; H-5), 6.08 (d, 2*J* (H-11inside,H-11outside) = -7.4 Hz, 4H; H-11outside), 7.28 (s, 4H; H-4); **^{13}C NMR** (100.6 MHz, CDCl3, 25°C): δ = 13.0 (C-10), 21.6 (C-9), 26.2 (C-8), 28.1 (C-6), 30.7 (C-7), 35.3 (C-5), 97.8 (C-11), 103.4 (C-1), 111.0 (-CN), 123.7 (C-4), 138.1 (C-3), 155.7 (C-2); **ESI-FTICR-MS** (negative mode, sprayed from acetone, 1 eq. Bu4NCl added): *m/z* = 951 ([M+Cl]-, 100%).

2.5 References

[1] For reviews on resorcinarene-based cavitands, see: a) P. Timmerman, W. Verboom, D. N. Reinhoudt, Tetrahedron 1996, 52,2663 – 2704; b) A. Jasat, J. C. Sherman, Chem. Rev. 1999, 99, 931 – 96.

[2] F. Hof, S. L. Craig, C. Nuckolls, J. Rebek, Jr., Angew. Chem. 2002, 114, 1556– 1578; Angew. Chem. Int. Ed. 2002, 41, 1488 – 1508.

[3] a) L. R. MacGillivray, J. L. Atwood, Nature 1997, 389, 469 – 472; b) T. Gerkensmeier,W. Iwanek, C. Agena, R. FrNhlich, S. Kotila, C. NPther, J. Mattay, Eur. J. Org. Chem. 1999, 2257 – 2262; c) A. Shivanyuk, J. Rebek, Jr., J. Am. Chem. Soc. 2003, 125, 3432 – 3433; d) L. Avram, Y. Cohen, Org. Lett. 2003, 5, 3329 – 3332; e) N. K. Beyeh, M. Kogej, A. Mhman, K. Rissanen, C. A. Schalley, Angew. Chem. 2006, 118, 5339 – 5342; Angew. Chem. Int. Ed. 2006, 45, 5214 – 5218

[4] L. Pirondini, F. Bertolini, B. Cantadori, F. Ugozzoli, C. Massera, E. Dalcanale, Proc. Natl. Acad. Sci. USA 2002, 99, 4911 – 4915.

[5] O. D. Fox, M. G. B. Drew, P. D. Beer, Angew. Chem. 2000, 112, 139 – 144; Angew. Chem. Int. Ed. 2000, 39, 135 – 140.

[6] L. Pirondini, E. Dalcanale, Chem. Soc. Rev. 2007, 36, 695 – 706.

[7] R. J. Hooley, S. M. Biros, J. Rebek, Jr., Angew. Chem. 2006, 118, 3597 – 3599; Angew. Chem. Int. Ed. 2006, 45, 3517 – 3519.

[8] a) H. J. Schneider, Angew. Chem. 1991, 103, 1419 – 1439; Angew. Chem. Int. Ed. Engl. 1991, 30, 1417 – 1436; b) A. Shivanyuk, K. Rissanen, E. Kolehmainen, Chem. Commun. 2000, 1107 – 1108; c) A. Shivanyuk, J. Rebek, Jr., Chem. Commun. 2001, 2374 – 2375; d) H. MPnsikkamPki, M. Nissinen, K. Rissanen, Chem. Commun. 2002, 1902 – 1903; e) H. MPnsikkamPki, M. Nissinen, C. A. Schalley, K. Rissanen, New J. Chem. 2003, 27, 88 – 97.

[9] a) A. Bianchi, K. Bowman-James, E. Garcia-Espana, Supramolecular Chemistry of Anions, Wiley-VCH, New York, 1997; b) P. A. Gale, Coord. Chem. Rev. 2003, 240, 191 – 221; c) J. L. Sessler, P. A. Gale, W.-S. Cho, Anion Receptor Chemistry, RCS Publishing, Cambridge, 2006.

[10] Selected examples: a) H. Boerrigter, L. Grave, J. W. M. Nissink, L. A. J. Chrisstoffels, J. H. van der Maas, W. Verboom, F. de Jong, D. N. Reinhoudt, J. Org. Chem. 1998, 63, 4174 – 4180; b) U. LQcking, D. M. Rudkevich, J. Rebek, Jr., Tetrahedron Lett. 2000, 41, 9547 – 9551; c) S. K. Kim, B.-G. Kang, H. S. Koh, Y. J. Yoon, S. J. Jung, B. Jeong, K.-D. Lee, J. Yoon, Org. Lett. 2004, 6, 4655 – 4658.

[11] Examples for aromatic C_H···anion interactions: a) D.-W. Yoon, H. Hwang, C.-H. Lee, Angew. Chem. 2002, 114, 1835 – 1837; Angew. Chem. Int. Ed. 2002, 41, 1757 – 1759; b) K. Chellappan, N. J. Singh, I.-C. Hwang, J.W. Lee, K. S. Kim, Angew. Chem. 2005, 117, 2959 – 2963; Angew. Chem. Int. Ed. 2005, 44, 2899 – 2903; c)W. J. Belcher, M. Fabre, T. Farhan, J.W. Steed, Org. Biomol. Chem. 2006, 4, 781 – 786.

[12] a) C. A. Ilioudis, D. A. Tocher, J.W. Steed, J. Am. Chem. Soc. 2004, 126, 12395 – 12402; b) H. Maeda, Y. Kusunose, Chem. Eur. J. 2005, 11, 5661 – 5666.

[13] a) C. L. D. Gibb, E. D. Stevens, B. C. Gibb, J. Am. Chem. Soc. 2001, 123, 5849 – 5850; b) Z. R. Laughrey, T. G. Upton, B. C. Gibb, Chem. Commun. 2006, 970 – 972.

[14] M. Meot-Ner (Mautner), Chem. Rev. 2005, 105, 213 – 284.

[15] Cavitand syntheses: a) D. J. Cram, L. M. Tunstad, C. B. Knobler, J. Org. Chem. 1992, 57, 528; b) J. A. Bryant, M. T. Blanda, M. Vincenti, D. J. Cram, J. Am. Chem. Soc. 1991, 113, 2167 – 2172;

c) N. Cuminetti, M. H. K. Ebbing, P. Prados, J. de Mendoza, E. Dalcanale, Tetrahedron Lett. 2001, 42, 527 – 530; d) F. Fochi, P. Jacopozzi, E.Wegelius, K. Rissanen, P. Cozzini, E. Marastoni, E. Fisicaro, P. Manini, R. Fokkens, E. Dalcanale, J. Am. Chem. Soc. 2001, 123, 7539 – 7552.

[16] A. I. Boldyrev, J. Simons, J. Phys. Chem. 1994, 98, 2298 – 2300.

[17] a) A. T. Blades, P. Kebarle, J. Am. Chem. Soc. 1994, 116, 10761 – 10766; b) X.-B. Wang, J. B. Nicholas, L.-S. Wang, J. Chem. Phys. 2000, 113, 10837 – 10840.

[18] This experiment is a variant of Cooks F kinetic method and used here only for a qualitative ranking, not for the determination of quantitative binding energies. For a review on this method, see: R. G. Cooks, J. S. Patrick, T. Kotiaho, S. A. McLuckey, Mass Spectrom. Rev. 1994, 13, 287 – 339.

[19] O. B. Berryman, V. S. Bryantsev, D. P. Stay, D. W. Johnson, B. P. Hay, J. Am. Chem. Soc. 2007, 129, 48 – 58, and references therein.

[20] A. D. Becke, J. Chem. Phys. 1993, 98, 5648 – 5652.

[21] M. J. Frisch, et al., Revision B.02 ed., Gaussian, Inc., Pittsburgh PA, 2003.

[22] K. Brandhorst, J. Grunenberg, ChemPhysChem 2007, 8, 1151 – 1156, and references therein

Self-assembly of a cavitand-based heteronuclear coordination cage*

3

3.1 Introduction

The self-assembly of coordination cages has reached a high level of sophistication with regard to ligand design and selection of metal precursors.[1] As a result, the shape, dimensions and polarity of the internal cavity can be engineered, allowing for inclusion of diverse neutral[2] and charged guests[3] in different solvents. The compartmentalization of these guests imparts a wide spectrum of useful properties, including catalysis,[4,5] storage,[6] and the stabilization of labile chemical species.[7].

A missing feature in these self-assembly protocols is the differentiation in metal/ligand reactivity necessary for the generation of heteronuclear coordination cages. As a first step to address this issue, Kobayashi and coworkers reported the preparation of heterocages, coordination cages featuring two different ligands.[8,9] Two complementary tetradentate cavitand ligands were prepared, each bearing four identical coordination groups at the apical positions, either nitriles[10] or pyridines.[8] By utilizing the two cavitands' different coordination ability, they devised self-assembly conditions leading to the formation of either homonuclear Pd or Pt heterocages as the dominant product under kinetic control.

The formation of heteronuclear cages introduces a further level of complexity, where at least two metal/ligand couples must undergo self-sorting during the assembly procedure. For instance, the choice of coordinating ligands and metal

*Part of this chapter has been published in Tetrahedron **2009**, in press

precursors must be well-defined to differentiate their cross-reactivity. At the same time, the different coordinating groups must be inserted at a single macrocyclic ligand site and organized in a precise relative spatial orientation.

In particular, for our purpose, we took into consideration Kobayashi's work. He carried out some experiments with two cavitands (Figure 1) having four benzonitriles or four ethynylpiridines at the apical positions.

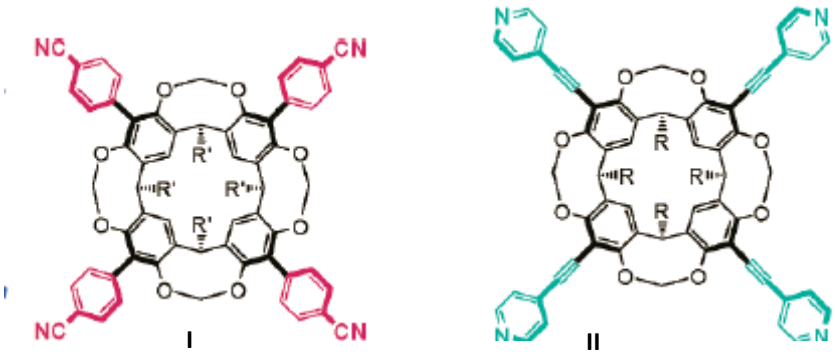

Figure 1 Structure of cavitand **I** and **II** synthesized by Kobayashi's group for the self-assembly of hetero- and homo-cages

He observed that, upon addition of four equivalents of Pt(dppp)OTf_2 to a 1:1 mixture of **I** and **II** in $CDCl_3$, the ^{1}H NMR spectrum showed the formation of a 1:1:*n* (*n* > 1) mixture of the two homocages **III** and **IV** as well as the heterocage **V**, as shown in Scheme 1

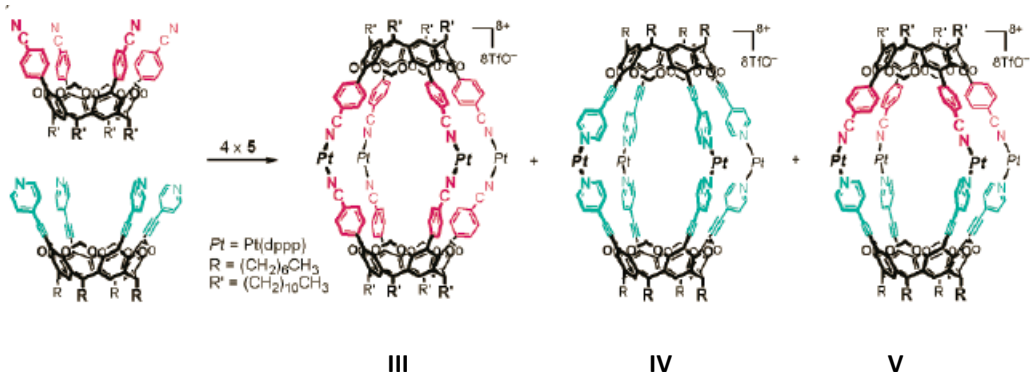

Scheme 1 Formation of homocages and heterocage starting from cavitand **I** and **II**, upon addition of Pt complex.

Addition of cyanophenyl cavitand **II** to the solution of homo cavitand cage **IV** and free Pt(dppp)OTf_2, gave only homo cavitand cages **III** and **IV** in a 1:1 ratio (Scheme 2)

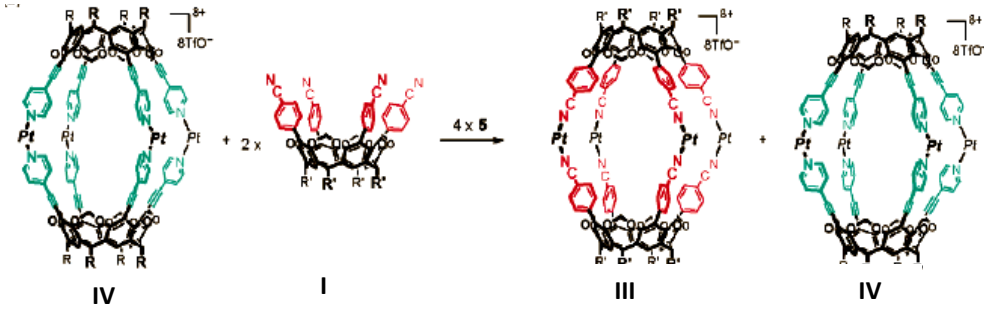

Scheme 2 formation of homocages reacting homocage **IV** and cavitand **I**

The only way to obtain selectively the heterocage was to add cavitand **II** to the homocage **III**; heterocage **V** and free cavitand **I** convert in the two homocages **III** and **IV**. (Scheme 3) This process is slow at room temperature whereas it is faster at 50°C.

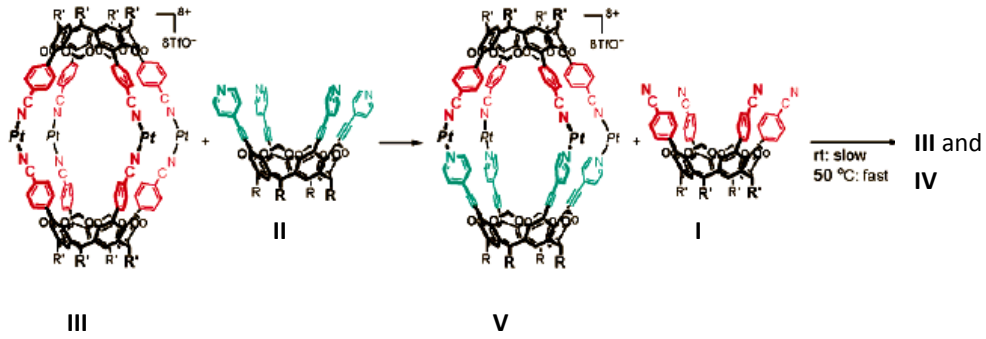

Scheme 3 Selective formation of heterocage **V**

This result suggested that heterocage was a kinetic product whereas homocage **IV** was a thermodynamic one. They observed that the homocage **IV** was the thermodynamic product with lower energy, whereas homocage **III** has

higher energy level and heterocage **V** is in between them. In Figure 2 is represented the average energy level of the three cages.

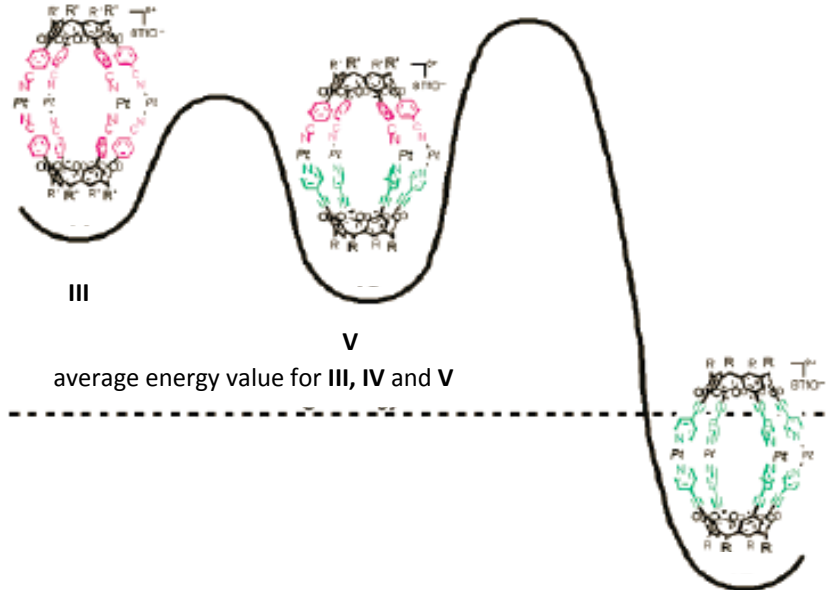

Figure 2 Average energy level for cages **III**, **IV** and **V**

In conclusion, the selectivity for the self-assembly of the homo or hetero cavitand cage is controlled by the balance between kinetic and thermodynamic stabilities of cages based on a combination of factors such as coordination ability and steric demand of the cavitands.

In this Chapter we report a thermodynamically controlled self-assembly protocol leading to the exclusive formation of a Pd/Pt heteronuclear cage. The protocol is based on a tetradentate cavitand ligand functionalized with three nitriles and one pyridine at the upper rim.

3.2 Result and Discussion

3.2.1 Synthesis of the cavitand 1

The tetradentate cavitand ligand **1**, designed for the self-assembly of heteronuclear coordination cages, presents three benzonitrile and one ethynylpyridine ligands, all of which inserted at the apical positions of a methylene-bridged cavitand (Figure 3). The choice of these different ligands at the upper rim of the cavitand was dictated by two factors: (i) their different coordination ability toward transition metals like Pt or Pd and (ii) their constant distance and orientation with respect to the cavitand scaffold, in order to avoid mismatch during self-assembly.[11] The four-step synthesis of cavitand **1** is presented in Scheme 1. Resorcinarene **2**, equipped with hexyl feet to assure solubility in organic solvents, was synthesized according to published procedure. Tetraiodo-resorcinarene **3** was obtained from the reaction of resorcinarene **2** with iodine in the presence of sodium hydrogencarbonate.[13]

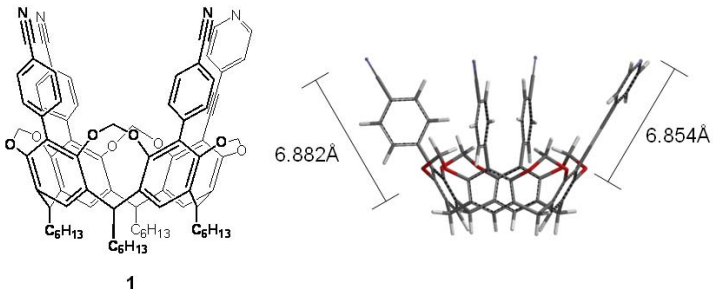

Figure 3 Structure of cavitand **1** and Spartan modeling showing the distance and orientation of the two ligands with respect to the cavitand scaffold.

The reaction was carried out at room temperature in a 1:1 mixture of water and diethyl ether. The desired product precipitated in pure form at the water-organic interface (36 % yield). Reaction of 3 with CH_2ClBr in a Schlenk apparatus[14] afforded methylene-bridged tetraiodo-cavitand **4** in very high yield (88%). Sonogashira coupling on **4** gave monoethynylpyridine derivative **5**, which underwent a multiple Suzuki coupling to give the desired cavitand 1. (Scheme 4).

3.2.2 Stepwise self-assembly of homonuclear cages.

We first explored the complexation behavior of tetradentate ligand **1** against a single metal precursor of general structure M(dppp)OTf_2. A stepwise protocol, depicted in Scheme 4, was devised for both Pt(dppp)OTf_2 and Pd(dppp)OTf_2. 0.5 equivalents of metal complex were added to a 5 mM solution of cavitand **1** in a mixture of CD_2Cl_2 (400 µL) and CD_3NO_2 (100 µL). CD_3NO_2 was added to accelerate the ligand exchange[15] in order to reach the thermodynamic equilibrium in a reasonable time. Subsequently, the remaining 1.5 equivalents of metal precursor were added to the solution. ^1H and ^{31}P NMR spectra were used to track the self-assembly process. The cages were identified by ESI mass

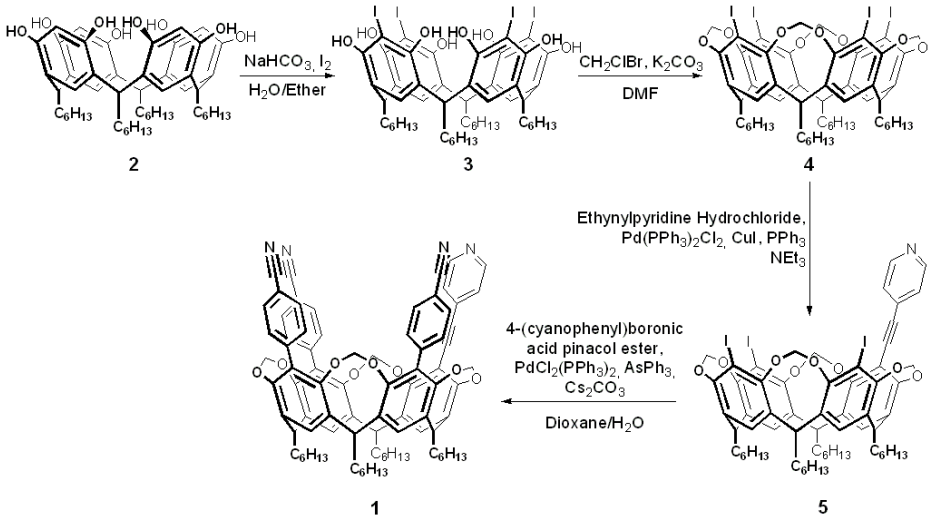

Scheme 4. Synthesis of tetradentate cavitand ligand **1**

spectrometry.

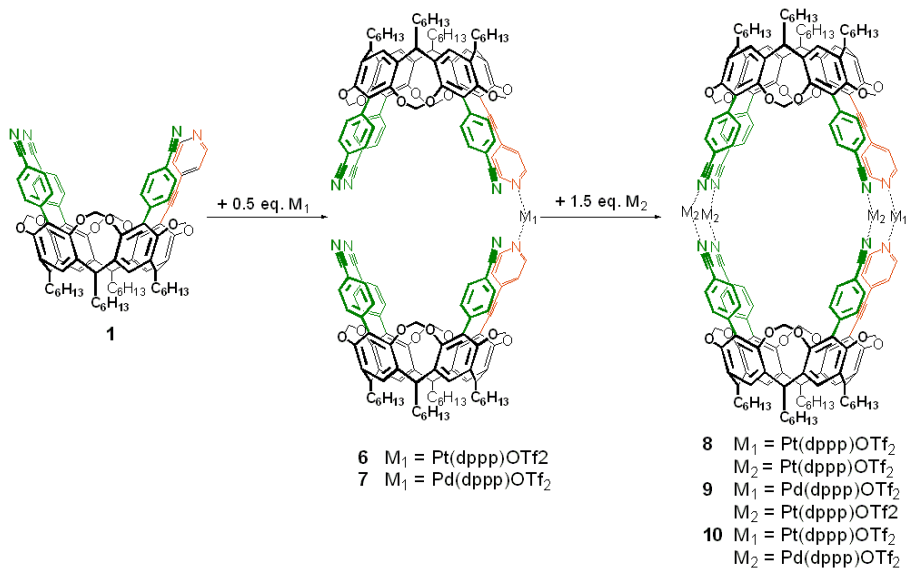

Scheme 5. Stepwise self-assembly protocol.

As shown in Figure 4a−b, upon addition of 0.5 equivalents of Pt(dppp)OTf_2 to a solution of cavitand **1**, the α-H peak a of ethynylpyridine ligand experienced a downfield shift of 0.3 ppm (from 8.52 to 8.82 ppm), while the H_{in} and H_{out} signals of the methylene bridges nearby the ethynylpyridine group moved upfield from 5.59 to 5.50 ppm. The ^{31}P NMR spectrum showed a single signal at − 15.60 ppm (with appropriate satellites); this peak was shifted upfield with respect to the free Pt(dppp)OTf_2 ($\Delta\delta = \delta_{hemicage} - \delta_{free\ Pt\ metal\ complex}$ = 5.63 ppm, from − 9.97 to − 15.60 ppm). These data are in agreement with the formation of hemicage **6**, in which the metal complex is coordinated to the ethynylpyridine ligands, leaving the benzonitrile ones free. The addition of further 1.5 equivalents of Pt(dppp)OTf_2 led to complete closure of the cage, as confirmed by ESI MS (Figure 5). The mass spectrum contained a prominent signal at 2938.2 *m/z*, corresponding to the doubled charged cage ion. However, as shown in Figure 2c−d, two NMR signals corresponding to the ethynylpyridine α-H were present at 8.81 and 8.61 ppm. The the intensity ratio of the two peaks was 1:1 immediately after the addition of the metal complex, but became 1:3 after 48 h and remained stable thereafter. Moreover, a splitting of the signals corresponding to H_{in} and H_{out} of the methylene bridges was observed. After the completion of the reaction, the ^{31}P NMR spectrum

presented a second signal at – 10.02 ppm, in addition to − 15.60 ppm peak in a 3:1 ratio.

Taken together these observations indicate the presence of more than one isomeric cage in solution. As shown in Figure 6, in addition to the structure in which the two ethynylpyridines are coordinated to the same metal center (**8a**) the formation of two other isomers is conceivable. In such isomers (**8b** and **8c**), one Pt(dppp)OTf_2 complex is coordinated to an ethynylpyridine and a benzonitrile ligand. In the case of **8b,** two equivalent structures are possible, obtained by rotating one cavitand ligand in **8a** by ± 90°.

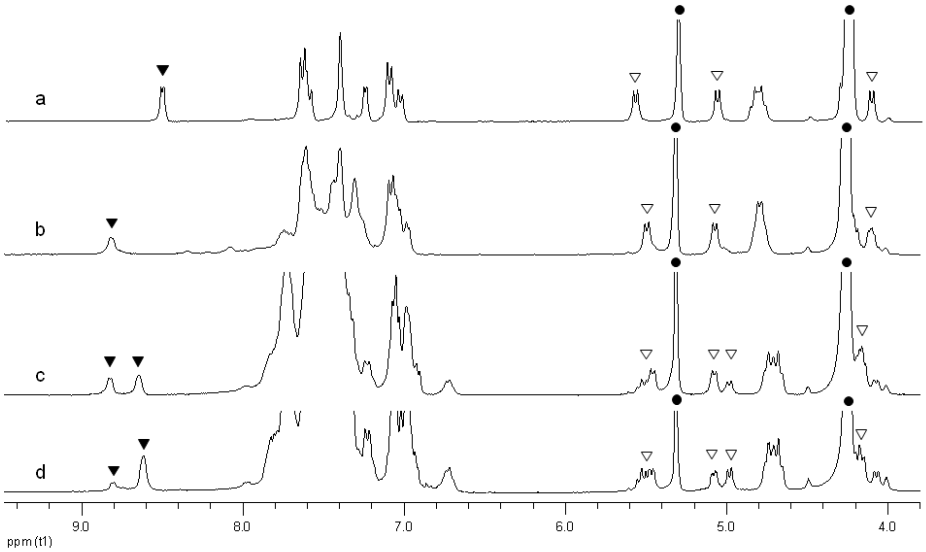

Figure 4. ^{1}H NMR (300 MHz, 400 µL CD_2Cl_2 and 100 µL CD_3NO_2) spectra of (a) 5 mM cavitand **1**, (b) 5 mM cavitand **1** and 0.5 eq. Pt(dppp)OTf_2, (c) 5 mM cavitand **1** and 2 eq. Pt(dppp)OTf_2, (d) 5 mM cavitand **1** and 2 eq. Pt(dppp)OTf_2 after 48 hours. ▲ethynylpyridine α-H protons, ▽ H_{in} and H_{out} methylene bridges protons, ● residual solvent peaks.

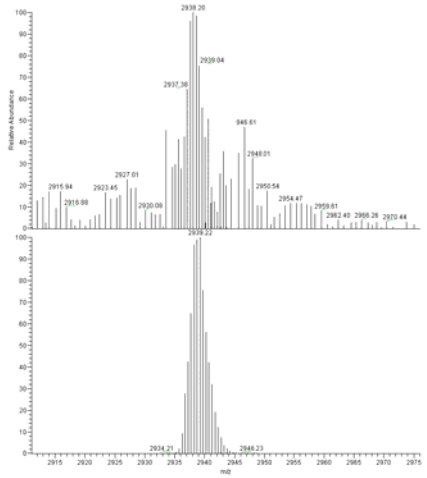

Figure 5. . Selected region of the experimental (top) and calculated (bottom) ESI MS spectrum of CD_2Cl_2/CD_3NO_2 solution of cage **8** showing $[M - 2CF_3SO_3]^{2+}$ signal at *m/z* 2938.2

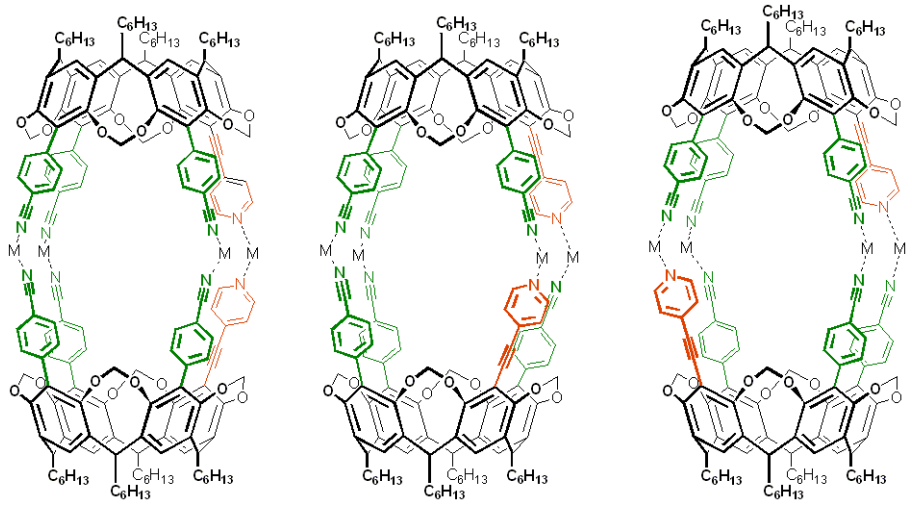

8a
9a

8b (× 2)
9b (× 2)

8c
9c

8a-c M = $Pt(dppp)OTf_2$
9a-c M = $Pd(dppp)OTf_2$

Figure 6. Isomeric coordination cages **8a – c** and **9a – c.**

As reported by Kobayashi,[8] the ^{1}H NMR signal corresponding to the α-H protons of the ethynylpyridine ligand is slightly upfield shifted for the EtPy−Pt−NCPh system compared to the EtPy−Pt−EtPy system. Therefore, the new signal detected at 8.61 ppm is consistent with cages **8b** and **8c,** which cannot be differentiated by NMR. Kobayashi and co-workers demonstrated that heterocages can be formed as kinetic products, whereas the thermodynamic products were always the homocages of ethynylpyridine and benzonitrile.[8] The driving force of the self-assembly was the higher coordination ability of the ethynylpyridine ligand. The homocage composed by two identical tetraethynylpyridine cavitand was the thermodynamically favored product. However, in our system all isomeric cages require the formation of the same set of coordinative bonds, namely two EtPy − Pt and six CNPh − Pt bonds. There is no energy gain in binding two ethynylpyridines to the same metal center, as opposed to bind them to two different Pt complexes. Therefore the three possible structures are energetically

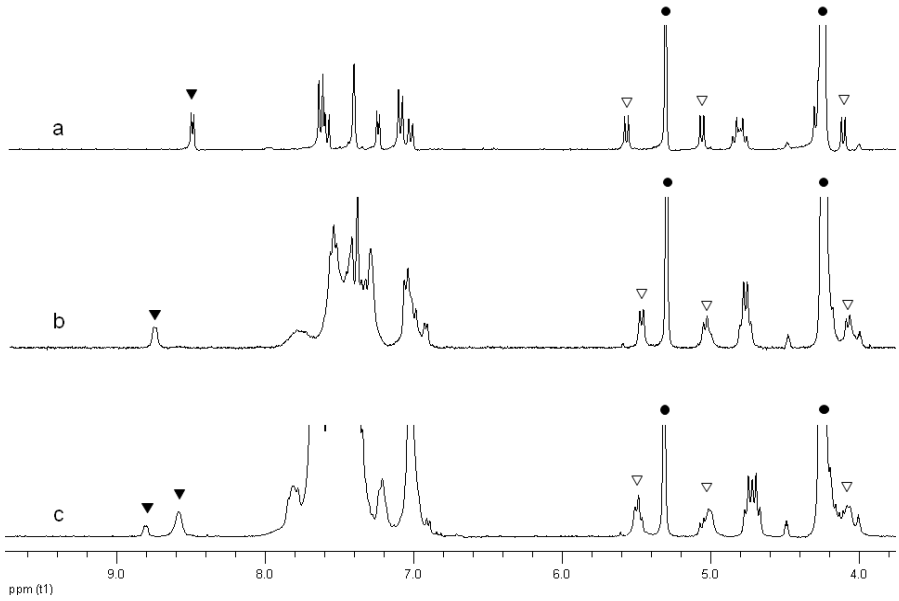

Figure 7. ^{1}H NMR (300 MHz, 400 µL CD_2Cl_2 and 100 µL CD_3NO_2) spectra of (a) 5 mM cavitand **1**, (b) 5 mM cavitand **1** and 0.5 eq. Pd(dppp)OTf_2, (c) 5 mM cavitand **1** and 2 eq. Pd(dppp)OTf_2, (d) 5 mM cavitand **1** and 2 eq. Pd(dppp)OTf_2 after 48 hours ▲ ethynylpyridine α-H protons, ▽H_{in} and H_{out} methylene bridges protons, ● residual solvent peaks.

equivalent, as demonstrated by the 3:1 observed **8b-c**:**8a** ratio.

The same protocol was utilized for the formation of Pd cages **9a-c** starting from Pd(dppp)OTf_2. Just as with the Pt cages, when 0.5 equivalents of Pd(dppp)OTf_2 were added to a 5 mM solution of cavitand **1** in CD_2Cl_2/CD_3NO_2 hemicage **7** was formed. Due to its higher coordination ability, ethynylpyridine sequestrated the whole amount of metal complex added and led to the exclusive formation of **7**. The ^{1}H NMR spectrum showed the characteristic downfield shift of the peak corresponding to the α-H of the ethynylpyridine ($\Delta\delta = \delta_{cage} - \delta_{free\ cavitand}$ = 0.26 ppm, from 8.51 to 8.77 ppm). In addition, the H_{in} and H_{out} signals of the methylene bridges adjacent to the ethynylpyridine shifted upfield from 5.59 to 5.49 ppm and from 4.12 to 4.09 ppm (Figure 7). The ^{31}P NMR signal shifted upfield from 17.26 to 6.14 ppm ($\Delta\delta = \delta_{hemicage} - \delta_{free\ Pd\ metal\ complex}$ = 11.12 ppm).

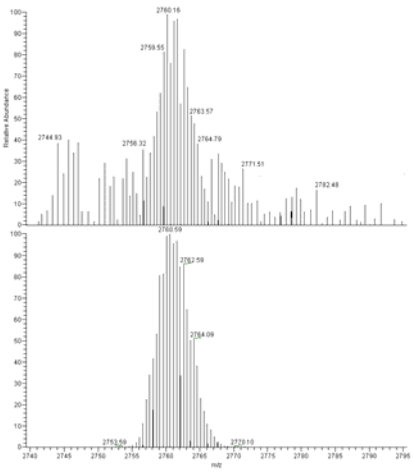

Figure 8 Selected region of the experimental (top) and calculated (bottom) ESI MS spectrum of CD_2Cl_2/CD_3NO_2 solution of cage **9** showing $[M - 2CF_3SO_3]^{2+}$ signal at *m/z* 2760.1.

After the addition of 1.5 further equivalents of metal complex, two signals for the α-H of the ethynylpyridine were observed at 8.81 and 8.59 ppm, as was the splitting of the H_{in} and H_{out} signals of the methylene bridges. The intensity of the two signals reached a ratio of 1:3 after ca. 48 hours (Figure 7c). Two of the six ^{31}P signals showed the $^2J_{P-P}$= 25 Hz, which is characteristic for the desymmetrization of the dppp signal in EtPy – CNPh systems. The diagnostic M^{2+} ion of coordination cages was observed via ESI MS at 2760.2 *m/z* (Figure 8). The whole trend is identical to the previous case. The different coordination

ability of the ligands in **1** could only be exploited for the first step of the self-assembly protocol, leading to homocages **6** and **7**. Further addition of the same metal led to ligand scrambling during subsequent cage closure, regardless of the metal used. We can conclude that, in itself, the presence of different ligands at the upper rim of the cavitand is not sufficient to drive self-assembly toward the formation of a single molecular cage. Therefore, an additional strategy was devised, involving two different metal centers, to obtain selectively a single cage.

3.2.3 Stepwise self-assembly of heteronuclear cage 10.

Addition of 1.5 equivalents of Pd(dppp)OTf_2 to a solution of Pt-hemicage **6** led to the exclusive formation of the heterocage **10**. Only one signal for the α-H protons of ethynylpyridine groups and two signals for H_{in} and H_{out} respectively

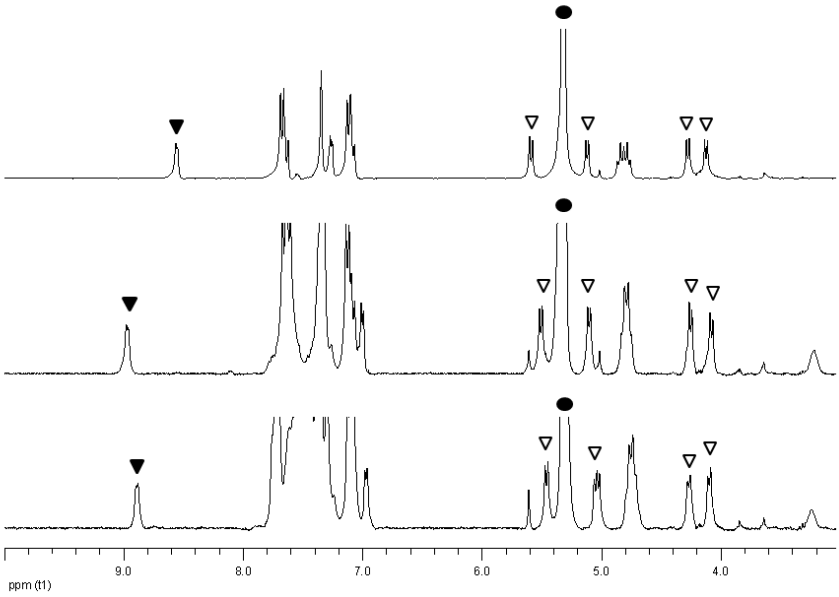

Figure 9 Stepwise approach: ^{1}H NMR (300 MHz, 500 µL CD_2Cl_2) spectra of (a) 5 mM cavitand **1**, (b) 5 mM cavitand **1** and 0.5 eq. Pt(dppp)OTf_2, (c) 5 mM cavitand **1** and 0.5 of Pt(dppp)OTf_2 and 1.5 eq. of Pd(dppp)OTf_2, ▼ethynylpyridine α-H protons, ▽H_{in} and H_{out} methylene bridges protons, ● residual solvent peaks.

were observed in the ^{1}H NMR spectrum.(Figure 9)

Moreover, α-H protons of the ethynylpyridine and H_{in} signals were shifted slightly upfield with respect to hemicage **6** due to the complete closure of the cage ($\Delta\delta = \delta_{cage} - \delta_{hemicage} = 0.11$ ppm from 8.98 to 8.89 ppm for ethynylpyridine group and $\Delta\delta = \delta_{cage} - \delta_{emicage} = 0.05$ ppm for H_{in}). ^{31}P NMR exhibited three peaks at – 15.48 (EtPy − Pt − PyEt), 11.82 (PhCN − Pd − CNPh), and 15.36 ppm (PhCN − Pd − CNPh) in a 1:2:1 ratio, consistent with the structure of **10**. The presence of the M^{2+} ion in the ESI MS at *m/z* = 2803.5 confirmed the formation of the heteronuclear cage. The absence of the M^{2+} ions corresponding to **8** and **9** excluded their presence in solution

3.2.4 One-Pot self-assembly of heteronuclear cage 10. The thermodynamic versus kinetic stability of cage **10** was determined by using a one pot procedure. Cavitand **1** was reacted with a mixture of Pd(dppp)OTf_2 and Pt(dppp)OTf_2 in a 3:1 ratio in the standard CD_2Cl_2/CD_3NO_2 solution. Initially,

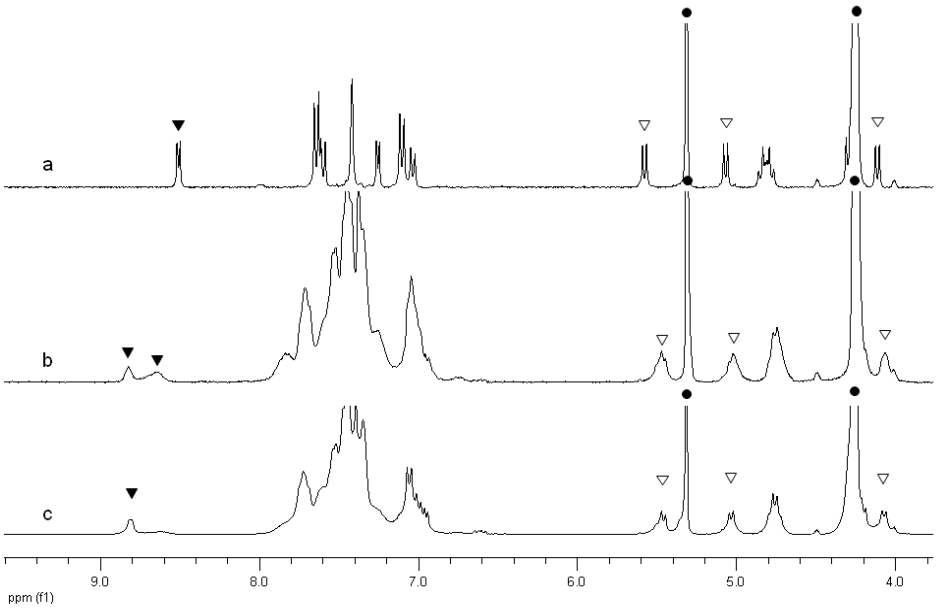

Figure 10. ^{1}H NMR (300 MHz, 400 µL CD_2Cl_2 and 100 µL CD_3NO_2) spectra of (a) 5 mM cavitand **1**, (b) 5 mM cavitand **1**, 0.5 eq. Pt(dppp)OTf_2, and 1.5 eq. Pd(dppp)OTf_2, (c) 5 mM cavitand **1**, 0.5 eq. Pt(dppp)OTf_2, and 1.5 eq. Pd(dppp)OTf_2 after one week. ▲ethynylpyridine α-H protons, ▽ H_{in} and H_{out} methylene bridges protons. ● residual solvent peaks

two peaks corresponding to the α-H protons of the ethynylpyridine appeared at 8.82 and 8.64 ppm, as did broad signals corresponding to H_{in} and H_{out}, suggesting the formation of a mixture of different cages (Figure 10b). Whithin

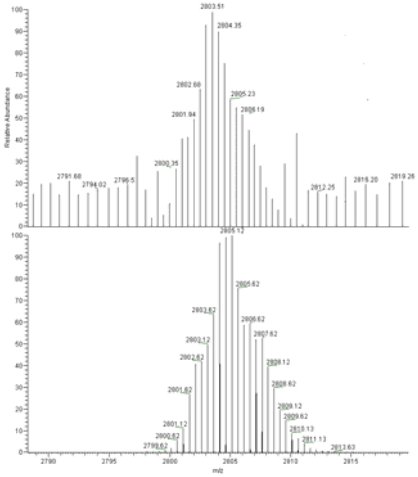

Figure 11. Selected region of the experimental (top) and calculated (bottom) ESI MS spectrum of CD_2Cl_2/CD_3NO_2 solution of cage **10** showing $[M - 2CF_3SO_3]^{2+}$ signal at *m/z* 2803.5.

several hours, however the two ethynylpyridine signals merged into a single peak at 8.82 ppm, and the broad H_{in} and H_{out} signals evolved into four doublets at 5.47, 5.05, 4.22 (partially obscured by residual nitromethane solvent signal), and 4.08 ppm. The ^1H NMR spectrum remained unchanged after one week (Figure 10c). These results indicate the initial formation of several isomeric cages (kinetic products), which interconvert into cage **10** (the thermodynamic product) over time. ^1H and ^{31}P NMR confirmed a complete transformation of the isomeric cages into structure **10**.

3.2.5 Concentration dependence

Titrations with $Pt(dppp)OTf_2$ were carried out at several concentrations in order to determine if this is an issue that could affect the formation of cages in solution. We took into consideration three concentrations:

- 2.5 mM,
- 5 mM (experiments already shown)
- 8 mM.

We observed that, at the very beginning, just after the addition of metal complex, the concentration influenced the formation of cages. Infact, in the less concentrated (2.5 mM) solution the predominant peak corresponding to the orto pyridine proton was due to Py-Pt-PhCN interaction at 8.69 ppm and the ratio between this and Py-Pt-Py was about 10:1, meaning that we mostly obtained the isomeric cages and a very tiny amount of cage having Py-Pt-Py interaction (Figure 12b). In the most concentrated one we observed the peak relative to Py-Pt-Py interaction and a very small peak that could be considered like an impurity, corresponding to the three isomeric cages (Figure 12a). In this case there was also the presence of very sharp peaks relative to H_{in} and H_{out} and the symmetry of the species in solution was the same as the starting cavitand.

After 48 hours we checked again the solution and we observed that new peaks appeared. In the case of the diluted solution the ratio between the two peaks turned into 1:3 as shown before for other experiments, and in the 8 mM solution a new peak at 8.69 ppm corresponding to Py-Pt-PhCN appeared; the

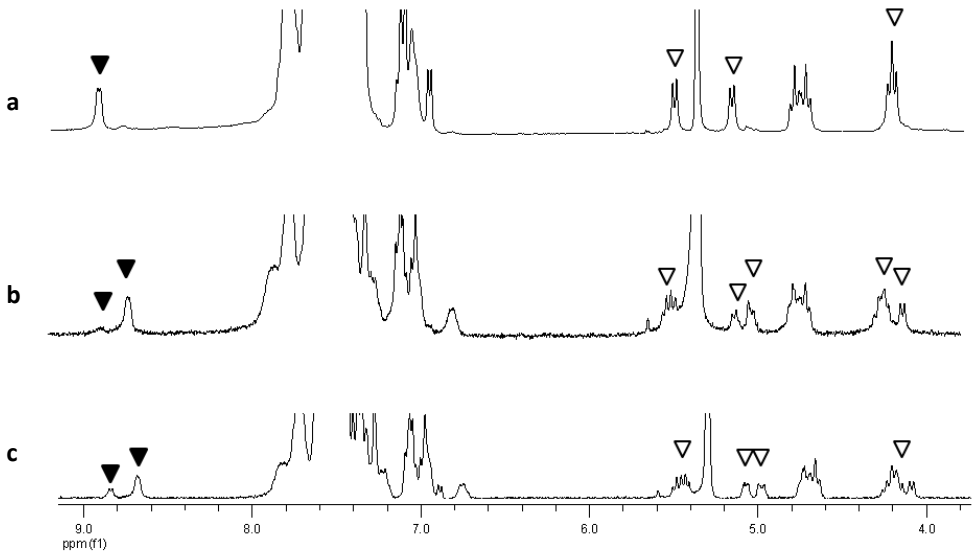

Figure 12 ^{1}H NMR (300 MHz, 400 µL CD_2Cl_2) spectra of (a) 8 mM solution of cavitand **1**, and 2 eq. Pt(dppp)OTf_2, (b) 2.5 mM solution of cavitand **1** and 2 eq. Pt(dppp)OTf_2, (c) cavitand **1** and 2eq. of Pt(dppp)OTf_2, after 48 hours. ▼ethynylpyridine α-H protons, ▽ H_{in} and H_{out}

relative intensity is 1:3 as previously reported (Figure 12c).

These results are the confirmation that the thermodynamic product is a mixture of both species due to the fact that there is no energy gain in binding respectively two ethynylpyridines and two benzonitriles.

3.2.6 New approach

Taking into consideration provious result, a cavitand having three ethynylpyridines and one benzonitrile (Figure 13), inserted at the apical positions, was synthesized. Synthesis of cavitand **12** was carried out reacting tetraiodocavitand **4** with an appropriate amount of boronic acid in order to obtain the monosostituted product **11**.

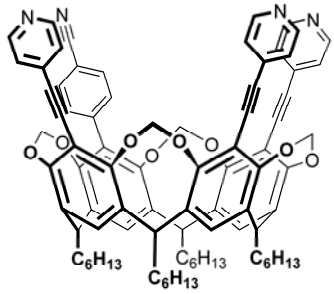

Figure 13 Structure of cavitand **12**

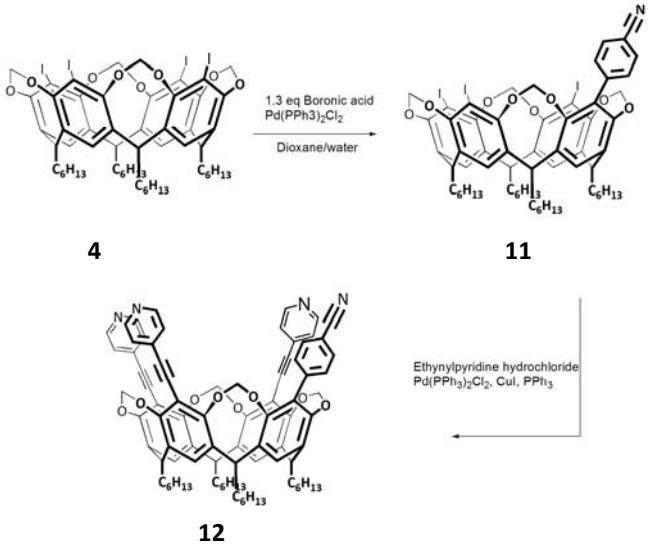

4 **11**

12

Scheme 6. Synthesis of tetradentate cavitand

This was subjected to a Suzuki coupling in order to obtain the final cavitand **12.** (Scheme 6). This possesses the same geometric properties as the one previously shown, same length and same orientation respect to the cavitand scaffold; although, the presence of three ethynylpyridines could affect its complexation ability.

The purpose was to observe if, also in the presence of more than one ethynylpyridine unit, the interaction with Pt complex led to several species in solution or to a one well define cage. In particular what we wanted to obtained was the selective formation of cages **13**

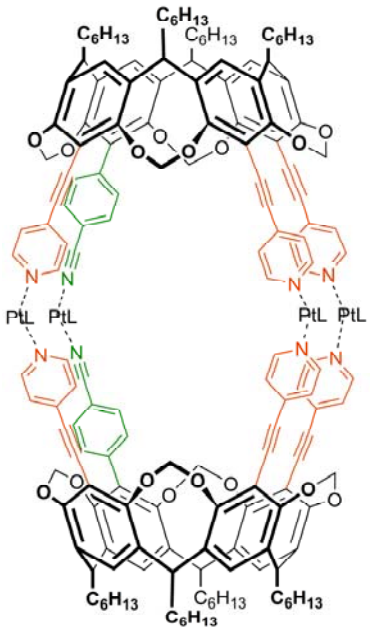

Figure 14 Structure of cages **13**

3.2.7 Self-assembly of homonuclear cage 13

To a solution 5 mM of cavitand **12** in CD_2Cl_2 2 equivalents of Pt(dppp)OTf_2 were added, we observed a low field shift of ethynylpyridines H_α from 8.55 ppm to 8.98 and 8.90 ppm; the presence of two distinct signals of pyridine, in this case, is due to the asymmetry of the cavitand. H_{in} and H_{out} corresponding to methylene bridges shifted from 6.04 to 5.98 ppm, from 5.51 to 5.42 ppm, from 4.45 to 4.28 and from 4.27 to 4.05 ppm; unfortunately it was possible to

observe very small doublets close to each one of these suggesting the presence of another species in solution. ^{31}P NMR confirmed it, we could observed two peaks corresponding to Py-Pt-Py interaction at -15 and 14.9ppm, at -5 the one corresponding to PhCN-Pt-PhCN interaction and also a smaller one due to Py-Pt-PhCN.

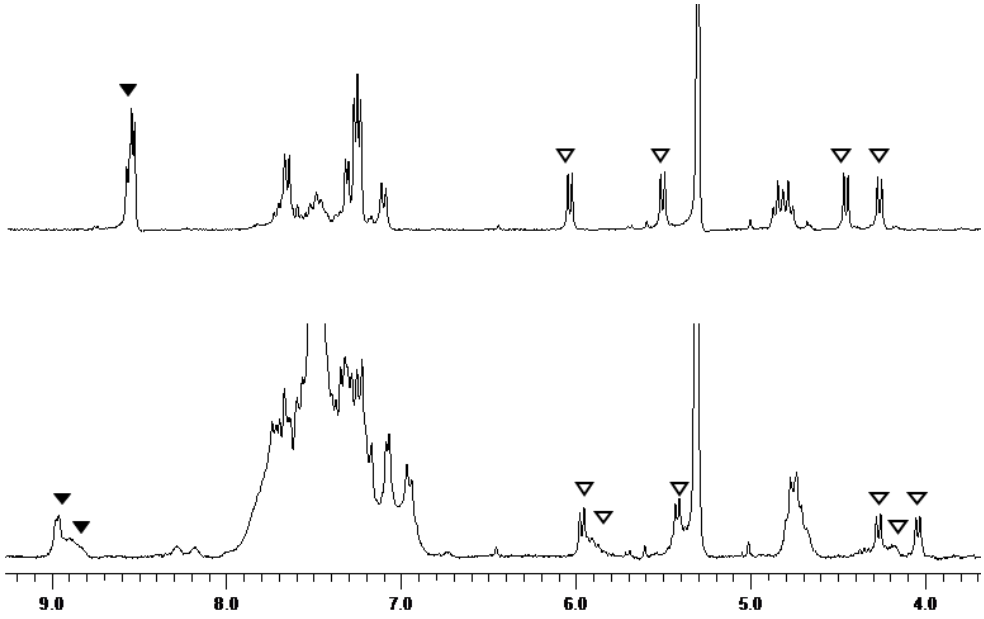

Figure 13. ^{1}H NMR (300 MHz, 400 µL CD_2Cl_2) spectra of (a) 5 mM cavitand **12**, (b) cavitand **12** and 2 eq. Pt(dppp)OTf_2, ▼ ethynylpyridine α-H protons, ▽ H_{in} and H_{out} methylene

Also in the case, we obtained more than one cage in solution; the presence of three ethynylpyridines is not sufficient to interact with Pt(dppp)OTf_2 giving selectively one cage.

3.3 Conclusion

The exclusive formation of heteronuclear coordination cage **10** demonstrates the versatility of this type of self-assembly procedure. The design of the appropriate tetradentate cavitand ligand is the key element in driving the self-assembly toward the formation of the desired product. In the specific case of the heteronuclear coordination cages reported here, it is crucial to

differentiate the type, number, and position of the ligands, to reach the correct metal/ligand cross reactivity. A single ligand substitution with respect to the parent tetrabenzonitrile cavitand[10] is sufficient to shift completely the outcome of the self-assembly protocol from homonuclear to heteronuclear cage. For the same reason, cavitand **1** is unfit for homocage self-assembly, as it leads to the formation of a set of isomeric cages. Efforts to extend this strategy to the self-assembly of large cage networks[16] are underway.

3.4 Experimental

General

Reagents and solvents were purchased as reagent grade and used without further purification. Analytical TLC was performed on Merck silica gel 60 F254 precoated plates. Column chromatography was performed using silica gel (Merck 70 − 230 mesh). ^{1}H NMR spectra were recorded at 300 MHz on a Bruker AC 300 Avance spectrometer with solvent peaks as reference..^{31}P NMR spectra were recorded at 162 MHz, on a Bruker 400 spectrometer. ESI MS spectra were measured on a Helwett-Packard 3395 Waters 74 spectrometer.

Tetraiodo-resorcinarene (3) To a solution of 0.496 g of resorcinarene **1** (6.02×10^{-4} mol) in a 1:1 mixture of water and diethyl ether (16 mL), 0.202 g of $NaHCO_3$ (2.41×10^{-4} mol) and 0.614 g of I_2 (2.41×10^{-4} mol) were added. The solution was stirred overnight at room temperature. Following Buchner filtration, the precipitate was washed with cold ethanol. The pure product was collected as white solid. (Yield 36%). **^{1}H NMR** (acetone d_6, 300 MHz) δ = 8.16 (s, 8H, ArO**H**), 7.65 (s, 4H, Ar**H**), 4.43 (t, 4H, ArC**H,** J = 8.6 Hz), 2.29 (m, 8H, ArCHC**H$_2$**), 1.24 (m, 32H, $CH_2C\mathbf{H_2}C\mathbf{H_2}C\mathbf{H_2}C\mathbf{H_2}CH_3$), 0.85 (t, 12H, $CH_2C\mathbf{H_3}$, J = 7.4 Hz); **ESI MS** (*m/z*): 1327 $[M]^-$ [M = $C_{52}H_{68}I_4O_8$].

Tetraiodo-cavitand (4) 0.593 g of **1** (4.46×10^{-4} mol) were dissolved in dry DMF (8 mL) in a dry Schlenk tube. To the solution were added 1.208 mL of CH_2ClBr (1.78×10^{-2} mol) and 0.493 g of K_2CO_3 (3.57×10^{-3} mol). The mixture was stirred at 85°C for 3 hours. After neutralization with HCl 2 %, a precipitate formed; foolowing Buchner filtration, the resulting solid was the pure product. (Yield 88%).**^{1}H NMR** ($CDCl_3$, 300 MHz) δ = 7.05 (s ,4H, Ar**H**), 5.96 (d, 4H, $OCH_{in}\mathbf{H_{out}}O$, J_2 = 8.2 Hz), 4.84 (t, 4H, ArC**H**, J = 9.0 Hz), 4.30 (d, 4H, $OCH_{in}\mathbf{H_{out}}O$, J_2 = 8.3 Hz), 2.18 (m, 8H, ArCHC**H$_2$**), 1.31 (m, 32H, $CH_2C\mathbf{H_2}C\mathbf{H_2}C\mathbf{H_2}C\mathbf{H_2}CH_3$), 0.89 (t, 12H, $CH_2C\mathbf{H_3}$, J = 7.4 Hz); **ESI MS** (*m/z*): 1399 $[M + Na]^+$ [M = $C_{56}H_{68}I_4O_8$].

Monobenzonitrile cavitand (11) To a solution of 0.100 g of **4** (7.26×10^{-5} mol) in 10 mL of dioxane 0.0157 g of $Pd(PPh_3)_2Cl_2$ (2.24×10^{-5} mol), 0.028 g of 4-(cyanophenyl)boronic acid pinacol ester, (9.43×10^{-5} mol), 0.057 of $AsPh_3$ (1.86×10^{-4} mol), and 0.4748 g of Cs_2CO_3 previously dissolved in 0.25 mL of water, were added. The mixture was stirred under Argon for 40 hours at 110°C. The solution was cooled at room temperature and concentrated under vacuum. The pure product was obtained by purification with silica gel cromatography with hexane and CH_2Cl_2 (25:75). **^{1}H NMR** ($CDCl_3$, 300 MHz) δ =7.22 (d, 2H, NCAr**H$_o$,** J = 8.1 Hz), 7.15 (d, 2H, NCAr**H$_m$**, J = 8.1 Hz), 7.11 (s, 4H, Ar**H**), 6.0 (d, 2H, OCH_{in}**H$_{out}$**O, J = 7.5 Hz), 5.50 (d,2H, OCH_{in}**H$_{out}$**O, J = 7.2), 4.90 **–** 4.77 (m, 4H**,** ArC**H),** 4.26 (d, 4H, OC**H$_{in}$**H_{out}O J = 6.9 Hz), 2.18 (m, 8H, ArCHC**H$_2$**), 1.31 (m, 32H, CH_2C**H$_2$**C**H$_2$**C**H$_2$**C**H$_2$**CH_3), 0.89 (t, 12H, CH_2C**H$_3$**, J = 7.4 Hz); **ESI MS** (*m/z*)= 1222.6 $[M]^+$.

Monoethynylpyridine-cavitand (5) 10 mL of dry Et_3N were degassed in a dry flask for 30 minutes. 0.5 g of **1** (3.63×10^{-4} mol), 0.084 g of ethynylpyridinehydrochloride (6.25×10^{-4} mol), 0.0102 g of $Pd(PPh_3)_2Cl_2$ (1.45×10^{-5} mol), 0.0051 g of CuI (3.5×10^{-5} mol), and 0.0057 g of PPh_3 (2.2×10^{-5} mol) were added and the mixture was stirred for 1 hour at 60°C and for 48 hours at 90°C. After cooling to room temperature, $CHCl_3$ was added and the crude product was washed with water and extracted with $CHCl_3$. The pure product was obtained by purification with silica gel flash chromatography with CH_2Cl_2:AcOEt (95:5) as eluent. (35% yield). **^{1}H NMR ($CDCl_3$, 300 MHz)** δ = 8.60 (d, 2H, Py**H$_o$,** J = 5.7 Hz), 7.30 (d, 2H, Py**H$_m$**, J = 6.6 Hz), 7.11 (s, 1H, Ar**H**), 7.08 (s, 1H, Ar**H**), 7.06 (s, 1H, Ar**H**), 5.95 (m, 4H, OCH_{in}**H$_{out}$**O), 4.84 (m, 4H, ArC**H**), 4.48 (d, 2H, O**CH$_{in}$**H_{out}O, J_2 = 8.1 Hz), 4.29 (d, 2H, O**CH$_{in}$**H_{out}O, J_2 = 8.2 Hz), 2.21 (m, 8H, ArCHC**H$_2$**), 1.28 (m, 40H, CH_2C**H$_2$**C**H$_2$**C**H$_2$**C**H$_2$**CH_3), 0.88 (t, 12H, CH_2C**H$_3$**, J = 7.2 Hz); **ESI-MS** (*m/z*): 1352.7 $[MH]^+$ [M = $C_{63}H_{72}I_3NO_8$].

Monoethynylpyridine-tribenzonitrile cavitand (1) To a solution of 0.1088 g of **5** (7.45×10^{-5} mol) in 10 mL of dioxane 0.0157 g of $Pd(PPh_3)_2Cl_2$ (2.24×10^{-5} mol), 0.208 g of 4-(cyanophenyl)boronic acid pinacol ester, (9.07×10^{-4} mol), 0.057 of $AsPh_3$ (1.86×10^{-4} mol), and 0.475 g of Cs_2CO_3 previously dissolved in 0.25 ml of water, were added. The mixture was stirred under Argon for 40 hours at 110°C. The solution was cooled at room temperature and concentrated under vacuum. Cavitand **1** was obtained as white solid by precipitation with diethyether in 36% yield. **^{1}H NMR** ($CDCl_3$, 300 MHz) δ = 8.55 (d, 2H, Py**H$_o$,** J = 5.5 Hz), 7.65 (d, 4H, NCAr**H$_o$,** J = 9.1 Hz), 7.59 (d, 2H, NCAr**H$_o$**, J = 9.1 Hz), 7.29 (s, 4H, Ar**H**), 7.21 (d, 2H, Py**H$_m$,** J = 6.4 Hz), 7.15 (d, 4H, NCAr**H$_m$**, J = 9.1 Hz), 7.09 (d, 2H, NCAr**H$_m$**, J = 9.2 Hz), 5.60 (d, 2H, OCH_{in}**H$_{out}$**O, J_2 = 7.8 Hz),

5.17 (d, 2H, $OCH_{in}\mathbf{H_{out}}O$, J_2 = 7.7 Hz), 4.80 (m, 4H, ArC**H**), 4.38 (d, 2H, $OC\mathbf{H_{in}}H_{out}O$, J_2 = 7.8 Hz), 4.15 (d, 2H, $OC\mathbf{H_{in}}H_{out}O$, J_2 = 7.7 Hz), 2.30 (m, 8H, ArCHC$\mathbf{H_2}$), 1.22 (m, 32H, $CH_2C\mathbf{H_2}C\mathbf{H_2}C\mathbf{H_2}C\mathbf{H_2}CH_3$), 0.90 (t, 12H, $CH_2C\mathbf{H_3}$, J=7.3 Hz); **ESI MS** (*m/z*): 1278.6 $[MH]^+$, [M = $C_{84}H_{84}N_4O_8$].

Triethynylpyridine-monobenzonitrile cavitand (12) 30 mL of dry Et_3N were degassed in a dry flask for 30 minutes. 0.3 g of **11** (2.22×10^{-4} mol), 0.309 g of ethynylpyridinehydrochloride (2.22×10^{-3} mol), 0.062 g of $Pd(PPh_3)_2Cl_2$ (1.32×10^{-5} mol), 0.0051 g of CuI (1.1×10^{-5} mol), and 0.0057 g of PPh_3 (2.2×10^{-5} mol) were added and the mixture was stirred for 1 hour at 60°C and for 48 hours at 90°C. After cooling to room temperature, $CHCl_3$ was added and the crude product was washed with water and extracted with $CHCl_3$. The pure product was obtained by purification with silica gel flash chromatography with CH_2Cl_2: Ethyl acetate(6:4) **^{1}H NMR** ($CDCl_3$, 300 MHz) δ =8.56 (d, 6H, Py$\mathbf{H_o}$, J = 5.5 Hz), 7.67 (d, 2H, NCAr$\mathbf{H_o}$, J = 8.1 Hz), 7.34 (d, 2H, , Py$\mathbf{H_m}$, J = 5.7 Hz), 7.30 (d, 4H, , Py$\mathbf{H_m}$ J = 5.7 Hz), 7.25 (s, 4H, Ar**H**), 7.11 (d, 2H, NCAr$\mathbf{H_m}$, J = 9.2 Hz), 6.04 (d, 2H, $OCH_{in}\mathbf{H_{out}}O$, J_2 = 7.2 Hz), 5.51 (d, 2H, $OCH_{in}\mathbf{H_{out}}O$, J_2 = 7.2 Hz), 4.80 (m, 4H, ArC**H**), 4.46 (d, 2H, $OC\mathbf{H_{in}}H_{out}O$, J_2 = 7.2 Hz), 4.27 (d, 2H, $OC\mathbf{H_{in}}H_{out}O$, J_2 = 7.2 Hz), 2.30 (m, 8H, ArCHC$\mathbf{H_2}$), 1.22 (m, 32H, $CH_2C\mathbf{H_2}C\mathbf{H_2}C\mathbf{H_2}C\mathbf{H_2}CH_3$), 0.90 (t, 12H, $CH_2C\mathbf{H_3}$, J=7.3 Hz); **ESI MS** (*m/z*): 1222.5 $[MH]^+$, [M = $C_{84}H_{84}N_4O_8$].

Stepwise self-assembly of Pt hemicage (6) and Pt cage (8) To a solution of 3.2 mg of **1** (5.0×10^{-3} M) in CD_2Cl_2 (0.4 mL) and CD_3NO_2 (0.1 mL) in the NMR tube 1.1 mg of $Pt(dppp)OTf_2$ were added to give hemicage **6** and ^{1}H NMR and ^{31}P NMR spectra were recorded. **^{1}H NMR (CD_2Cl_2 + CD_3NO_2, 300 MHz)**: δ = 8.82 (d, 4H, Py$\mathbf{H_o}$), 7.76 – 6.98 (m, 48H, P$\mathbf{Ph_2}$ + NCAr$\mathbf{H_o}$ + Py$\mathbf{H_m}$ + NCAr$\mathbf{H_m}$), 5.50 − 5.48 (d, 4H, $OCH_{in}\mathbf{H_{out}}O$), 5.08− 5.06 (d, 4H, $OCH_{in}\mathbf{H_{out}}O$), 4.80 − 4.78 (m, 8H, ArC**H**), 4.21 − 4.19 (d, 4H, $OC\mathbf{H_{in}}H_{out}O$ partially under residual solvent peak), 4.11 − 4.08 (d, 4H, $OC\mathbf{H_{in}}H_{out}O$), 2.29 (m, 16H, ArCHC$\mathbf{H_2}$), 1.29 (m, 64H, $CH_2\mathbf{CH_2CH_2CH_2CH_2}CH_3$) 0.90 (bt, 24H, $CH_2\mathbf{CH_3}$) **^{31}P NMR (CD_2Cl_2 + CD_3NO_2, 162 MHz)**: −15.60 ppm (J_{P-Pt} = 3033 Hz). An additional 3.4 mg of $Pt(dppp)OTf_2$ were added to same solution and ^{1}H NMR and ^{31}P NMR spectra were recorded again. **^{1}H NMR (CD_2Cl_2 + CD_3NO_2, 300 MHz):** δ = 8.81 (d, 4H, Py$\mathbf{H_o}$), 8.61 (d, 12H , Py$\mathbf{H_o}$), 7.82 − 6.98 (m, 416H, P$\mathbf{Ph_2}$ + NCAr$\mathbf{H_m}$ + NCAr$\mathbf{H_o}$), 6.93 − 6.91 (d, 4H, Py$\mathbf{H_m}$), 6.74 − 6.71 (d, 12H, Py$\mathbf{H_m}$), 5.55 − 5.42 (m, 16H, $OCH_{in}\mathbf{H_{out}}O$), 5.09 − 5.07 (d,8H, $OCH_{in}\mathbf{H_{out}}O$), 4.99 − 4.96 (d,8H, $OCH_{in}H_{out}O$), 4.75 − 4.65 (m, 32H, ArCH), 4.26 − 4.22 (m, 16H, $OCH_{in}H_{out}O$), 4.25 − 4.20 (d, 8H, $OC\mathbf{H_{in}}H_{out}O$ partially under residual solvent peak) 4.20 − 4.16 (d, 16H, $OC\mathbf{H_{in}}H_{out}O$), 2.90 (m, 64H, dppp), 2.75 (m, 32H, dppp) 2.29 (m, 64H, ArCH$\mathbf{CH_2}$), 1.29 (m, 256H, $CH_2\mathbf{CH_2CH_2CH_2CH_2}CH_3$) 0.90 (bt, 96H, $CH_2\mathbf{CH_3}$); **^{31}P NMR (CD_2Cl_2 + CD_3NO_2, 162 MHz)**: −15.60, −10.02 (J_{P-Pt} = 3444 Hz).

ESI MS (*m/z*): 2938.2 $[(M - 2OTf)]^{2+}$, [M = C_{284} $H_{272}F_{24}N_8O_{40}P_8Pt_4S_8$].

Stepwise self-assembly of Pd hemicage (7) and Pd cage (9) To a solution of 3.1 mg of **1** (4.85×10^{-3} M) in CD_2Cl_2 (0.4 mL) and CD_3NO_2 (0.1 mL) in the NMR tube 1 mg of Pd(dppp)OTf_2 was added to give hemicage **7** and ^{1}H NMR and ^{31}P NMR spectra were recorded. **^{1}H NMR (CD_2Cl_2 + CD_3NO_2, 300 MHz)**: δ = 8.77 (d, 4H, Py**H$_o$**), 7.67 – 7.30 (m, 32H, P**Ph$_2$** + NCAr**H$_o$**), 7.08 − 7.00 (d, 12H, NCAr**H$_m$**), 7.94 − 6.93 (d, 4H, Py**H$_m$**), 5.49 − 5.47 (d, 4H, OCH_{in}**H$_{out}$**O), 5.06 − 5.04 (d, 4H, OCH_{in}**H$_{out}$**O), 4.81 − 4.75 (m, 8H, Ar**CH**), 4.22 − 4.19 (m, 4H, OC**H$_{in}$**H_{out}O, partially under residual solvent peak), 4.09 − 4.07 (d, 4H, OC**H$_{in}$**H_{out}O), 3.12 – 2.91 (dppp signals), 2.32 (m, 16H, ArCHC**H$_2$**), 1.29 (m, 64H, CH_2**$CH_2CH_2CH_2CH_2$**CH_3) 0.87 (bt, 24H, CH_2**CH_3**); **^{31}P NMR: (CD_2Cl_2 + CD_3NO_2, 162 MHz)**: δ = 6.14 ppm.

An additional 2.9 mg of Pd(dppp)OTf_2 were added to same solution and ^{1}H NMR and ^{31}P NMR spectra were recorded again**. ^{1}H NMR (CD_2Cl_2 + CD_3NO_2, 300 MHz)**: δ = 8.81 d, 4H, Py**H$_o$**), 8.59 (d, 12H, Py**H$_o$**), 7.84 − 6.89 (m, 432H, P**Ph$_2$** + NCAr**H$_m$** + NCAr**H$_o$** + Py**H$_m$**), 5.51 − 5.46 (m, 16H, OCH_{in}**H$_{out}$**O), 5.07 − 4.99 (d, 16H, OCH_{in}**H$_{out}$**O), 4.77 − 4.66 (m, 32H, ArC**H**), 4.19 − 4.07 (m, 32H, OC**H$_{in}$**H_{out}O partially under residual solvent peak), 2.90 − 2.75 (m, 3 signals of dppp), 2.29 (m, 64H, ArCHC**H$_2$**), 1.40 − 1.29 (m, 256H, CH_2**$CH_2CH_2CH_2CH_2$**CH_3), 0.87 (bt, 96H, CH_2CH_3); **^{31}P NMR** (CD_2Cl_2 + CD_3NO_2, 162 MHz**):** δ = 15.77, 12.41, 11,50 (d, $^2J_{P-P}$ = 25 Hz), 10.90 (d, $^2J_{P-P}$ = 25 Hz), 6.14, 4.91 ppm.

ESI MS (*m/z*): 2760.16 $[(M - 2OTf)]^{2+}$, [M = C_{284} $H_{272}F_{24}N_8O_{40}P_8Pd_4S_8$].

Self-assembly of heteronuclear cage (10)

a) Stepwise procedure: to a solution of 3.2 mg of **1** (5×10^{-3} M) in CD_2Cl_2 (0.5 mL) in the NMR tube 1.1 mg of Pt(dppp)OTf_2 were added to form Pt-hemicage **6**. 3 mg of Pd(dppp)OTf_2 were added to same solution and ^{1}H NMR and ^{31}P NMR spectra were recorded. **^{1}H NMR** (CD_2Cl_2, 300 MHz): δ = 8.89 (d, 4H, Py**Ho**), 7.73 – 7.30 (m, 92H, P**Ph$_2$** + NCAr**H$_o$**), 7.13 – 7.07 (d, 12H, NCAr**H$_m$**), 6.99 − 6.97 (d, 4H, Py**H$_m$**), 5.47 − 5.44 (d, 4H, OCH_{in}**H$_{out}$**O), 5.06 − 5.03(d, 4H, OCH_{in}**H$_{out}$**O), 4.80 − 4.72 (m, 8H, Ar**CH**), 4.28 − 4.26 (m, 4H, OC**H$_{in}$**H_{out}O), 4.10 − 4.08 (d, 4H, OC**H$_{in}$**H_{out}O), 3.24 (m, 8H, dppp), 2.90 (m, 8H, dppp) 2.30 (m, 24H, dppp + ArCHC**H$_2$**), 1.42 − 1.34 (m, 64H, CH_2C**H$_2$**C**H$_2$**C**H$_2$**CH_3) 0.93 (bt, 24H, CH_2C**H$_3$**); **^{31}P NMR** (CD_2Cl_2, 162 MHz): δ =15.36, 11.82, − 15.48 J_{P-Pt} = 3189 Hz)

b) One pot procedure: to a solution of 3.5 mg of **1** (5.4×10^{-3} M) in CD_2Cl_2 (0.4 mL) and CD_3NO_2 (0.1 mL) in the NMR tube 1.25 mg of Pt(dppp)OTf_2 and 3.3 mg of Pd(dppp)OTf_2 were added. ^{1}H NMR and ^{31}P NMR spectra were recorded. **^{1}H**

NMR (CD_2Cl_2 + CD_3NO_2, 300 MHz): δ = 8.82 (d, 4H, Py**H$_o$**), 7.72 – 7.25 (m, 92H, PPh_2 + NCAr**H$_o$**), 7.07 − 6.94 (m, 16H, Py**H$_m$** + NCAr**H$_m$**), 5.47 − 5.44 (d, 4H, OCH_{in}**H$_{out}$**O), 5.05 − 5.02 (d, 4H, OCH_{in}**H$_{out}$**O), 4.79 − 4.74 (m, 8H, ArC**H**), 4.22 − 4.18 (d, 4H, OC**H$_{in}$**H_{out}O partially under residual solvent peak), 4.08 − 4.06 (d, 4H, OC**H$_{in}$**H_{out}O), 3.23 − 2.83 (m, dppp) 2.30 (m, 16H, ArCHC**H$_2$**), 1.40 − 1.29 (m, 64H, $CH_2CH_2CH_2CH_2CH_2CH_3$), 0.87 (bt, 24H, CH_2**CH_3**); **^{31}P NMR** (CD_2Cl_2 + CD_3NO_2, 162 MHz): δ = 15.84, 12.35, − 15.07 J_{P-Pt} = 3075 Hz)

ESI MS (*m/z*): 2803.51 $[(M - 2OTf)]^{2+}$, [M = C_{284} $H_{272}F_{24}N_8O_{40}Pd_3P_8PtS_8$].

Self-assembly of homonuclear cage (13): to a solution of 3.6 mg of cavitand **12** in CD_2Cl_2 (0.4 mL) we added 2.6 mg of Pt(dppp)OTf_2(2.86×10^{-6} mol), ^{1}H NMR and ^{31}P NMR were recorded. **^{1}H NMR (CD_2Cl_2 300 MHz)**: δ = 8.97 **–** 8.81 (d, 12H, Py**H$_o$**), 7.84 **–** 6.94 (m, 108H, P**Ph$_2$** + NCAr**H$_o$** + Py**H$_m$** + NCAr**H$_m$** +Ar**H**), 5.98 − 5.95 (m, 4H, OCH_{in}**H$_{out}$**O), 5.43 − 5.40 (m, 4H, OC**H$_{in}$**H_{out}O), 4.80 − 4.65 (m, 8H, ArC**H**), 4.38 − 4.22 (d, 4H, OC**H$_{in}$**H_{out}O), 4.07 − 4.03 (m, 4H, OC**H$_{in}$**H_{out}O), 3.23 − 2.83 (m, dppp) 2.25 (m, 16H, ArCHC**H$_2$**), 1.40 − 1.29 (m, 64H, CH_2**$CH_2CH_2CH_2CH_2$**CH_3), 0.87 (bt, 24H, CH_2**CH_3**); **^{31}P NMR (CD_2Cl_2, 162 MHz)**: δ = −15 and −14.9, −5.

3.5 References

1. Pirondini, L.; Dalcanale, E. In *Modern Supramolecular Chemistry*, WILEY-VCH, Weinhem, Eds F. Diedrich, P. J. Stang, R. R. Tykwinski, Chapter 7, pp 233–276.
2. (a) Harrison, R. G.; Burrows, J. L.; Hansen, L. D. *Chem. Eur. J*. **2005**, *11*, 2881–2888; (b) Haino, T.; Kobayashi, M.; Fukazawa, Y. *Chem. Eur. J*. **2006**, *12*, 3310–3319.
3. (a) Caulder,D.L.; Powers, K.N.; Parac, T. N.; Raymond, K. N. *Angew. Chem. Int. Ed*. **1998**, *37*, 1840–1843; (b) Fochi, F.; Jacopozzi, P.; Wegelius, E.; Rissanen, K.; Cozzini, P.; Marastoni, E.; Fisicaro, E.; Manini, P.; Fokkens, R.; Dalcanale, E. *J. Am. Chem. Soc.* **2001**, *123*, 7539–7552; (c) Fujita, M.; Yoshizawa, M. In *Modern Supramolecular Chemistry*, WILEY-VCH, Weinhem, Eds F. Diedrich, P. J. Stang, R. R. Tykwinski, Chapter 8, pp 277–313.
4. (a) Chen, J.; Köner, S.; Craig, S. L.; Rudkevich, D. M.; Rebek, J. Jr. *Nature*, **2002**, *415*, 385–386; (b) Yoshizawa, M.; Sato, N.; Fujita, M. *Chem. Lett.* **2005**, *34*, 1392–1393.

5. Koblenz, T. S.; Dekker, H. L.; de Koster, C. G.; van Leeuwen, P. W. N. M.; Reek, J. N. H. *Chem*. *Commun*. **2006** 1700–1702.
6. Rudkevich, D. M. *Angew. Chem. Int. Ed.* **2004**, *43*, 558–571.
7. (a) Warmuth, R. *Eur. J. Org. Chem*. **2001**, 423–437; (b) Yoshizawa, M.; Kusukawa, T.; Fujita, M.; Yamaguchi, K. *J. Am. Chem. Soc.* **2000**, *122*, 6311–6312.
8. Yamanaka, M.; Yamada, Y.; Sei, Y.; Yamaguchi, K.; Kobayashi, K. *J. Am. Chem. Soc.* **2006**, *128*, 1531–1539.
9. For the self-assembly of heterocages on surfaces see: (a) Menozzi, E.; Pinalli, R.; Speets, E. A.; Ravoo, B. J.; Dalcanale, E.; Reinhoudt, D. N. *Chem. Eur. J*. **2004**, *10*, 2199–2206; (b) Busi, M.; Laurenti, M.; Condorelli, G. G.; Motta, A.; Favazza, M.; Fragalà, I. L.; Montalti, M.; Prodi, L.; Dalcanale, E. *Chem. Eur. J.* **2007**, *13*, 6891–6898.
10. Cuminetti, N.; Ebbing, M. H. K.; Prados, P.; de Mendoza, J.; Dalcanale, E. *Tetrahedron Letters* **2001**, *42*, 527–530.
11. Pinalli, R.; Cristini, V.; Sottili, V.; Geremia, S.; Campagnolo, M; Caneschi, A.; Dalcanale, E. *J. Am. Chem. Soc.* **2004**, *126*, 6516–6517.
12. Tunstad, L.M.; Tucker, J.A.; Dalcanale, E.; Weiser J.; Bryant, J.A.; Sherman, C. J.; Helgeson, R.C.; Knobler. C.B.; Cram, D. *J. Org. Chem*. **1989**, *54*, 1305–1312.
13. Tanaka, Y.; Sasada, A.; Fujita, Y. Procedings of *9th International Conference on Calixarene Chemistry* **2007** p 96
14. Román, E.; Peinador, C.; Mendoza, S.; Kaifer, A. E. *J. Org. Chem*. **1999**, *64*, 2577–2578.
15. Zuccaccia, D.; Pirondini, L.; Pinalli, R.; Dalcanale, E.; Macchioni, A. *J. Am. Chem. Soc.* **2005**, *127*, 7025–7032.
16. Menozzi, E.; Busi, M.; Massera, C.; Ugozzoli, F.; Zuccaccia, D.; Macchioni, A.; Dalcanale, E. *J. Org. Chem*. **2006**, 71, 2617–2624.

Rhenium based coordination cages

4

4.1 Introduction

The most fundamental definition of self-assembly is the spontaneous formation of higher order structures from simpler building blocks. This definition implies a thermodynamically driven process close to, or at, equilibrium. In contrast with the kinetics regime familiar to standard covalent syntheses, these conditions - where entropy-enthalpy compensation effects predominate – often yield discrete highly complex architectures.
The first method exploited in pursuit of this latter goal, involving self-assembly followed by covalent modification, has been pursued, amongst others, by the Stoddart and Sauvage groups[1], who have used this strategy to construct interlocked functional molecular architectures.

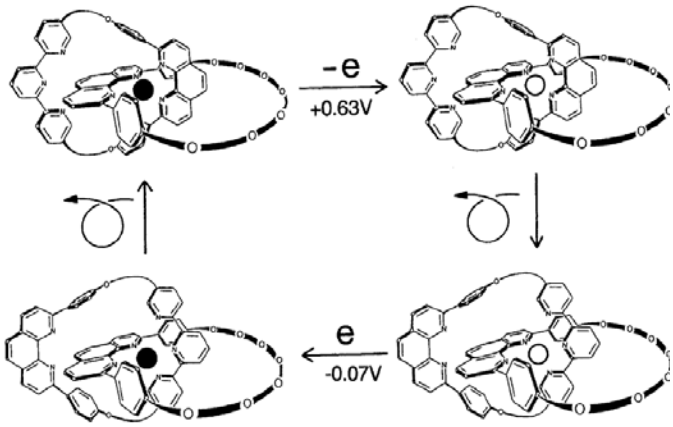

Figure 1 Example of molecular machines synthesized by Sauvage group

However, this method often requires judicious selection of specific reactions and very careful, not to say demanding, design of components that the biological molecular recognition of receptor-substrate complexes as well as in the final covalent steps. An emerging alternative strategy involves construction by self-assembly followed by whole-system switching into the kinetic regime, thus ‘‘locking’’ the resultant architecture into a structurally resilient entity.

Infact, in many cases is very advantageous to allow labile “building blocks” to assemble and then, when the target structure is formed, to “lock them” to create a kinetically stabile architecture that can be easily isolated and that can later be used as “building block” for more complex structures .[2]

The first example of intentional kinetic locking came from the work of Williams and co-workers[3] during their studies on helicate complexes; they found that by using relatively simple achiral ligands with more than one metal binding site, and various classically labile metal ion templates, the targeted assembly of both double and triple helicates could be realized.

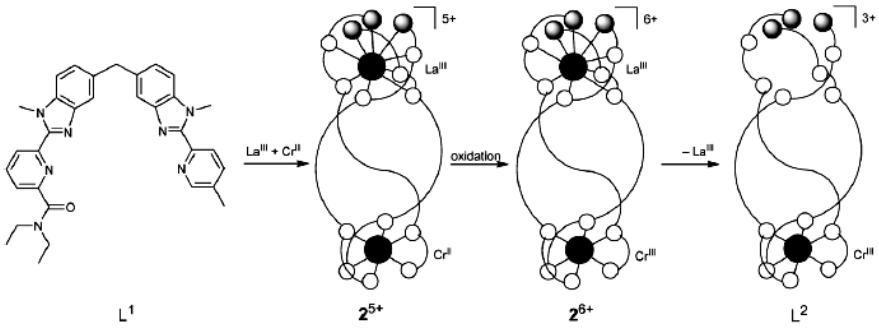

Figure 2 Synthesis of kinetically locked helicate L^2

This process resulted in racemic mixtures of both right- and left-handed helices. In 1994, a method for the separation of enantiomers of the triple helicates was described, using a well-known characteristic of cobalt coordination chemistry.

Another method to obtain kinetically stable structure is to use a metal that can give kinetically stable compounds at room temperature, like Rhenium. Re(I) is one of the most used metals in the formation of complex molecular architectures, despite the fact that, being a low-spin d^6 metal, is considered to

be a classic inert metal center. Hupp and colleagues studied, in particular, the complex $Re(CO)_5Cl$[4].

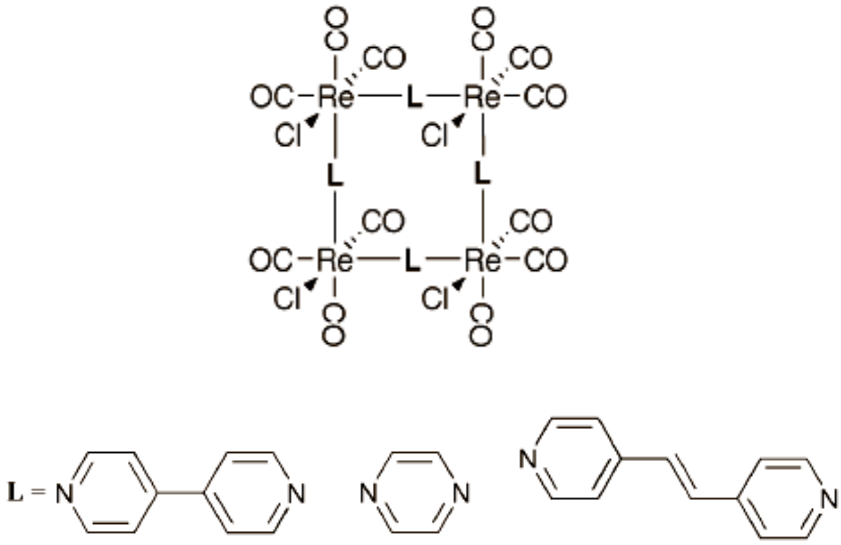

Figure 3 General scheme of Re(I) complexes

Unlike many other architectures, the metallomacrocycles assembled using these building blocks are neutral and, since they do not require any charge compensating anions that may block the central aperture, they are particularly suited to the construction of thin-films that have been used for molecular sieving and nano-filtration or for any kind of application where charged species are not desired. In order to create three dimensional molecular architectures the starting building block could be a kinetically "locked" metal complex with the required connective geometry or function obtained using Re(I).
This can be then reacted with another metal that is used as the templating "assembler" (Figure 4)[5].

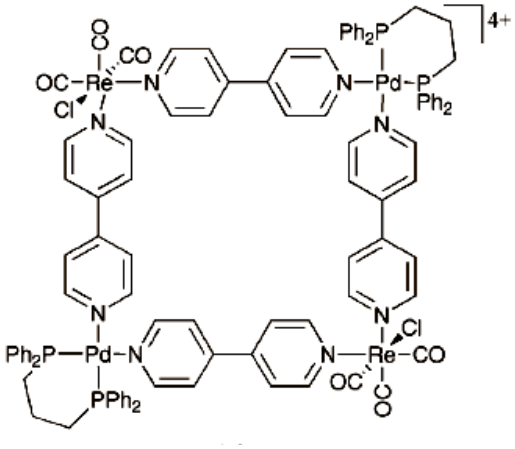

Figure 4 Example of the architecture obtained by using Re(I) as building block and a Pd complex as "templating assembler"

Cavitands could be used as ligands when they are decorated with pyridines moieties. An example of how Re(I) could be used with them was reported by Busi and Cantadori [6] where a cavitand possessing one phenylpyridine on the bridge was reacted with $Re(CO)_5Br$ in order to give a hemicage (Scheme 1a). The same approach was then extended to a cavitand having two pyridine moieties on the bridges in *AC* geometry to create a cage with very wide lateral portals (Scheme 1b). The presence of phosphonate bridges, that conferred complexation ability to the structure, didn't allow the addition of more than two pyridines due to a difficult purification step. The goal was to extend this procedure to cavitands having three and four pyridines in order to obtain a completely "closed cage"; to do that new cavitands had to be designed. The final aim were both the synthesis of cavitands as building blocks for more complex molecular architectures, as well as the synthesis of Rhenium cages possessing complexation ability for molecular recognition.

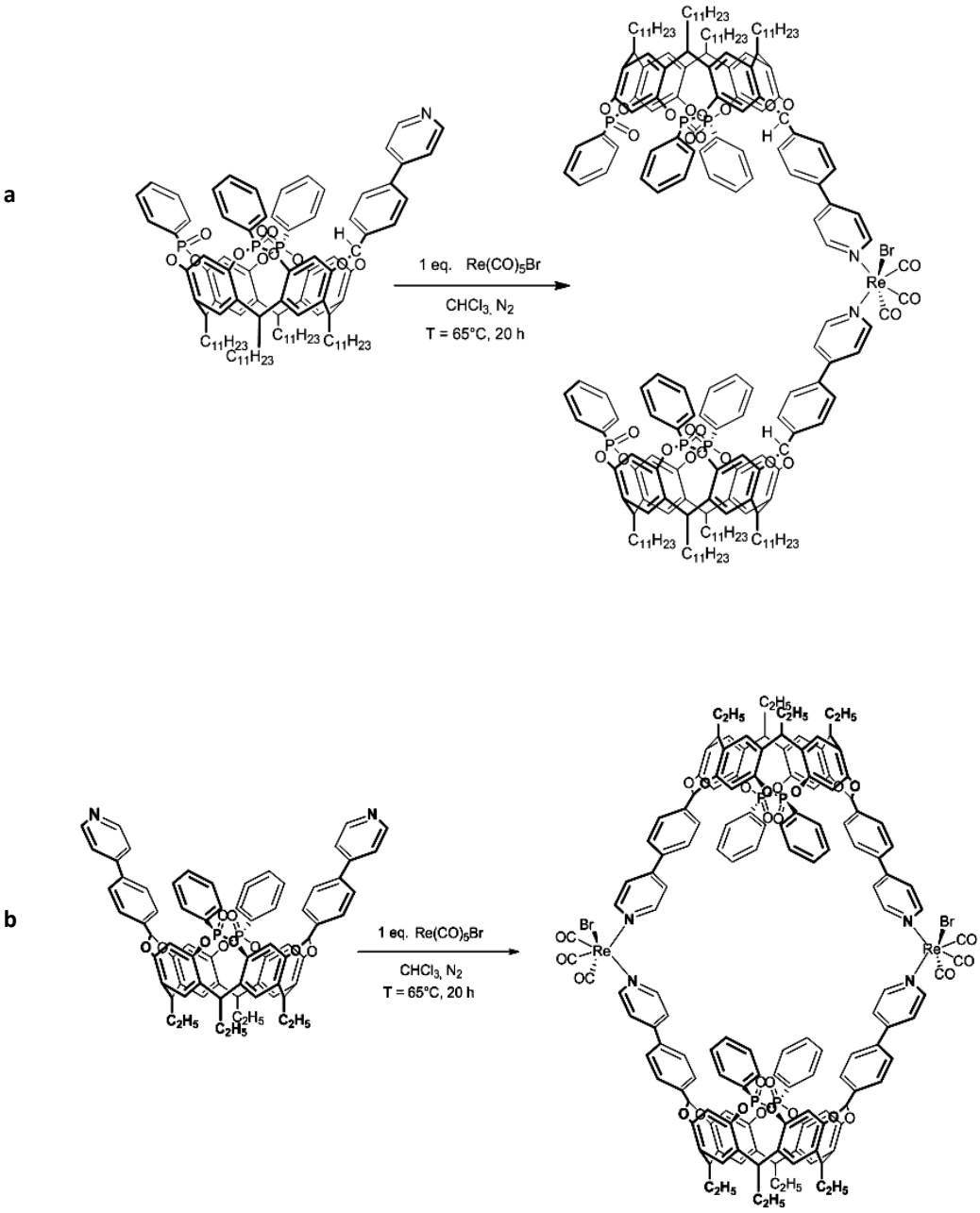

Scheme 1 Synthesis of Re hemicage **a**) and cage **b**) using cavitands having phenylpyridines groups on the bridges

4.2 Result and Discussion

The aim of the work reported in this chapter is to explore the coordination chemistry of pyridine cavitand ligands for the formation of kinetically stable Re-based coordination cages.$Re(CO)_5Br$ has been chosen as metal precursor because is one of the few octahedral complexes that undergoes *cis* ligand exchange exclusively, due to the remarkable trans effect of carbonyl ligands. Typically, nitrogen ligands replace two equatorial *cis*-CO units of $Re(CO)_5Br$ to give neutral *fac*-$Re(CO)_3L_2Br$. The other advantage in this approach is that, leaving the bridges free from complexation duties, we can to functionalize them in several ways according to our purpose.

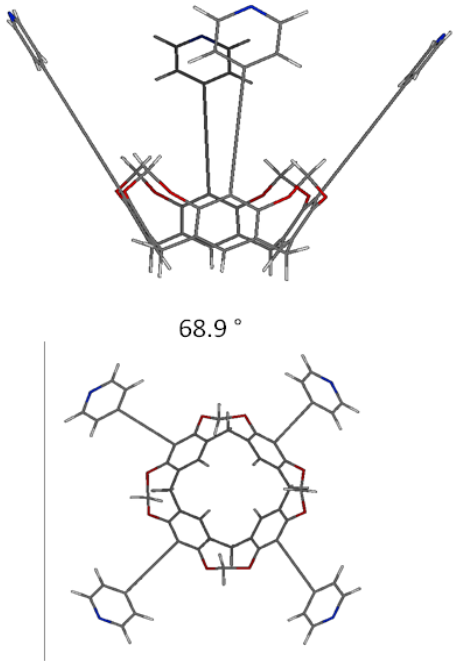

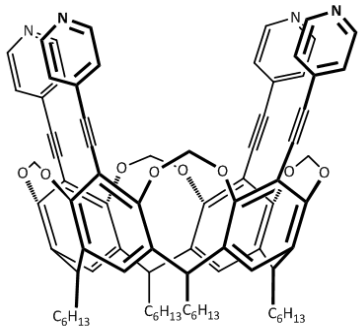

6

Figure 5 Modeling and structure of tetraethynylpyridines cavitand **6**

The chosen ligand is ethynylpyridine, to be connected to the cavitand skeleton at the apical positions. We envisioned a whole class of pluridentate cavitand ligands having one, two, three and four ethynylpyridine moieties (Scheme 2). The modeling of cavitand **6,** shown in Figure 5, allowed to estimate an angle of 68.9° between the planes containing two of the ethynylpyrydines; whereas in Scheme 1b, where the ligands are on the bridges, the angle between the same

two planes is about 90°. As reported in literature, Rhenium shows complexation angles that vary according to different pyridinic ligands from 86° to 91°, consequently the angle calculated by the modeling in Figure 5 is smaller than the optimal one , forcing the Re-*fac* complex to assume a larger angle.

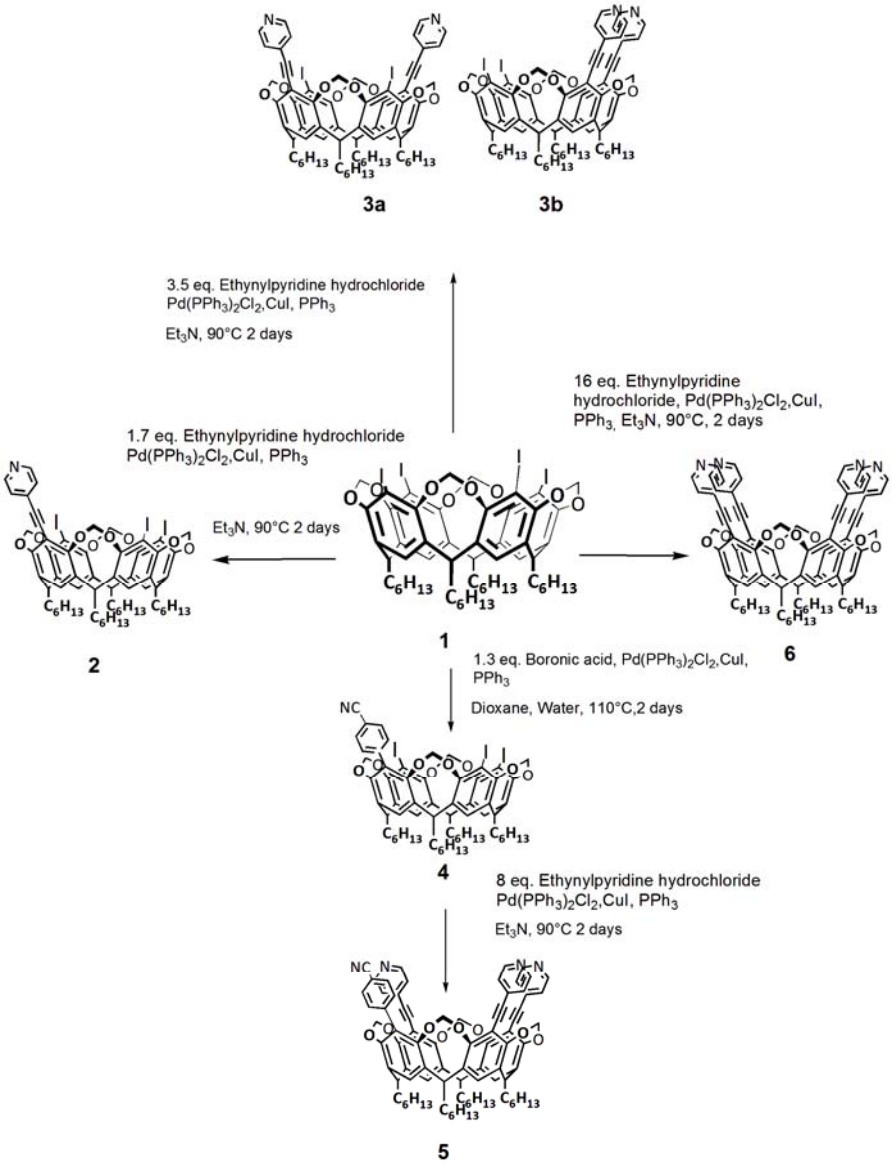

Scheme 2 Synthesis of cavitand having 1, 2, 3 and 4 ethynylpyridine lignads at the apical position

4.2.1 Synthesis of monoethynylpyridines cavitand 2

The first cavitand synthesized was cavitand **2**; as previously reported in Chapter 3, this was prepared reacting cavitand **1** (whose synthesis is shown in Chapter 3) with 1.7 equivalents of ethynylpyridine hydrochloride, $Pd(PPh_2)_3Cl_2$, PPh_3 and CuI in dry Et_3N for 2 days at 90°C. This reaction gave our desired product and, as byproduct the starting material, cavitand **1**. The yield of the reaction was only 35%, although, being able to recover the starting material, this reaction was particularly convenient.

4.2.2 Synthesis of diethynylpyridines cavitand 3a and 3b

The second target molecule was the di-substituted cavitand **3**. The reaction was conducted in dry triethylammine with Pd(II)catalyst using 3.5 equivalents of ethynylpyridine hydrochloride (Scheme 2) in order to make the reaction selective toward the di-substitution. We obtained, as expected, both *AC* and *AB* isomers in a 1,6:2 ratio. The yield of this reaction was around 5.2% for the *AB* isomer and 4.5% for the *AB* isomer. The low yield was due to the difficult separation of the two isomers. We observed that, at the end of the reaction, we had tetraiodocavitand left and, as byproduct, we had monoethynylpyridine cavitand **1**. The addiction of higher amount of ethynylpyridine hydrochloride (4 or 5 equivalents) led to the formation also of tri substituted and tetra substituted cavitands, leaving unchanged the yield of **3.** Moreover, the advantage of the strategy proposed in Scheme 2 is that we can recover the starting material and the byproduct and reacting them again.

4.2.3 Synthesis of triethynylpyrydines monobenzonitrile cavitand 5.

The first approach involved the reaction of **1** with ten equivalents of ethynylpyridine hydrochloride, but we obtained a mixture of our desired product and cavitand **6;** moreover, the yield of the trisubstituted cavitand was very low. In order to make our reaction more selective, and avoid the formation of undesired byproduct, we perfomed at first a Suzuki coupling to obtain the monosubstituted benzonitrile cavitand **4**, as shown in Scheme 2 and as reported in Chapter 3. We then reacted **4** with a slight excess of ethynylpyridine hydrochloride (8 equivalents) in order to have the desired cavitand **5**. The presence of one benzonitrile does not affect the reactivity of cavitand **5** toward Re complexes due to the fact Re does not complex nitrile ligands.

4.2.4 Synthesis of tetraethynylpyrydine cavitand 6

The last target molecule, tetraethynylpyridine cavitand **6**, was then synthesized using the procedure previously shown, increasing to 16 the equivalents of ethynylpyrydine hydrochloride, as reported by Kobayashi. The yield of this reaction is just 25% due to the presence of several homocoupling byproducts**.**

4.2.5 Microwave assisted Sonogashira coupling

Transition-metal-catalyzed carbon–carbon and carbon– heteroatom bond reactions are of prime interest in chemistry due to their widespread applications in the synthesis of drug-like molecules and natural products. Microwave-assisted organic synthesis (MAOS) is a relatively new technique and has grown extensively in the last decade from a mere academic tool to a heartily used technique in the industrial research laboratory. Homogeneous transition-metal-catalyzed reactions, typically needing rather long reaction times, represent one of the most important and best studied reaction types in MAOS. It is apparent that microwave irradiation mostly results in a dramatic acceleration of reactions, most often resulting in cleaner outcomes and increased yields.[7, 8].Due to our need to improve the yield of Sonogashira coupling, a new approach involving microwave assisted reactions, was developed; in particular for **3a**, **3b** and **6**; we also wanted to observe if there was any kind of selectivity in the formation of one of the two isomer (*AC* vs. *AB*) in the synthesis of the di substituted cavitand.

4.2.6 Microwave-assisted synthesis of diethynylpyridines cavitand 3 and tetraethynylpyrydines cavitand 6. (Scheme 3)

The synthesis was carried out in the appropriate microwave tube, adding, to tetraiodocavitand in dry DMF, Pd(II) catalyst, 3.5 eq. and 16 eq. of ethynylpyrydinehydrochloride, , CuI and PPh_3. We irradiated at 300 W for one hour and 45 minutes reaching 140°C of temperature. We didn't obtain the desired product but just undesired byproducts. We conducted the reaction changing the solvent from DMF to dry triethylammine as we did in reactions previously shown. In this case, due to the solvent nature, the temperature reached 128°C but we observed the formation of the diethynylpyrydines cavitands, (both *AC* and *AB*) and tetraethynylpyridine cavitand. The yield after purification was respectively 5.0 % and 6.0% for **3a** and **3b** and 35% for **6.** Even

though we didn’t observe a significant increment in the yield, the advantage in the use of this approach lies in the drastically reduced reaction times (Scheme 3).

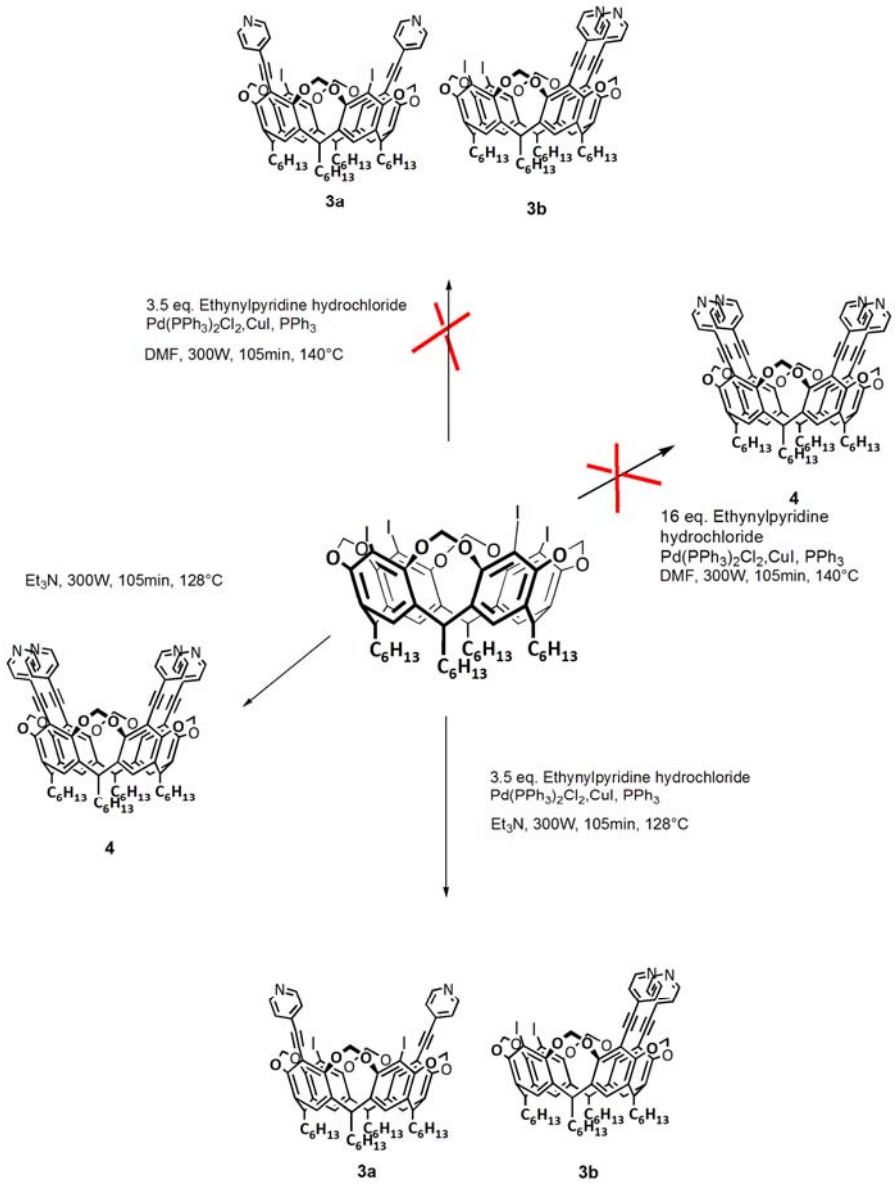

Scheme 3 Synthesis of diethynylpyridine cavitand *AC* and *AB* isomer **3a** and **3b** and tetraethynynylpyridines cavitand

Rhenium cages synthesis

4.2.7 Synthesis of Re-monoethynyl cavitand hemicage 7

Cavitand **2** was reacted with $Re(CO)_5Cl$ in $CHCl_3$ at 60°C for 12 hours to give the hemicage **7** (Scheme 4) in 80% of yield. ^1H NMR spectrum of the product showed the characteristic low field shift of the α-H of the pyridine from 8.58 ppm to 8.74 ppm and H_{down} of the aromatic ring from 8.10 to 8.21 ppm, due to the complexation. Since Rhenium complexes are kinetically stable at room temperature, it was possible to perform a silica gel chromatography purification; we also obtained, as byproduct, the species having only one cavitand ligand connected to Rhenium.

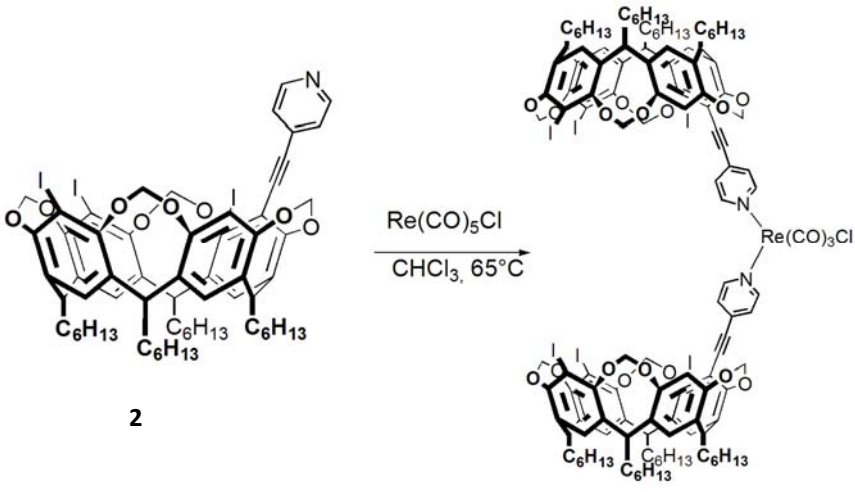

2 **7**

Scheme 4 Synthesis of Re-hemicage **7**

4.2.8 Synthesis of Re-diethynylpyridine cavitand cages 8 and 9.

We wanted to investigate the diethynylpyridine cavitand coordination ability toward Re(I) complex in order to create a building block useful for the formation of complex molecular architectures.

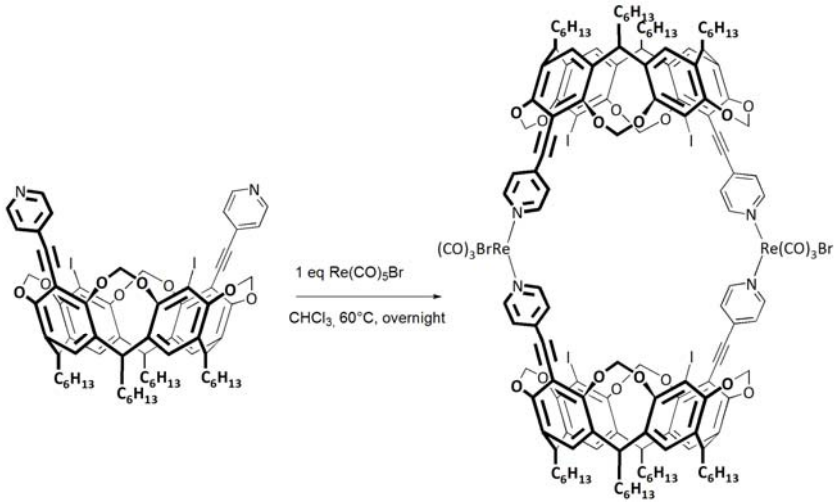

Scheme 5 Synthesis of *AC* Re-cage **8**

Reacting the *AC* isomer with one equivalent of Re(I) complex (Scheme 5 and Figure 6) we observed the formation of cage **8**, that was obtained as pure product after purification by silica gel chromatography. The yield of this reaction was about 40% due to the formation of "partially closed" cages.
^{1}H NMR spectrum showed low field shift of the α-H of pyridines from 8.57 to 8.79 ppm; there was a clear splitting of the H_{down} of the aromatic ring, in fact one at 7.07 ppm remained unchanged, whereas the other at 7.09 shifted to 7.14 ppm.

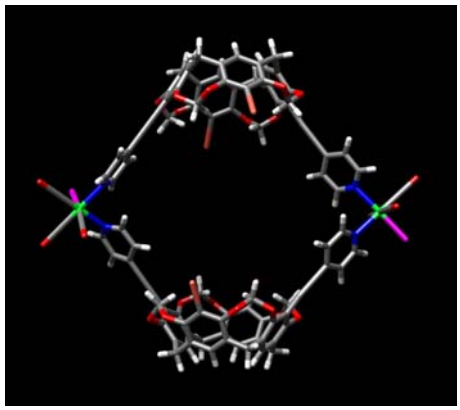

Figure 6 Spartan model of *AC* Rhenium cage

Moreover, H_{in} ,corresponding to the bridges close to the ethynylpyrydines, slightly moved upfield from 4.44 to 4.40 ppm: the whole molecule's symmetry remained unchanged respect to the starting cavitand, suggesting a complete complexation.
This result is very important: the presence of the two pyridine ligands in apical positions does not hamper the formation of the cage, despite of the smaller angle between the two ligands (see Figure 5).
Therefore for the formation of Re cages the ligands can be positioned not only on the bridges (see Scheme 1b) but also on apical positions, leaving the bridges free to be decorated with phosphonate groups.

The same approach was used for the *AB* isomer but, in this case, the ^{1}H NMR showed a more complex spectrum: this was partially due to the cavitand asymmetry, and partially to the fact that there were two possible configurations of the final product (Scheme 6). ^{1}H NMR showed partially overlapped peaks for the α-H of pyridines, from 8.80 to 8.74 ppm; moreover, we observed several broad peaks corresponding to H_{in} and H_{out} 6.04 – 5.85 ppm, 4.4.3 –4.38 ppm and 4.24 – 4.2; suggesting the presence of more than one species in solution. This configurations are called Clamshell or *C shaped configuration* and *S shaped configuration,* respectively. Molecular modeling confirms the formation of two possible structures (Figure 7).

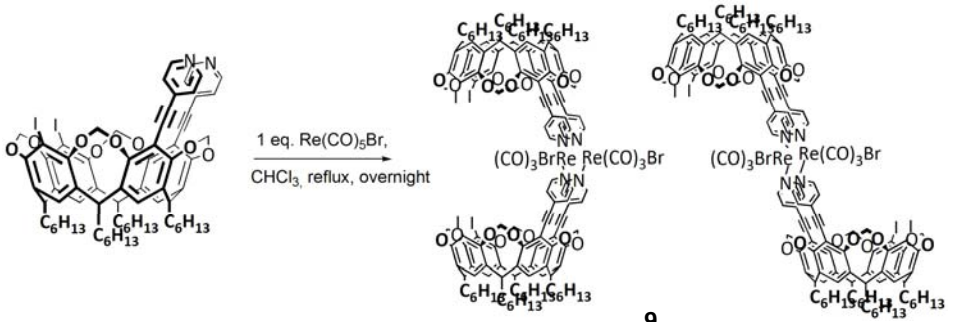

Scheme 6 Synthesis of the AB Rhenium hemicages **9** in the two configurations **A** and **B**

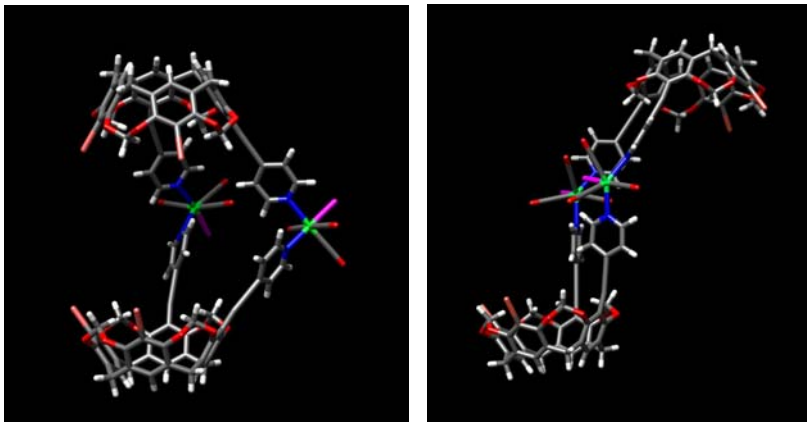

Figure 7 Spartan model of *AB* cages **9**. **A**: C shaped configuration; **B**: S shaped

In order to examine the complexation behavior of the cavitand having pyridine moieties at the apical positions, we reacted cavitand **5**, having three ethynylpyridines and one benzonitrile (Figure 8) with Rhenium pentacarbonyl bromide in chloroform at 60° for 12 hours.

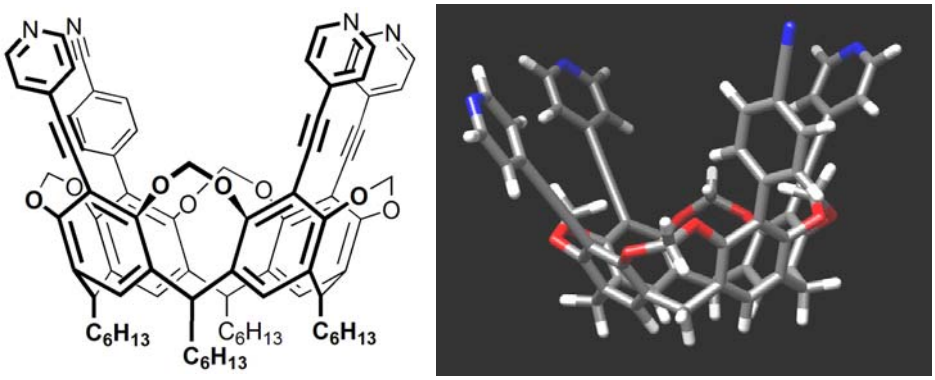

Figure 8 Structure and Spartan model of cavitand **5**

TLC of the crude showed several spots; after separation we weren't able to assign any compound to the desired one. The explanation of the high number of products-byproducts was due to the fact that there are several routes

available due to the asymmetry of the starting cavitand (Figure 9). In the case of **10a** three Re metal centers are involved, while for **10b-d** only two are required. Since Re complexation is not reversible due to the loss of CO, once structures **10b-d** are formed they cannot interconvert back to **10a**.

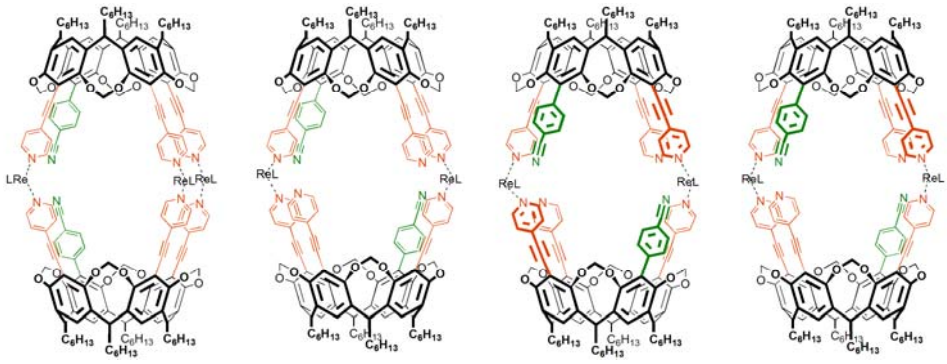

10a **10b** **10c** **10d**

Figure 9 Structure of the isomeric cages **10 a-d**

4.2.9 Synthesis of tetra Re-tetraethynylpyridines cage 11

The last step was the synthesis of tetra Rhenium tetraethynylpyridine cage; we reacted cavitand **6** with four equivalents of $Re(CO)_5Br$ for 2 days. The TLC of crude showed the presence of several byproducts. The yield of this reaction was quite low probably due to the formation of polymeric species; moreover, the difficult purification step drastically affected the final yield and the purity of the product itself. Although, it was possible to detect in ^1H NMR characteristic peaks corresponding to the desired molecule (Figure 10). The difficult in forming cage **11** cannot be associated with the apical positioning of the four pyridine ligands: in fact the same problem was observed for tetradentate pyridyl cavitands having the pyridines on the bridges.

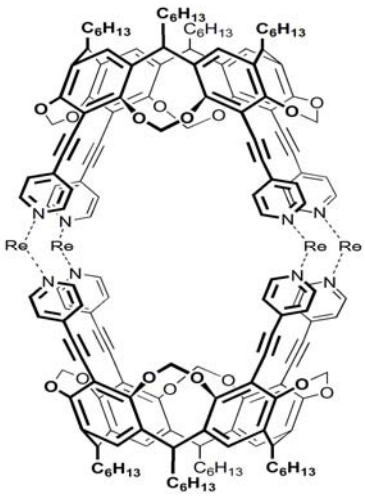

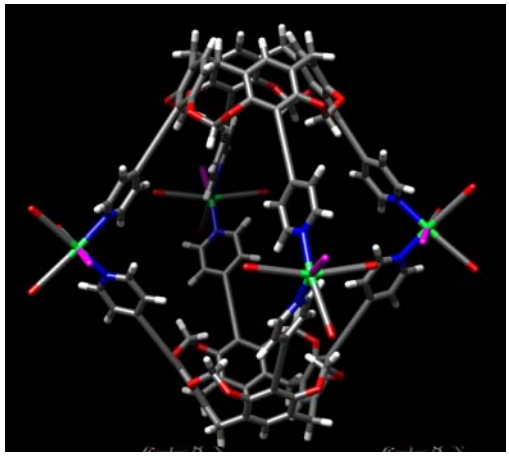

11

Figure 10 Structure and Spartan model of tetra rhenium cage **11**

One of the main issues in the synthesis of these cages is the characterization *via* mass spectrometry; it is possible to observe the mass peak just in the case of the mono-Re-monoethynylpyridine hemicage, however, the intensity of this peak is very low. The reason of this behavior is that the cage itself is not charged and, it is reported, that usually the CO-Re bond is broken during the analysis making the cage charged. Unfortunately, we observe that the Py-Re bond is more easily broken in respect with CO-Re bond. This results in the breaking of the cage itself. The decomposition pathway becomes dominant with an increasing number of Py-Re bonds, like for cage **9** and **11.**

4.3 Conclusions

The outcome of this study can be summarized as follow: (i) the introduction of one Re metal connecting two cavitand ligands is an easy process; (ii) connection of two *AC* cavitands *via* two Re metals to form cage **8** is valuable despite of the non optimal orientation of the two apical pyridyl ligands; (iii) the *AB* isomer instead leads to a mixture of two configurational isomers **9a** and **9b**, useless for any further reaction; (iv) the presence of three pyridyl ligands leads to the formation of several isomeric cages; (v) tetrapyridyl cavitand ligand **6** does not form the desired cage **11** as the major product.

4.4 Experimental

General

Reagents and solvents were purchased as reagent grade and used without further purification. Analytical TLC was performed on Merck silica gel 60 F254 precoated plates. Column chromatography was performed using silica gel (Merck 70 − 230 mesh). ^{1}H NMR spectra were recorded at 300 MHz on a Bruker AC 300 Avance spectrometer with solvent peaks as reference.. ^{31}P NMR spectra were recorded at 162 MHz, on a Bruker 400 spectrometer. ESI MS spectra were measured on a Helwett-Packard 3395 Waters 74 spectrometer.

Monoethynylpyridine-cavitand (2) 10 mL of dry Et_3N were degassed in a dry flask for 30 minutes. 0.5 g of **1** (3.63×10^{-4} mol), 0.084 g of ethynylpyridinehydrochloride (6.25×10^{-4} mol), 0.0102 g of $Pd(PPh_3)_2Cl_2$ (1.45×10^{-5} mol), 0.0051 g of CuI (3.5×10^{-5} mol), and 0.0057 g of PPh_3 (2.2×10^{-5} mol) were added and the mixture was stirred for 1 hour at 60°C and for 48 hours at 90°C. After cooling to room temperature, $CHCl_3$ was added and the crude product was washed with water and extracted with $CHCl_3$. The pure product was obtained by purification with silica gel flash chromatography with CH_2Cl_2: AcOEt (95:5) as eluant. (35% yield). **^{1}H NMR ($CDCl_3$, 300 MHz)** δ = 8.60 (d, 2H, Py**H$_o$,** J = 5.7 Hz), 7.30 (d, 2H, Py**H$_m$**, J = 6.6 Hz), 7.11 (s, 1H, Ar**H**), 7.08 (s, 1H, Ar**H**), 7.06 (s, 1H, Ar**H**), 5.95 (m, 4H, OCH_{in}**H$_{out}$**O), 4.84 (m, 4H, ArC**H**), 4.48

(d, 2H, O**CH$_{in}$**H$_{out}$O, J_2 = 8.1 Hz), 4.29 (d, 2H, O**CH$_{in}$**H$_{out}$O, J_2 = 8.2 Hz), 2.21 (m, 8H, ArCHC**H$_2$**), 1.28 (m, 40H, $CH_2C\mathbf{H_2}C\mathbf{H_2}C\mathbf{H_2}C\mathbf{H_2}CH_3$), 0.88 (t, 12H, $CH_2C\mathbf{H_3}$, J = 7.2 Hz); **ESI-MS** (*m/z*): 1352.7 $[MH]^+$ [M = $C_{63}H_{72}I_3NO_8$].

Diethynylpyridine-cavitand (3): a) standard preparation: 30 mL of dry Et_3N were degassed in a dry flask for 30 minutes. 0.3 g of **1** (2.17×10^{-4} mol), 0.104 g of ethynylpyridinehydrochloride, 0.00902 g of $Pd(PPh_3)_2Cl_2$ (1.30×10^{-6} mol), 0.0045 g of PPh3 (1.085×10^{-6}), 0.0045 g of CuI were added and the mixture was stirred for 1 hour at 60°C and for 48 hours at 90°C. After cooling to room temperature, $CHCl_3$ was added and the crude product was washed with water and extracted with $CHCl_3$. **3** was obtained as a mixture of the two isomers by purification with silica gel flash chromatography with CH_2Cl_2:AcOEt (95:5) as eluant. In order two separate AC from AB isomer a preparative TLC was performed using as eluant CH_2Cl_2:AcOEt: EtOH (97:3:2). (5.2% yield *AB* isomer, 4.5% *AC* isomer).

Diethynylpyridine-cavitand (3): b) microwave assisted preparation: to a solution of 0.050 g (3.63×10^{-5} mol) of **1** in 3 mL of dry triethylammine in a microwave tube were added 0.0177 g of ethynylpyridinehydrochloride (1.27×10^{-4} mol), 0.0015 g of $Pd(PPh_3)_2Cl_2$ (7.26×10^{-6} mol), 0.00045 g of PPh_3 (1.81×10^{-6} mol) and 0.00027 g of CuI (5.80×10^{-6} mol; the mixture was stirred at 127°C and 300 W for 75 minutes. After cooling to room temperature $CHCl_3$ was added and the crude product was washed with water and extracted with $CHCl_3$. Purification was carried out as in **a**). AC isomer yield: 5.0%.AB isomer yield 6.0%

***AC* isomer ^{1}H NMR ($CDCl_3$, 300 MHz):** δ = 8.58 (d, 4H, Py**H$_o$**, J = 5.7 Hz), 7.33(d, 4H, PyH$_m$, J = 6.6 Hz) 7.12 (s, 2H, Ar**H**), 7.06 (s, 2H, Ar**H**), 5.96 (m, 4H, $OCH_{in}\mathbf{H_{out}}O$), 4.84 (m, 4H, ArC**H**), 4.60 (d, 1H, d, 2H, O**CH$_{in}$**H$_{out}$O, J_2 = 6.9 Hz), 4.43 (d, 2H, O**CH$_{in}$**H$_{out}$O J_2 = 7.5 Hz), 4.25 (d, 2H, O**CH$_{in}$**H$_{out}$O, J_2 = 7.5 Hz), 2.21 (m, 8H, ArCHC**H$_2$**), 1.28 (m, 40H, $CH_2\mathbf{CH_2CH_2CH_2CH_2}CH_3$), 0.88 (t, 12H, $CH_2\mathbf{CH_3}$, J = 7.2 Hz)

ESI MS (*m/z*)**:** 1327.4 $[MH]^+$ 664.5 $[MH_2]^{2+}$ [M = $C_{70}H_{76}I_2N_2O_8$]

***AB* isomer ^{1}H NMR ($CDCl_3$, 300 MHz):** 8.58 (d, 4H, Py**H$_o$**, J = 5.7 Hz), 7.33 (d, 4H, PyH$_m$, J = 6.6 Hz), 7.10 (s, 2H, Ar**H**), 7.07 (s, 2H, Ar**H**), 5.96 (m, 4H, $OCH_{in}\mathbf{H_{out}}O$ J_2 = 7.2 Hz), 4.84 (m, 4H, ArC**H**), 4.25 (d, 4H, O**CH$_{in}$**H$_{out}$O, J_2 = 7.5 Hz), 2.21 (m, 8H, ArCHC**H$_2$**), 1.28 (m, 40H, $CH_2\mathbf{CH_2CH_2CH_2CH_2}CH_3$), 0.88 (t, 12H, $CH_2\mathbf{CH_3}$, J = 7.2 Hz); **ESI MS** (*m/z*)**:** 1327.4 $[MH]^+$ 664.5 $[MH_2]^{2+}$ [M = $C_{70}H_{76}I_2N_2O_8$]

Tetraethynylpyridine-cavitand (6): a) standard preparation: 20 mL of dry Et_3N were degassed in a dry flask for 30 minutes. 0.2 g of **1** (1.45×10^{-4} mol), 0.320 g of ethynylpyridinehydrochloride (2.30×10^{-3} mo), 0.0064 g of $Pd(PPh_3)_2Cl_2$ (8.71×10^{-6} mol), 0.0015 g of PPh3 (5.8×10^{-6}), 0.0018 g of CuI (7.25×10^{-6}) were added and the mixture was stirred for 1 hour at 60°C and for 48 hours at 90°C. After cooling to room temperature, $CHCl_3$ was added and the crude product was washed with water and extracted with $CHCl_3$. The pure product was obtained after purification with silica gel flash chromatography with AcOEt:EtOH (8:2) with addition of 1% of Et_3N. The yield was 25%.

Tetraethynylpyridine-cavitand (6) : b) microwave assisted preparation: to a solution of 0.050 g (3.63×10^{-5} mol) of **1** in 3 mL of dry triethylammine, in a microwave tube, were added 0.080 g of ethynylpyridinehydrochloride (5.8×10^{-4} mol), 0.0015 g of $Pd(PPh_3)_2Cl_2$ (7.26×10^{-6} mol), 0.00045 g of PPh_3 (1.81×10^{-6} mol) and 0.00027 g of CuI (5.80×10^{-6} mol); the mixture was stirred at 127°C and 300 W for 75 minutes. After cooling to room temperature $CHCl_3$ was added and the crude product was washed with water and extracted with $CHCl_3$. Purification was carried out as in **a**). The yield was 35% **^{1}H NMR** ($CDCl_3$, 300 MHz)**:** 8.54 (d, 8H, Py**H_o**), 7.28 (d, 8H, Py**H_m**), 7.12 (s, 4H, Ar**H**), 5.95 (d, 4H, OCH_{in}**H_{out}**O, J = 6.6 Hz), 4.82 (m, 4H, Ar**CH**), 4.51 (d, 4H, OC**H_{in}**H_{out}O, J = 6.6 Hz) 2.21 (m, 8H, $ArCHCH_2$), 1.28 (m, 32H, CH_2**$CH_2CH_2CH_2CH_2$**CH_3), 0.88 (t, 12H, CH_2CH_3, J = 7.2 Hz).
ESI MS (*m/z*): 1278.7 $[MH]^+$, 1318.5 $[M+Na]^+$, 639.3 $[MH_2]^{2+}$

Re-Monoethynylpyridine cavitand cage (7) To a solution of 0.1 g (7.4×10^{-5} mol) of cavitand **2** in 15 mL of dry $CHCl_3$ under argon, were added 0.013 g of $Re(CO)_5Cl$ (3.7×10^{-5}mol). The solution was refluxed overnight. After cooling to room temperature the solution was concentrated under vacuum and the crude purificated by silica gel chromatography using as eluent Hexane and CH_2Cl_2 (4:6). **^{1}H NMR** ($CDCl_3$, 300 MHz): δ = 8.72 (d, 4H, Py**H_o**, J = 5.7 Hz), 7.29 (d, 4H, Py**H_m**, J = 6.6 Hz), 7.13 (s, 2H, Ar**H**), 7.06 (s, 6H, Ar**H**), 5.97 (m, 8H, OCH_{in}**H_{out}**O), 4.82 (m, 8H, Ar**CH**), 4.45 (d, 4H, OC**H_{in}**H_{out}O, **J_2 = 8.1 Hz**), 4.26 (d, 4H, OC**H_{in}**H_{out}O, J_2 = 8.2 Hz), 2.21 (m, 8H, $ArCHCH_2$), 1.28 (m, 32H, $CH_2CH_2CH_2CH_2CH_2CH_3$), 0.88 (t, 12H, CH_2CH_3, J = 7.2 Hz).**ESI MS** not available.

***AC*-di-Re-diethynylpyridine cavitand cage (8):** To a solution of 0.015 g (1.13×10^{-5} mol) of cavitand **3a** in 10 mL dry $CHCl_3$ under argon, were added 0.0045 g of $Re(CO)_5Br$ (1.13×10^{-5} mol). The solution was refluxed overnight. After cooling to room temperature the solution was concentrated under vacuum and the crude purificated by silica gel chromatography using as eluent Hexane

and CH_2Cl_2 (5:5). **^{1}H NMR** ($CDCl_3$, 300 MHz): δ = 8.79 (d, 8H, Py**H_o**, J = 5.7 Hz), 7.33 (d, 8H, Py**H_m**, J = 6.6 Hz), 7.14 (s, 2H, Ar**H**), 7.08 (s, 6H, Ar**H**), 5.94 (m, 8H, OCH_{in}**H_{out}**O), 4.84 (m, 8H, Ar**CH**), 4.42 (d, 8H, OC**H_{in}**H_{out}O, **J_2 = 8.1 Hz**, 2.21 (m, 8H, $ArCHCH_2$), 1.28 (m, 64H, CH_2**$CH_2CH_2CH_2CH_2$**CH_3), 0.88 (t, 24H, CH_2CH_3, J = 7.2 Hz). **ESI MS** not obtained.

***AB*-di-Re-diethynylpyridine cavitand cage (9):** To a solution of 0.015 g (1.13× 10^{-5} mol) of cavitand **3b** in 10 mL of dry $CHCl_3$ under argon, were added 0.0045 g of $Re(CO)_5Br$ (1.13 × 10^{-5} mol). The solution was refluxed overnight. After cooling to room temperature the solution was concentrated under vacuum and the crude purificated by silica gel chromatography using as eluent Hexane and CH_2Cl_2 (5:5). **^{1}H NMR** ($CDCl_3$, 300 MHz): δ = 8.80 – 8.72(m, 8H, Py**H_o**,), 7.31–7.29 (m, 8H, Py**H_m** solvent partially overlapped), 7.16 (s, 4H, Ar**H**), 7.06 (s, 4H, Ar**H**), 6.04 – 5.87 (m, 8H, OCH_{in}**H_{out}**O), 4.88 – 4.74 (m, 8H, Ar**CH**), 4.43 – 4.35 (m, 4H, OC**H_{in}**H_{out}O) 4.26 – 4.20 (m, 4H, OC**H_{in}**H_{out}O) 2.21 (m, 8H, $ArCHCH_2$), 1.28 (m, 32H, CH_2**$CH_2CH_2CH_2CH_2$**CH_3), 0.88 (t, 12H, CH_2CH_3, J = 7.2 Hz).**ESI MS** not obtained.

Tri Re-triethynylpyridine monobenzonitrile cage 10: To a solution of 0.025 g (2.04× 10^{-5} mol) of cavitand **5** in 25 mL of dry $CHCl_3$ under argon, were added 0.0124 g of $Re(CO)_5Br$ (3.07 × 10^{-5} mol). The solution was refluxed overnight. After cooling to room temperature the solution was concentrated under vacuum and the crude purificated by silica gel chromatography using as eluent Ethylacetate and CH_2Cl_2 (3:7). **^{1}H NMR** ($CDCl_3$, 300 MHz): δ = 8.80 – 8.70 (m, 12H**,** PyH_o)**,** 7.65 (d, 4H, NCAr**H_o**), 7.27 **–** 7.09m, 24 H,Py**H_m**, + Ar**H** + NCAr**H_m**), 5.98 – 5.89 (m, 4H, OCH_{in}**H_{out}**O), 5.52**–** 5.47 (m, 4H, OCH_{in}**H_{out}**O), 4.84 **–** 4.76 (m, 8H, ArC**H**), 4.44 **–** 4.38 (m, 4H, OC**H_{in}**H_{out}O), 4.23 **–** 4.19 (m, 4H, OC**H_{in}**H_{out}O), 2.30 (m, 8H, $ArCHCH_2$), 1.22 (m, 32H, $CH_2CH_2CH_2CH_2CH_2CH_3$), 0.90 (t, 12H, CH_2CH_3, J=7.3 Hz). **ESI MS** not obtained.

Tetra Re-Tetraethynylpyridine-cavitand cage 11: To a solution of 0.015 g (1.17× 10^{-5} mol) of cavitand **4** in 10 mL of dry $CHCl_3$ under argon, were added 0.013 g of $Re(CO)_5Br$ (3.04 × 10^{-5} mol). The solution was refluxed overnight. After cooling to room temperature the solution was concentrated under vacuum and the crude purificated by silica gel chromatography using as eluent Hexane and CH_2Cl_2 (5:5). **^{1}H NMR** ($CDCl_3$, 300 MHz) Tentative attribution: δ = 8.74 (m, 16H, Py**H_o**,), 7.32 (m, 16H, Py**H_m**), 7.12 (s, 4H, Ar**H**), 7.07 (s, 4H, Ar**H**), 5.98 (d, 8H, OCH_{in}**H_{out}**O), 4.88 – 4.74 (m, 16H, Ar**CH**), 4.38 (m, 4H, OC**H_{in}**H_{out}O)) 2.21 (m, 16H, $ArCHCH_2$), 1.28 (m, 64H, CH_2**$CH_2CH_2CH_2CH_2$**CH_3), 0.88 (t, 24H, CH_2CH_3, J = 7.2 Hz) **ESI MS** not obtained.

4.4 References

1. J. P. Collin, C. Dietrich-Buchecker, P. Gavina, M. C. Jimenez-Molero and J. P. Sauvage, *Acc. Chem.Res.*, 2001, **34**, 477-487.
2. J. A. Thomas, *Chem Soc. Rev.*, 2007, **36**, 856-868.
3. S. Rigault, C. Piguet, G. Berardinelli and G. Hopfgartner, *Angew. Chem., Int. Ed*., 1998, **37**, 169;
4. R. V. Sloane and J. T. Hupp, L. Stern, T. E. Albrecht-Schmitt *Inorg. Chem.* 1996**, 35***,* 4096-4097.
5. R. V. Slone, K. D. Benkstein, S. Belanger, J. T. Hupp, I. A. Guzei and A. L. Rheingold, *Coord. Chem. Rev.*, **171**, 1998, 221**–**243.
6. E. Menozzi, M. Busi, C. Massera, F. Ugozzoli, D. Zuccaccia, A. Macchioni and E. Dalcanale, *J. Org. Chem.*, 2006, **71**, 2617-2624.
7. P. Appukkuttan and E. Van der Eycken, *Eur. J. Org. Chem.*, 2008, **35**, 1133-1155.
8. B. K. Singh, N. Kaval, S. Tomar, E. Van der Eycken and V. S. Parmar, *Org. Proc. Res. Dev.*, 2008, **12**, 468-474.

Heteronuclear dimeric cages

5

5.1 Introduction

Self assembly refers to the spontaneous assembly of non-covalently linked molecular clusters of unique shape and composition. This requires both a driving force and a dynamic system so that all possible molecular structures can be explored to generate the thermodynamically favored, pre-desired assembly.[1]

In Nature we can find such a structure in the protein apoferritin, an iron storage protein, (Figure 1) which is composed of 24 non covalently linked protein subunits that form a nearly spherical shell of octahedral symmetry.

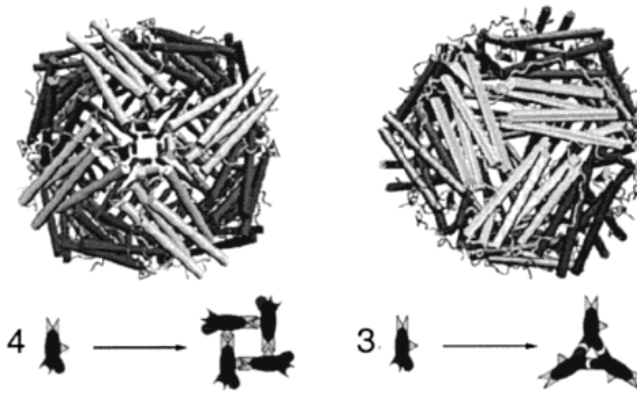

Figure 1 Human H chain ferritin,the octahedral 24-subunit iron storage protein as viewed down the 4-fold (left) and 3-fold (right) axes. The interaction at the 4-fold axis, in which the lock and key are 90° apart, requires the formation of tetramers. Similarly, the interaction at the 3-fold axis, in which the lock and key are 60° apart, requires the formation of trimers.

Several studies have been conducted with the aim of imitating such natural structures. This field of chemistry has demonstrated various applications involving both the biological molecular recognition of receptor-substrate complexes as well as the design of innovative and dynamic materials and catalytic processes [2,3,4].

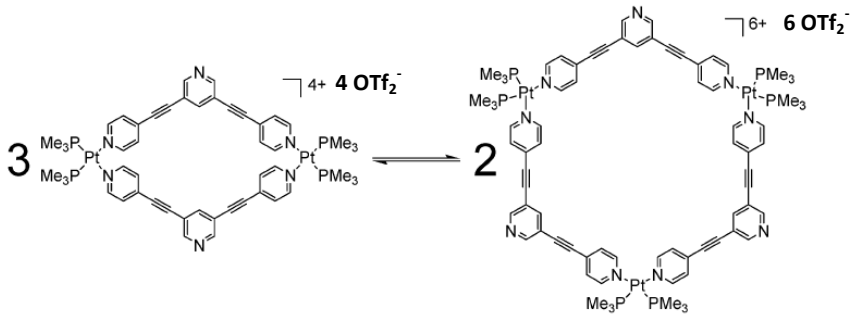

Figure 2 Stang's hexagon

Most of the designed systems involve labile metal-ligand interactions between fundamental components or precursors, which spontaneously generates structures in dynamic equilibrium. Thermodynamic and kinetics factors influence and determine the formation of the final product. The metal coordination geometry and the orientation of the interaction sites in a given ligand provide the blueprint for the self-assembly of the desired structures. [1]
The use of transition metal ions to direct self-assembly of supramolecular structures has become very popular due to their rich coordination ability allowing one to tune the self assembly in terms of coordination ability, geometry and bond energy. Fujita[5] reported the formation of molecular squares structure, as well as their extension to three-dimensional architectures, using transition metal such as Pd(II). Using a chelating square-planar Pd complex like [enPd(II)] and a ligand like (4,4'-bipyridine) they obtained squares (figure2) in which the metal units occupy the square corners.

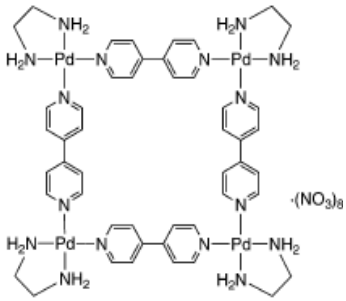

Figure 3 Fujita's square obtained by using [Pd(II)en] and (4,4'-bipyridine)

The same metal unit was then used to create three-dimensional structure, replacing (4,4'-bipyridine) by an exo-tridentate triangular ligand, 2,4,6-tris(4-pyridyl)-1,3,5-triazine.

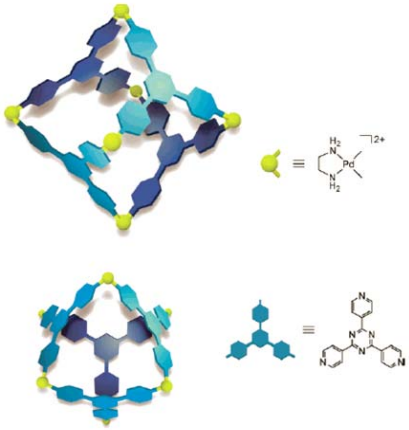

Figure 4 Fujita's three-dimensional structures obtained by using [Pd(II)en] and 2,4,6-tris(4-pyridyl)-1,3,5-triazine. as

Among the several building blocks employed, resorcinarene-based cavitands have proven to be particularly interesting as multidentate ligands. These molecules are characterized by rigidly-preorganized cavities of set molecular dimension, and allow for the introduction of diverse ligand moieties.

Upper rim functionalized cavitands have been used to create metallosupramolecular cages with more than four units, as reported by Volkmer and Mattay [6]. A cavitand possessing four terpyridyl units was used as

building block, in connection with $[Zn(NCMe_6)][TFPB]_2$ as metal precursor where TFPB = tetrakis-(
3,5-bis-(trifluormethyl)-phenyl)-borate). (Figure 5).

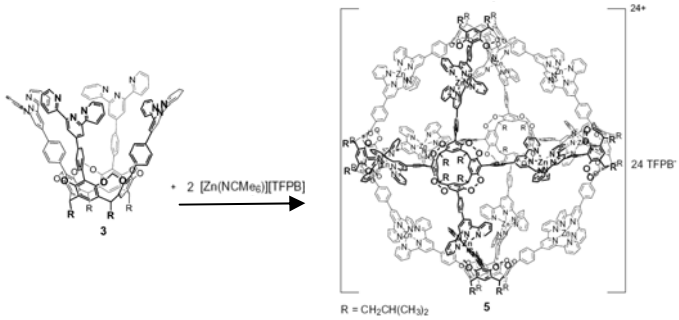

Figure 5 Volkmer and Mattay $[Zn(NCMe_6)]$ resorcinarene complex

In our laboratory numerous efforts have been made to create more complex molecular architectures, in particular dimeric cages. Busi and Menozzi [7] reported the self assembly of a dinuclear tetratopic cavitand hemicage obtained by reacting mono-pyridyl or mono-phenylpirydyl cavitands with a Pd(II) or Pt (II) ditopic complex (Scheme 1). The subsequent goal was to create a double cage, where the two cages are connected via a dinuclear metal precursor (Figure 6). The aim of this experiment was to self-assemble a complete-close double cage structure.

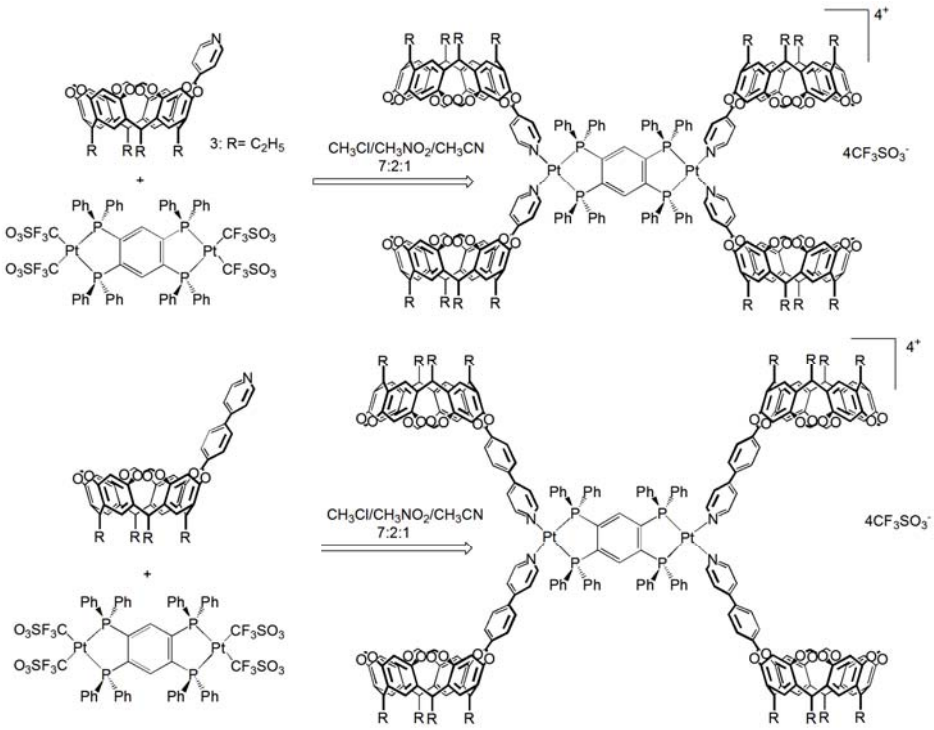

Scheme 1 Synthesis of Re-pyridine and Re-phenylpiridine dimeric hemicages.

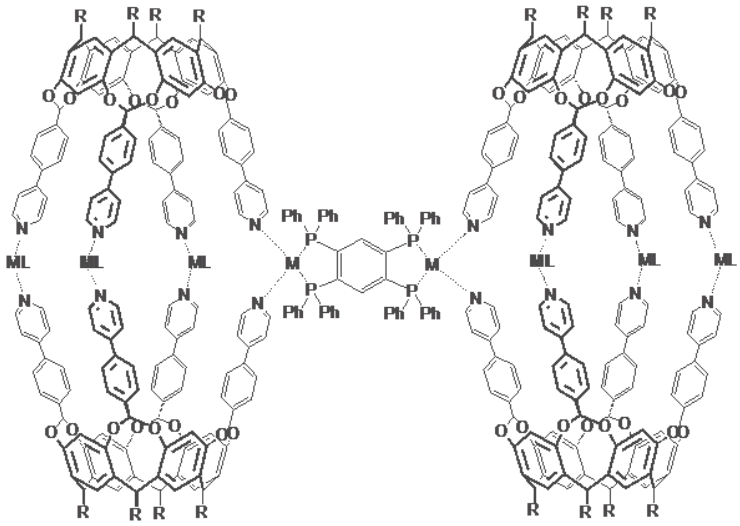

Figure 6 Structure of the dimeric cage designed by Busi and Menozzi

This experiment was conducted as a one pot experiment, in which the cavitand, Pd(dppp)OTf_2 or Pt(dppp)OTf_2 complexes and ditopic Pd(tppb)OTf_2 or Pt(tppb)OTf_2 in the ratio 4:6:1 were mixed together in a NMR tube. They observed the formation of the corresponding monomeric cage rather than the dimeric one: this was due to the fact that the former was entropically favored with respect to the latter. As we demonstrated in Chapter 3, it is necessary to differentiate metal-ligand cross reactivity to avoid undesired synthetic pathways.

In this Chapter, we report several innovative approaches for synthesizing dimeric cages, involving the use of different metal complexes to confer unique properties.

5.2 Results and discussion

5.2.1 Hemicage self-assembly

The aim of this project was to synthesize a cavitand suitable as building block for the self-assembly of a dimeric cage.
We took into consideration the results of Chapter 3 in which the different reactivity of the metal complexes as well as the different coordination ability of the two ligands in cavitand **1** were the only possible choices to obtain our desired molecule (Figure 7). We selected 1,2,4,5-tetrakis(diphenylposphino)benzene as a ligand for our metal precursor, as previously reported by Busi and Menozzi. This tetradentate chelating ligand can coordinate two metal ions by forming two equivalent square-planar complexes connected via a rigid spacer. Therefore our final supramolecular target was constituted by four cavitand **1** units , one Pt(II) dinuclear metal complex and six units of Pd(II) mononuclear complex (Figure 7).
In this approach Pt(tppb)OTf_2 complex should interact at first with the ethynylpyridine moieties, giving hemicage **8a** which in turn would react with Pd(dppp)OTf_2 to give the final dimeric cage **8b**.

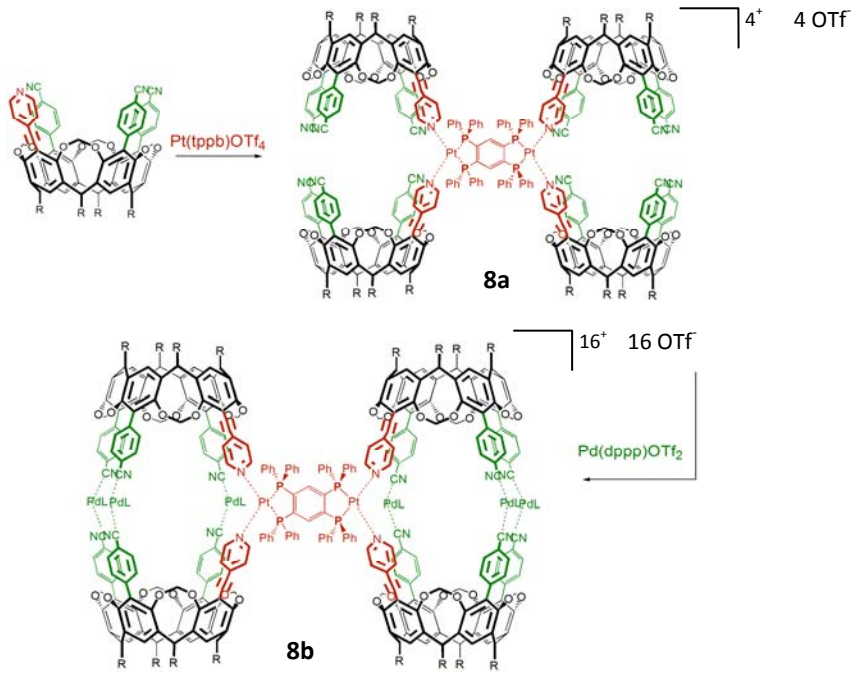

Figure 7 Stepwise self-assembly of dimeric hemicage **8a** and cage **8b**

We performed the stepwise self-assembly in a mixture of CD_2Cl_2 and CD_3NO_2 in the NMR tube: the first step was the formation of the dimeric hemicage (Figure 7, compound **8a**) by reacting four equivalents of cavitand **1** with one equivalent of Pt ditopic complex. The formation of this structure was confirmed by ^{1}H NMR, ^{31}P NMR, PGSE experiments and ESI MS.
^{1}H NMR showed the characteristic down field shift of the α-H of the pyridine from 8.58 ppm to 8.86 ppm, whereas the typical up-field shift was showed by H_{in} and H_{out} corresponding to the bridges: from 5.59 to 5.50 ppm, from 5.09 to 5.08 and from 4.11 to 4.10, respectively. One of the doublets corresponding to the bridges is covered by the peak of the residual solvent. ^{31}P NMR showed up-field shifted peak from 29.9 ppm to 17.1 ppm typical for Py-Pt-Py interaction. ESI MS confirmed the presence of the desired species showing a peak at *m/z*= 1522.6 corresponding to M^{4+} and *m/z* = 2082 corresponding to M^{3+}.

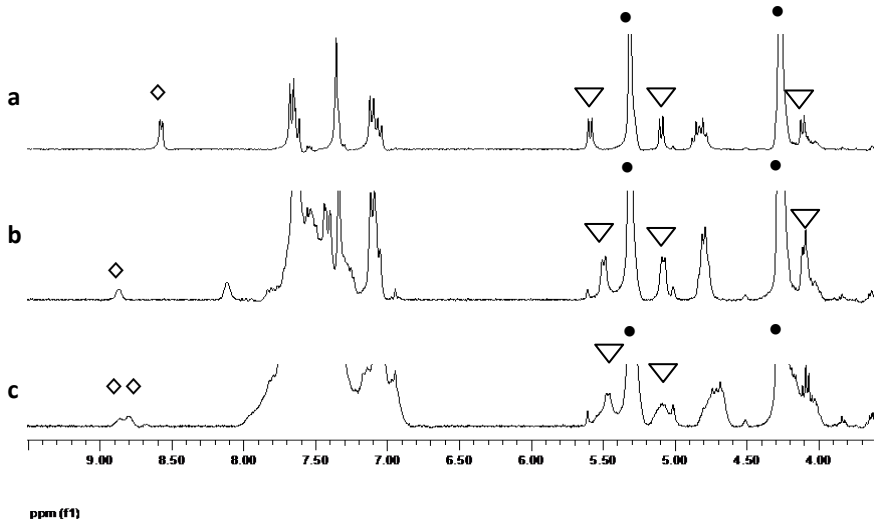

Figure 8 ^{1}H NMR (300 MHz, 400 µL CD_2Cl_2 and 100 µL CD_3NO_2) spectra of (a) 5 mM cavitand **1**, (b) 5 mM cavitand **1** and 0.25 eq. Pt(tppb)OTf_4, (c) 5 mM cavitand **1**, 0.25 eq. Pt(tppb)OTf_4. and 1.5 eq. of Pd(dppp)OTf_2, ◇ethynylpyridine α-H protons, ▽ H_{in} and H_{out} methylene bridges protons, ● residual solvent peaks.

5.2.2 PGSE experiment of hemicage 8a

Complex **8a** was characterized in solution by mono and bi-dimensional NMR experiments including ^{1}H PGSE (Pulsed-Field-Gradient-spin –Echo)[8,9,10,11]. The latter allows us to determine the transitional self-diffusion coefficient (Dt) and consequently, estimating the size of diffusing particle in solution. In fact, from (Dt) the average hydrodynamic radius (r_H) of the diffusing particles can be derived using Stockes-Einstein equation

$$Dt= kT/(c\pi\mu r_H), \quad (1)$$

where k is Boltzman constant, T is the temperature, μ is the solution viscosity and c is a numerical factor dipending on the molecule size (for our supramolecular structure was chosen to be 6). D_t can be measured by a number of pulse sequences based on standard stimulated Spin-Echo. The dependence of the resonance intensity (I) on a constant waiting time and on a varied gradient strength (G) is described by the equation (2)

$$\ln\left(\frac{I}{I_0}\right) = -(\gamma\delta)^2 D_t\left[\Delta - \frac{\delta}{3}\right]G^2 \quad (2)$$

where I, is the intensity of the observed Spin-Echo, I_0 is the intensity of the Spin-Echo without gradient, D_t is the diffusion coefficient, Δ is the delay between the midpoint of the gradient, δ is the length of the gradient pulse and γ is the magnetogyric ratio. D_t is directly proportional to the slope of the line obtained by plotting $\ln(I/I_0)$ vs G^2. As internal standard were used both TMSS (tetrakis-(trymethylsilyl)silane] and the solvent, CD_2Cl_2.

Figure 10 shows the plot we obtained from data elaboration. We monitored several signals corresponding to the cavitand and to Pt(tppb)OTf_2; in particular we wanted to observe the decreasing of the signals intensity in relation with the variation of the field applied (gradient applied during the PGSE experiment). We took into consideration three signals: **C** corresponding to H_α of the ethynylpyridine, **D** corresponding to H_{out} and **E** to the two aromatic protons of dinuclear metal complex. In Figure 10 we can observe that data, corresponding to different signals, (C,D and E) of both cavitand and Pt ditopic complex, lies on the same slope. That means that they possess the same diffusion coefficient due to the fact that they belong to the hemicage. The different slope of both TMMS and CD_2Cl_2 lines validate our measurements.

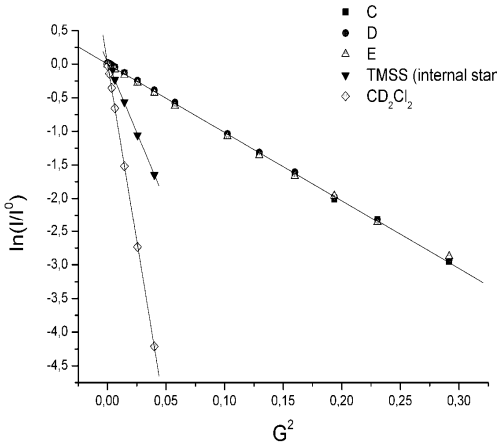

Figure 9 PGSE experiment data plot**.**

We extrapolated from Spartan model the radius and the volume of cavitand **1** and we compared these values with radius and volume calculated with PGSE experiment for hemicage **8a**, that are 16.4 Å and 17900 $Å^3$, respectively (Table 1). The values experimentally found were in agreement with models as shown in Figure 10. In PGSE experiment we extrapolated radius and volume data considering a spherical approximation even if the molecule is not a perfect sphere. In Figure 10 is shown the Spartan model of the molecule where three radii were calculated: The average of this three values is a good approximation of the experimental one.

Table 1 Calculated radius of cavitand **1** compared to the experimental one of hemicage **8a**

	D_t	R (Å)	V($Å^3$)
Cavitand	5.5×10^{-10}	8.9	2900 (calculated with Spartan model)
Hemicage	2.9×10^{-10}	16.4	17900 (experimentally determined)

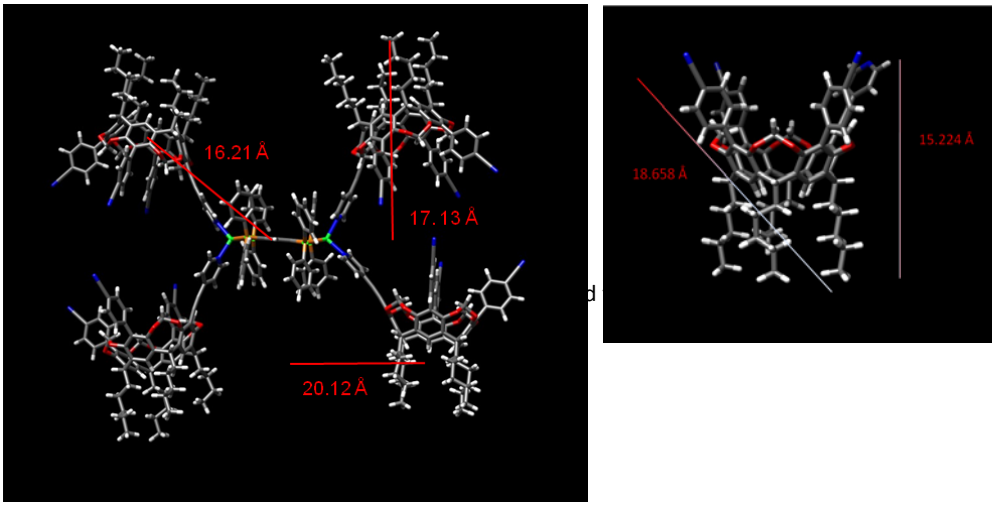

Figure 10 Radius and Volume for **8a** and cavitand **1** obtained from Spartan models

Table 2 Radii of hemicage **8a** in the three dimensions x, y and z calculated with Spartan model

	R_x (Å)	R_y (Å)	R_z (Å)	Average
Hemicage	20.1	17.1	16.2	17.8

In the second step we added, in the NMR tube, six equivalents of Pd(dppp)OTf_2 in order to complex the six remaining benzonitrile groups and close the dimeric hemicage. ^{1}H NMR showed two broad peaks for the α-H of the pyridine at 8.86 ppm and 8.79 ppm. We observed the presence of very broad signals for H_{in} and H_{out}. H_{out}, corresponding to the bridge close to ethynylpyridine, shifted from 5.49 ppm to 5.46 ppm the other one, close to benzonitriles, from 5.08 ppm to 5.08 – 5.16 ppm giving a multiplet. The H_{in} split into two partially overlapped doublets shifted from 4.10 ppm to 4.11-4.07 ppm. ^{31}P NMR exhibited three peaks at 17.10 ppm (PhCN − Pd − PhCN), 15.53 ppm (Py − Pt − Py), and 10.56 ppm (PhCN − Pd – CNPh). The presence of two signals for α-H of the pyridine suggested the presence of more than one species in solution. Ideally, we should have one signal for ethynylpyridine protons slightly up-field shifted with respect to the dimeric hemicage due to the closure of the cage; as well as sharp signals for the H_{in} and H_{out} dublets.

5.2.3 PGSE experiment of cage 8b

We can assume that the radius shouldn't change significantly from **8a** to **8b** because the addition of Pd complex shouldn't modify the molecule dimension (if we consider a sperical approssimation). In fact PGSE experiment of cage **8b**, carried out in the same conditions as the previous one, showed a value for the radius that was 17.9 Å and a volume of 24553 $Å^3$ that are in agreement with models. (Table 3)

Table 3 PGSE data for **8a** and **8b** compared to cavitand **1**

	R (Å)	**V($Å^3$)**
Cavitand	8.9	2900 (calculated with Spartan model)
Dimeric Hemicage	16.4	17900 (experimental determined)
Dimeric-cage	17.9	24553 (experimental determined)

We can conclude that the first step was selective toward the formation of the hemicage, whereas in the second step we didn't obtain a complete complexation but a "partially closed dimeric cage". The reason of this behavior could be that complexation ability of benzonitriles group is lower that pyridine moieties; and the possible formation of Pd (aquo)complexes could affect the self-assembly process. This approach presents some disadvantages: a)it is not easy to characterize the final molecule by mass spectrometry since the molecular weight is very high and the interaction PhCN-Pd is weak and is easily broken in ESI MS, b) from **8a** to **8b** there isn't a significant increment in radius to use PGSE technique as main experiment to confirm the formation of the dimeric cage.

5.2.4 The Rhenium approach

We developed a new approach focused on the use of Rhenium. As reported in Chapter 4 Rhenium presents several advantages: a) it forms kinetically stable complexes at room temperature, b) it interacts just with pyridine groups leaving benzonitriles free, c) Rhenium complexes are stable and they can be purified via silica gel chromatography. Hupp and coworkers K. [12] synthesized , a series of cationic and neutral rectangles with large cavities by using dinuclear 2,2'-bipyrimidine (bpym)and 2,2'-bisbenzimidazolate . While both these latter macrocycles bind to aromatic guest molecules, the kinetically inert nature of the rectangles has also meant that in-depth electrochemical and electrooptic studies can be carried out on these architectures. (Figure 11)

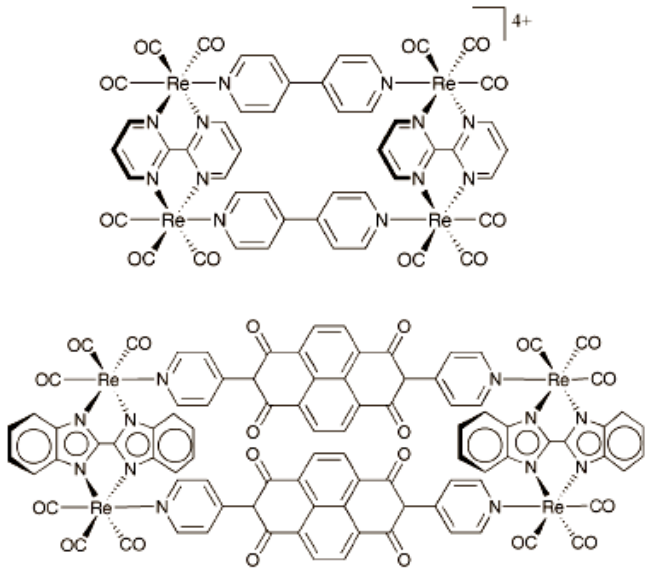

Figure 11 Hupp's rectangles obtained by using Rhenium complexes and bypyridine ligands

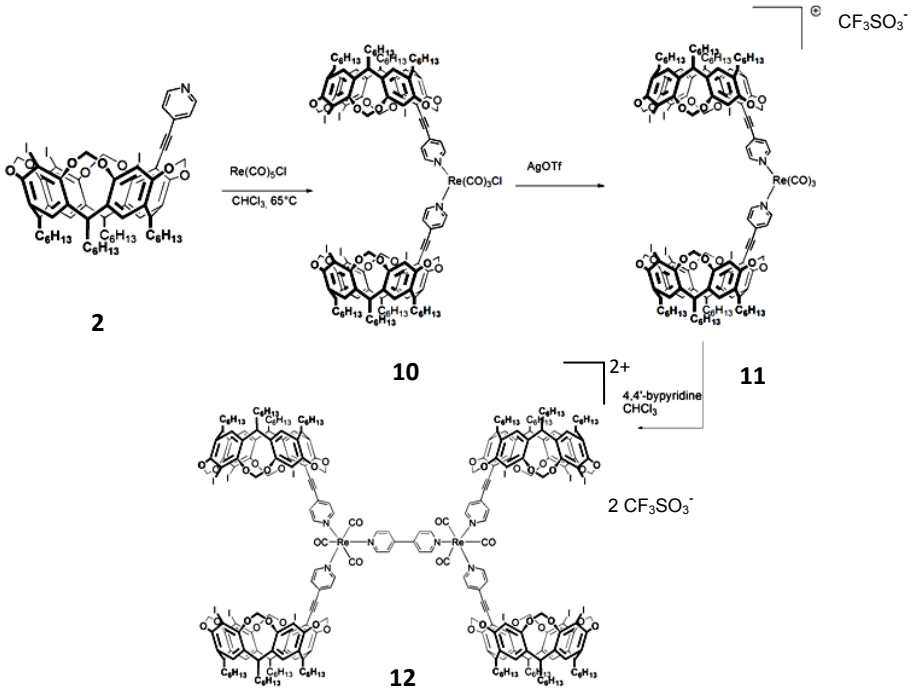

Scheme 2 Synthesis of Re-dimeric hemicage cage **12** obtained from single hemicage **10** and 4,4'-bypyridine ligand

We wanted to exploit the same approach using cavitand as building block and 4,4'-bypyridine as link in order to synthesize a new dimeric hemicage. The key point of this approach is the versatility of the link and the possibility to carry out the assembly of the final structure in two separate steps followed by purification. Moreover, the use of cavitands confers a very large cavity to the structure, that could be exploited for molecular recognition. The designed cavitand was the monoethynylpyrydil cavitand already shown in Chapter 3. We reacted cavitand **2** with $Re(CO)_5Cl$ in order to create a hemicage. The reaction was carried out as previously described, in dry $CHCl_3$ at 65°C for 12 hours. The pure product was obtained by flash chromatography in CH_2Cl_2 and hexane (9:1). Hemicage **10** was then reacted in dry acetone at 65°C overnight with silver trifluoromethanesulfonate (AgOTf) in order to exchange chloride with

triflate to give **11**. ^{1}H NMR of this hemicage showed up-field shift of the α-H of the ethynylpyridine from 8.72 ppm to 8.55 ppm due to the exchange of chloride with triflate, and a corresponding down-field shift of the meta proton of the ethynylpyridine from 7.29 ppm to 7.44 ppm. All the other peaks remained unchanged. Hemiage **11** reacted with 4,4, bypyridine in dry $CHCl_3$ at 60°C for two days. **12** was obtained by precipitation with hexane and was characterized by ^{1}H NMR.

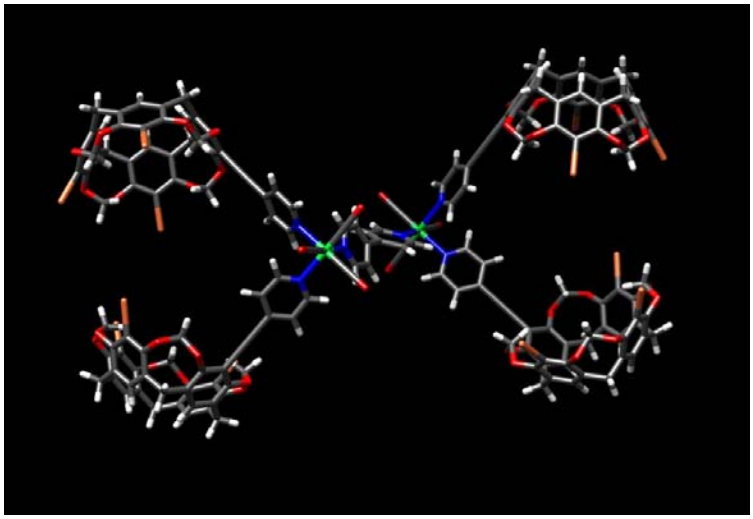

Figure 12 Spartan model of Re-hemicage **12**

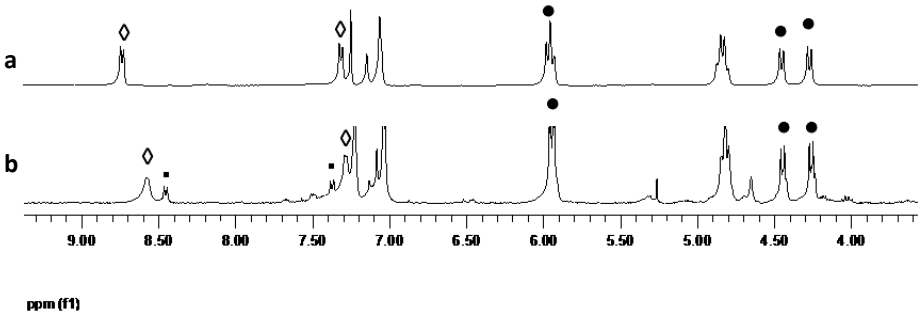

Figure 13 ^{1}H NMR ($CDCl_3$, 300 MHz) a) spectrum of hemicage **11** and b) spectrum of dimeric hemicage **12**. ◊ correspond to H_α and H_β proton of ethynylpyridine, ▪ correspond to Hα and H_β of bypyridinic link and ● to H_{in} and H_{out} of the cavitand bridges

^{1}H NMR of dimeric hemicage **12** showed new peaks at 8.49 ppm and 7.39 ppm with respect to the NMR of hemicage **11** (Figure 13 a and b); these correspond to the H_α and H_β the bypyridinic link, respectively. Moreover,the signal of H_α proton of ethynylpyridine shifted from 8.55 to 8.58 ppm and the symmetry of the molecule remained unchanged with respect to the starting cavitand and the hemicage.
The next step was to combine the approaches of Figure 7 with the hemicage **10** in Scheme 2. In particular, our approach involved at first the formation of a stable hemicage like **10** when additional free ligands are present, followed by a reaction of these ligands with dinuclear complexes such as Pt(tppb)OTf_4 or Pd(tppb)OTf_4 (see Figure 16)

5.2.5 Synthesis of single Re-Pt heteronuclear cage 14

The first goal was to check if the two metals, rhenium and platinum, were compatible on the same molecule. We performed an experiment involving cavitand **1**; we reacted it with 0.5 equivalent of $Re(CO)_5Br$ to create a single hemicage (Scheme 3 hemicage **13**) that was characterized by ^{1}H NMR and ESI MS. We then reacted **13**, in NMR tube, with 1.5 equivalents of Pt(dppp)OTf_2 in order to close the cage (Scheme 3, cage **14**).

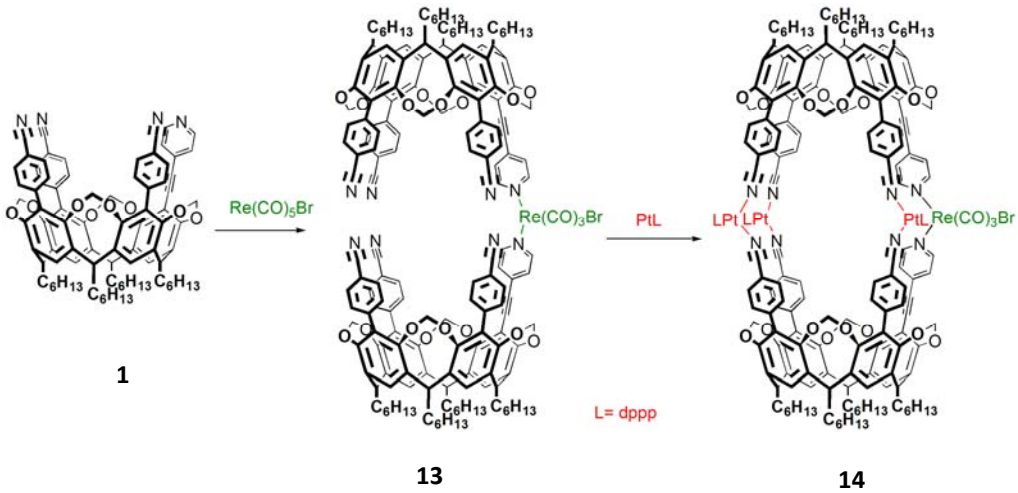

Scheme 3 Synthesis of Re-hemicage **13** and Re-Pt cage **14** starting from cavitand **1** as a building block

^{1}H NMR showed an up field shift for the α-H of the pyridine from 8.72 to 8.43 ppm in agreement with the closure of the cage; H_{out} and H_{in} were splitted with respect to single hemicage giving in total eight doublets, at 5.58 – 5.52 and 5.18 – 5.12 ppm for H_{out} and at 4.35 – 4.25 and 4.22 – 4.17 ppm for H_{in}. The asymmetry of the species in solution was also confirmed by the splitting of the triplet corresponding to the Ar**CH** at 4.81 – 4.77 and 4.75 – 4.65 ppm (Figure 14). ^{31}P NMR showed two signals at – 15.5 ppm and –5.1 ppm correspondent to Pt(dppp) –PhCN interactions. It was not possible to have a complete complexation of all the benzonitrile groups by Pt(II) complex. The mismatch between the angle requirements of Re and Pt complexes, which cannot be accommodated by the rigidly held ligands, can explain the experimental evidence. In any case at least one Pt complex has been coordinated by two benzonitriles.

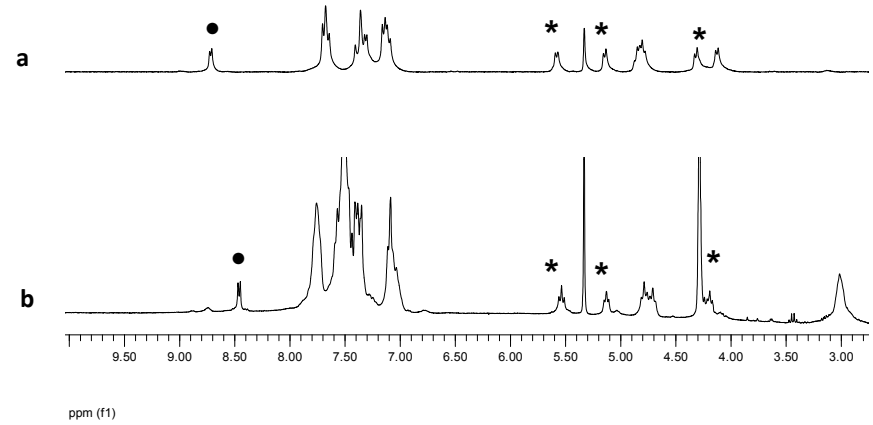

Figure 14 ^{1}H NMR (300 MHz,$CDCl_3$) spectrum of: a) Re-hemicage **13** and b) cage **14** ● correspond to H_α proton of the ethynylpyridine group while * correspond to H_{in} and H_{out} protons of cavitand bridges

5.2.6 Synthesis of cavitand 15 for the heteronuclear dimeric cage 16

To simplify the system we designed a molecule having two ligands at the upper rim of the cavitand: one benzonitrile and one ethynylpyridine. The *AC* isomer is the ideal one for symmetry reasons (Figure 15). In fact some requirements were needed for the design of the new cavitand: a) the presence of one ligand that could react with Re, b) no interaction of the other ligands with Re, c) strong interaction of the second ligand with Pt(II) or Pd(II), d) presence of just

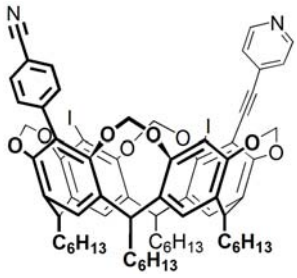

Figure 15 *AC* isomer of cavitand **15**

one benzonitrile, due to the fact that it was not possible to have a single species for cage **14**.

Cavitand **15** is the ideal building block for the synthesis of an innovative dimeric cage as shown in Figure 16. The formation of this heteronuclear dimeric cage involves a stepwise self-assembly, reversed respect to the one we presented in Figure 7: at first a reaction between two cavitands **15** with $Re(CO)_5Br$ to create a single hemicage which, complexing $Pt(dppp)OTf_2$, should lead to the dimeric cage **16**. In this way the PGSE experiments would be truly diagnostic.

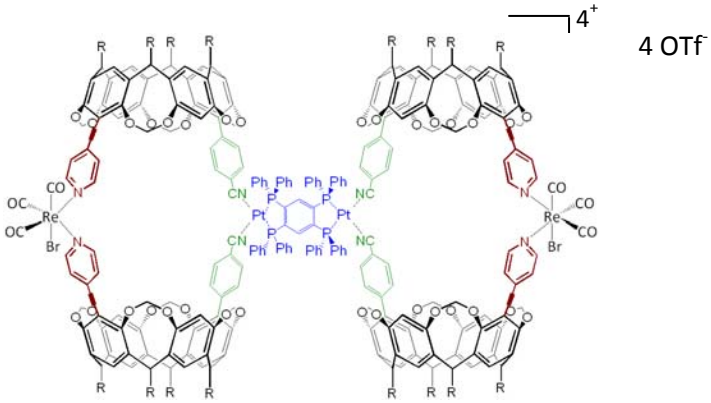

16

Figure 16 Pt-Re dimeric heteronuclear cage **16**

Synthesis of cavitand **15** was carried out reacting the monoethynylpyridine cavitand **2** (see Scheme 2) with 1.5 equivalents of the appropriate boronic acid in dioxane and water for two days at 110 °C. The purification step was difficult due to the presence of several byproducts obtained by partial or complete loss of iodide at the apical positions. We conducted the purification by silica gel chromatography but obtained the *AB* isomer (Figure 17) rather than the *AC* one. The product was characterized by ^{1}H NMR, ESI MS and ^{1}H COSY.

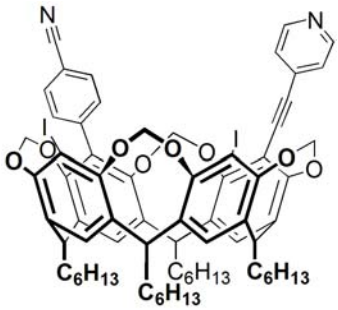

Figure 17 *AB* isomer of cavitand **15**

5.2.7 Synthesis of Re –Pt heteronuclear single cage 18

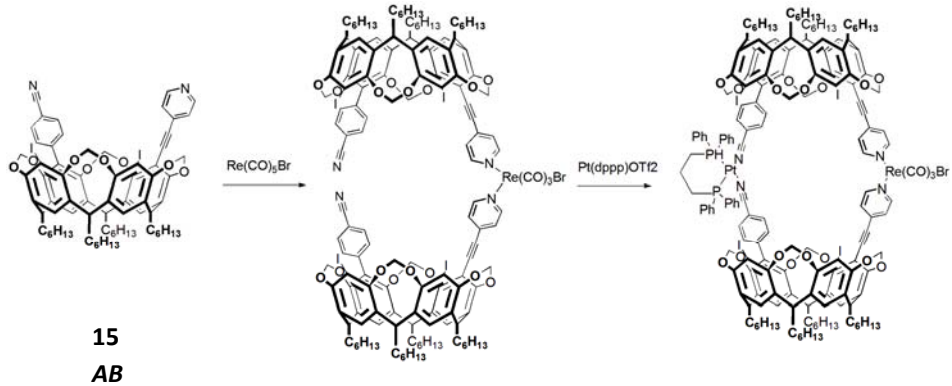

15
AB

17

18

Scheme 4 Stepwise synthesis of Re-single hemicage **17** and Re-Pt single cage **18**

Even if our ideal target was the *AC* isomer, we carried out the synthesis of the Re-Pt heteronuclear cage with the *AB* isomer instead (Figure 18a). At first, we wanted to synthesize a heteronuclear single cage in order to check if, in this case, the formation of our desired product was favored by geometric and steric factors. We reacted cavitand **15** ***AB*** (Scheme 4) with 0.5 equivalent of Rhenium complex to obtain the hemicage **17**. ^{1}H NMR confirmed the formation of this product by showing the typical low field shift of α-H of the pyridine from 8.57 to 8.72 ppm; H_{out} were shifted from 6.01 ppm to 5.97 and from 5.50 ppm to 5.49 – 5.40 ppm ppm. H_{in} were shifted from 4.40 ppm to 4.41– 4.39 ppm and from 4.24 to 4.22 – 4.21 ppm, showing splitted signals (Figure 18b).

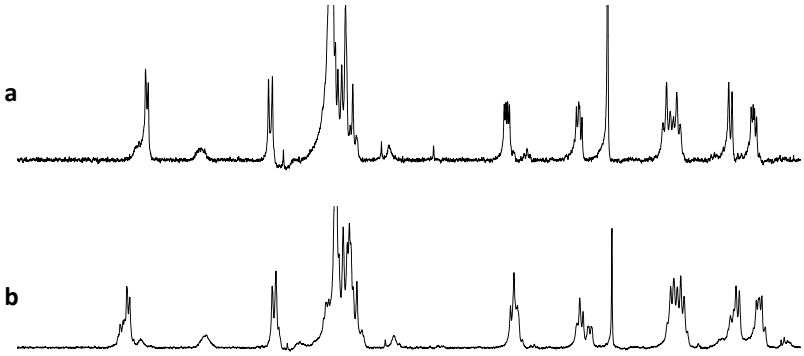

Figure 18 ^{1}H NMR (300 MHz,$CDCl_3$) spectrum of: a) AB isomer of cavitand **15,** b) Re-hemicage **17**

However, in Figure 18b, it was possible to observe that the α-H of the pyridine shows a slightly broad peak. This is due to the fact that cavitand **15** ***AB*** is present as racemic mixture of two enantiomers (Figure 19); in the synthesis of Re-hemicage **17** we observed a broad peak corresponding to α-H proton of pyridine moieties because of the formation of two diastereomeric products (see Figure 20). Only the RS/SR diastereomeric hemicage are suitable for cage closure, whereas the RR/SS diastereomeric hemicage can only lead to oligomeric products.

We carried out anyway the second step, reacting hemicages **17**, in the NMR tube, with 1 equivalent of Pt(dppp)OTf_2 in order to obtain **18.** ^{1}H NMR showed a complicated spectra with broad signals; in particular it was possible to observe that α-H of the pyridine were up-field shifted with respect to the hemicage from 8.72 to 8.47 ppm, in agreement with the formation of the cage. However, the signal was not a doublet but it was possible to observe the presence of two partially overlapped doublets. H_{in} and H_{out} gave very broad

and overlapped signals as a confirmation of the fact that we had more than one species in solution. The ^{31}P NMR exhibited a single peak at – 4.75 ppm, diagnostic of PhCN-Pt-CNPh complexation. From this spectrum it appears that ^{31}P NMR is unable to discriminate between Pt complexes of **17a** and **17b**. On the other side this result bodes well for cage **18** formation. Due to the impossibility to separate cage **18** from the other self-assembly products, this approach has been abandoned.

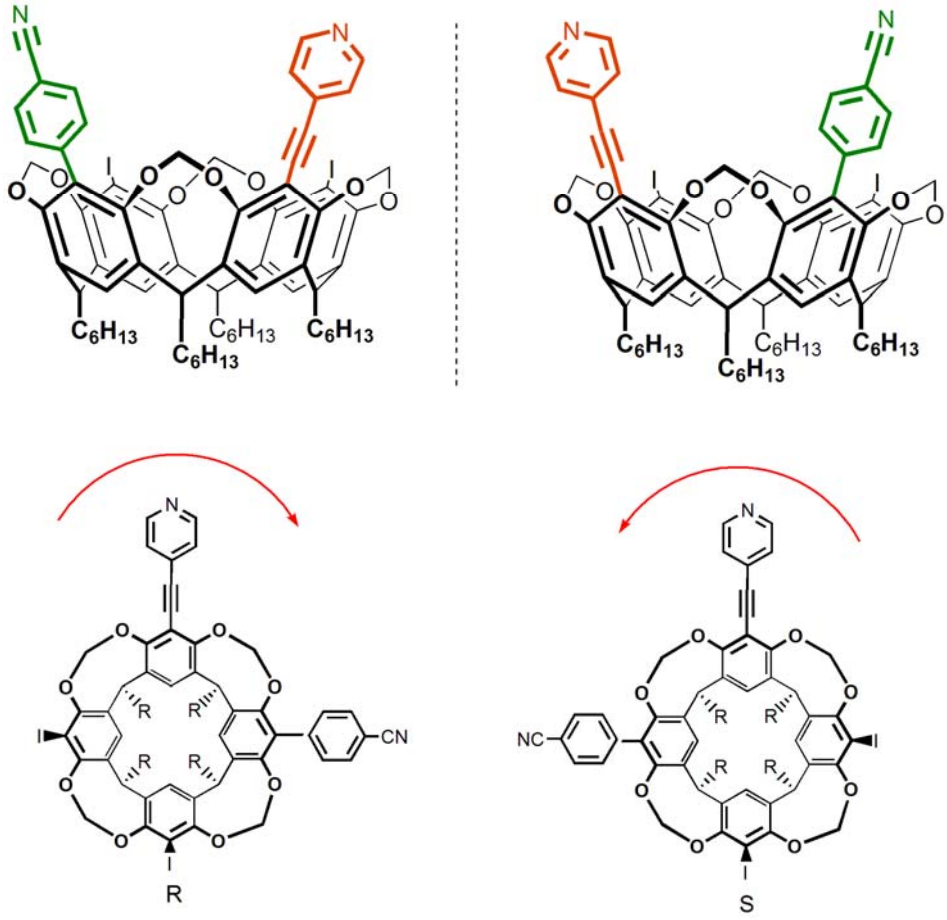

Figure 19 Two enantiomers **15** ***AB***

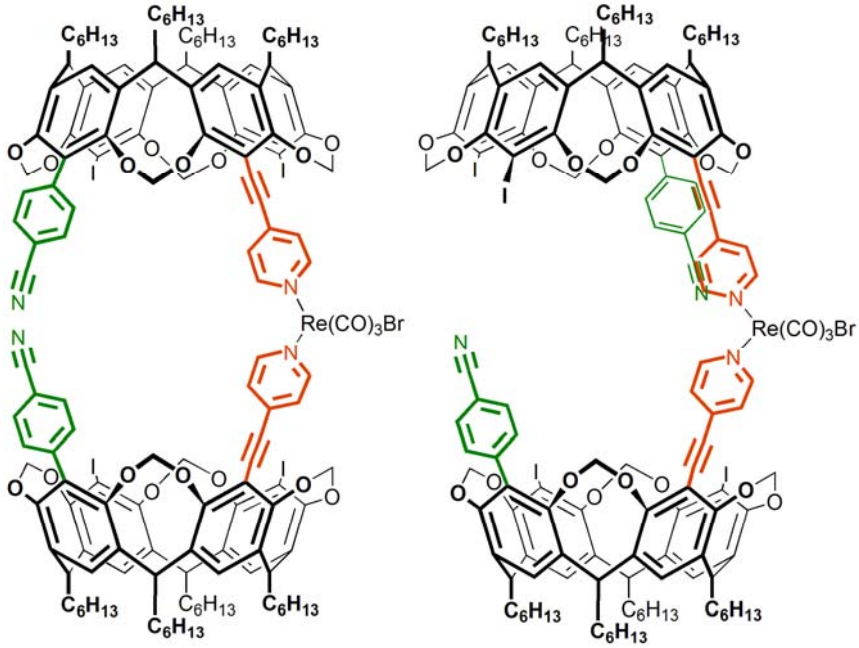

17a: SR compound.shown **17b: RR compound shown.**

Figure 20 Two of the four diastereomers obtained by reacting **15** ***AB*** with Re complex. Just in case of **17a** we have the desired hemicage

In order to obtain heteronuclear dimeric cage **16** we need to start from *AC* isomer of cavitand **15** to avoid the formation of undesired byproducts like in Figure 20.

5.3 Conclusions

We have synthesized tetradentate cavitands differently substituted with the final aim the self-assembly of dimeric cages. We have demonstrated that it is possible to have the dimeric hemicage using a ditopic metal complex whereas it is difficult to have a complete complexation in the following step. We also showed a new successful approach involving a Rhenium complex, that could be applied also in the assembly of more complex cage networks. Access to the ***AC*-15** cavitand is needed to obtain Re-Pt heteronuclear dimeric cage.

5.4 Experimental

General

Reagents and solvents were purchased as reagent grade and used without further purification. Analytical TLC was performed on Merck silica gel 60 F254 precoated plates. Column chromatography was performed using silica gel (Merck 70 − 230 mesh). ^{1}H NMR spectra were recorded at 300 MHz on a Bruker AC 300 Avance spectrometer with solvent peaks as reference.^{31}P NMR spectra were recorded at 162 MHz, on a Bruker 400 spectrometer. ESI MS spectra were measured on a Helwett-Packard 3395 Waters 74 spectrometer.

Pulse gradient spin echo (PGSE) spectroscopy: All the PGSE NMR measurements were performed by using the standard stimulated echo pulse sequence on a Brucker Avance DRX 400 spectrometer equipped with a Great 1/10 gradient unit and QNP probe with a Z-gradient coil, at 296K without spinning. The shape of the gradient was rectangular, their duration (δ) was 4-5 ms, and their strength was varied during the experiments. Different values of relaxtion time were used for different samples and ranging between 130 us and 900 us. The semi-logaririthmic plots of $\ln(I/I_0)$ vs G^2 were fitted using the linear regression for the hemicage **8a** and the cage **8b**. Different values of Δ, "nt" (number of transients) and number of different gradient strengths (G) were used for different samples. The diffusion coefficient D_t that is directly proportional to the slope of the regression line obtained plotting $\log(I/I_0)$ vs G^2 (eq 1), was estimated by measuring the proportional constant using a TMSS that is introduced as internal standard.

Monoethynylpyridine-cavitand (2) 10 mL of dry Et_3N were degassed in a dry flask for 30 minutes. 0.5 g of 2 (3.63×10^{-4} mol), 0.084 g of ethynylpyridinehydrochloride (6.25×10^{-4} mol), 0.0102 g of $Pd(PPh_3)_2Cl_2$ (1.45×10^{-5} mol), 0.0051 g of CuI (3.5×10^{-5} mol), and 0.0057 g of PPh_3 (2.2×10^{-5} mol) were added and the mixture was stirred for 1 hour at 60°C and for 48 hours at 90°C. After cooling to room temperature, $CHCl_3$ was added and the crude product was washed with water and extracted with $CHCl_3$. The pure product was obtained by purification with silica gel flash chromatography with CH_2Cl_2:AcOEt (95:5) as eluant. (35% yield). **^{1}H NMR** ($CDCl_3$, 300 MHz) δ = 8.60 (d, 2H, Py**H$_o$**, J = 5.7 Hz), 7.30 (d, 2H, Py**H$_m$**, J = 6.6 Hz), 7.11 (s, 1H, Ar**H**), 7.08 (s, 1H, Ar**H**), 7.06 (s, 1H, Ar**H**), 5.95 (m, 4H, OCH_{in}**H_{out}**O), 4.84 (m, 4H, ArC**H**), 4.48 (d, 2H, O**CH_{in}**H_{out}O, J_2 = 8.1 Hz), 4.29 (d, 2H, OCH_{in}**H_{out}**O, J_2 = 8.2 Hz), 2.21 (m,

8H, ArCHC**H$_2$**), 1.28 (m, 32H, CH$_2$**CH$_2$CH$_2$CH$_2$CH$_2$**CH$_3$), 0.88 (t, 12H, CH$_2$C**H$_3$**, J = 7.2 Hz); **ESI MS** (*m/z*): 1297.5 [MH]$^+$ [M = $C_{59}H_{64}I_3NO_8$].

Monoethynylpyridine-tribenzonitrile cavitand (1) To a solution of 0.1088 g of **2** (7.45×10^{-5} mol) in 10 mL of dioxane 0.0157 g of Pd(PPh$_3$)$_2$Cl$_2$ (2.24×10^{-5} mol), 0.208 g of 4-(cyanophenyl)boronic acid pinacol ester, (9.07×10^{-4} mol), 0.057 of AsPh$_3$ (1.86×10^{-4} mol), and 0.4748 g of Cs_2CO_3 previously dissolved in 0.25 ml of water, were added. The mixture was stirred under Argon for 40 hours at 110°C. The solution was cooled at room temperature and concentrated under vacuum. Cavitand **1** was obtained as white solid by precipitation with diethylether in 36% yield. **^{1}H NMR** ($CDCl_3$, 300 MHz) δ = 8.55 (d, 2H, PyH$_o$, J = 5.5 Hz), 7.65 (d, 4H, NCAr**H$_o$**, J = 9.1 Hz), 7.59 (d, 2H, NCAr**H$_o$**, J = 9.1 Hz), 7.29 (s, 4H, Ar**H**), 7.21 (d, 2H, Py**H$_m$**, J = 6.4 Hz), 7.15 (d, 4H, NCAr**H$_m$**, J = 9.1 Hz), 7.09 (d, 2H, NCAr**H$_m$**, J = 9.2 Hz), 5.60 (d, 2H, OCH$_{in}$**H$_{out}$**O, J_2 = 7.8 Hz), 5.17 (d, 2H, OCH$_{in}$**H$_{out}$**O, J_2 = 7.7 Hz), 4.80 (m, 4H, ArC**H**), 4.38 (d, 2H, OC**H$_{in}$**H$_{out}$O, J_2 = 7.8 Hz), 4.15 (d, 2H, OC**H$_{in}$**H$_{out}$O, J_2 = 7.7 Hz), 2.30 (m, 8H, ArCHC**H$_2$**), 1.22 (m, 32H, CH$_2$**CH$_2$CH$_2$CH$_2$CH$_2$**CH$_3$), 0.90 (t, 12H, CH$_2$C**H$_3$**, J=7.3 Hz); **ESI MS** (*m/z*): 1222 [MH]$^+$, [M = $C_{80}H_{76}N_4O_8$].

Stepwise self-assembly of Pt dimeric hemicage (8a) and Pt dimeric cage (8b): to a solution of 0.0059 g of cavitand **1** (4.8×10^{-6} mol) in CD_2Cl_2 (0.4 mL) and CD_3NO_2 (0.1 mL, in the NMR tube, 0.00219 g of Pt(tppb)OTf$_2$ were added to give hemicage **8a.** ^{1}H NMR and ^{31}P NMR were recorded. **^{1}H NMR** (CD_2Cl_2 + CD_3NO_2, 300 MHz): δ = 8.87 (d, 8H, Py**H$_o$**) 7.63-7.07 (m, 96H, PPh$_2$ + NCAr**H$_o$**, + NCAr**H$_m$**, + Py**H$_m$**), 5.49 (d, 8H, OCH$_{in}$**H$_{out}$**O, J= 9.6 Hz), 5.08 (d, 8H, OCH$_{in}$**H$_{out}$**O J= 9.6 Hz), 4.82 – 4.78 (m, 16H, ArC**H**), 4.23 (d, 8H, under residual solvent peak), 4.07 (d, 8H, OC**H$_{in}$**H$_{out}$O 9.6 Hz), 2.30 (m, 32H, ArCHC**H$_2$**), 1.22 (m, 128H, CH$_2$**CH$_2$CH$_2$CH$_2$CH$_2$**CH$_3$), 0.90 (t, 96H, CH$_2$C**H$_3$**, J=7.3 Hz); **^{31}P NMR** (CD_2Cl_2 + CD_3NO_2, 300 MHz): 15.53; **ESI MS** (*m/z*): 1522.6 [M^{4+}], 2082 [M^{3+}], M=[$C_{378}H_{346}F_{12}N_{16}O_{44}P_4Pt_2S_4$].

0.0059 g of Pd(dppp)OTf$_2$ were added to the solution to obtain **8b**. ^{1}H NMR and ^{31}P NMR were recorded again. **^{1}H NMR** (CD_2Cl_2 + CD_3NO_2, 300 MHz): 8.80 (m, 8H, Py**H$_o$**) 7.70-7.07 (m, 336H, PPh$_2$ + NCAr**H$_o$**, + NCAr**H$_m$**, + Py**H$_m$**), 5.47 –5.43 (m, 8H, OCH$_{in}$**H$_{out}$**O), 5.06 – 5.01 (m, 8H, OCH$_{in}$**H$_{out}$**O), 4.80 – 4.67 (m, 16H, ArC**H**), 4.24 – 4.21 (m, 8H, under residual solvent peak), 4.11 – 4.05 (m, 8H, OC**H$_{in}$**H$_{out}$O 9.6 Hz), 2.30 (m, 32H, ArCHC**H$_2$**), 1.22 (m, 128H, CH$_2$**CH$_2$CH$_2$CH$_2$CH$_2$**CH$_3$), 0.90 (t, 96H, CH$_2$C**H$_3$**, J=7.3 Hz); **^{31}P NMR** (CD_2Cl_2 + CD_3NO_2, 300 MHz): 17.01, 15.53.

Re-Monoethynylpyridine hemicage (10) To a solution of 0.1 g (7.4×10^{-5} mol) of cavitand **2** in dry $CHCl_3$ under argon, were added 0.013 g of $Re(CO)_5Cl$ (3.7×10^{-5}mol). The solution was refluxed overnight. After cooling to room temperature the solution was concentrated under vacuum and the crude purificated by silica gel chromatography using as eluant Hexane and CH_2Cl_2 (4:6). Yield 85%. **^{1}H NMR** ($CDCl_3$, 300 MHz)**:** δ = 8.72 (d, 4H, Py**H$_o$**, J = 5.7 Hz), 7.29 (d, 4H, Py**H$_m$**, J = 6.6 Hz), 7.13 (s, 2H, Ar**H**), 7.06 (s, 6H, Ar**H**), 5.97 (m, 8H, OCH_{in}**H$_{out}$**O), 4.82 (m, 8H, Ar**CH**), 4.45 (d, 4H, OC**H$_{in}$**H_{out}O, **J_2 = 8.1 Hz**), 4.26 (d, 4H, OC**H$_{in}$**H_{out}O, J_2 = 8.2 Hz), 2.21 (m, 8H, $ArCHCH_2$), 1.28 (m, 32H, CH_2**$CH_2CH_2CH_2CH_2$**CH_3), 0.88 (t, 12H, CH_2C**H$_3$**, J = 7.2 Hz). **ESI MS** not obtained.

Re-Monoethynylpyridine triflate hemicage (11): 0.050 g of **10** (1.6×10^{-5} mol) were dissolved in 10 mL of dry acetone; 0.0085 g of silver trifluoromethansulfunate were added (3.32 1.6×10^{-5} mol) and the mixture was stirred under argon over night at 65°C. After cooling, the solution was concentrated under vacuum and the pure product was precipitated with hexane. **^{1}H NMR** ($CDCl_3$, 300 MHz): δ = 8.55 (d, 4H, Py**H$_o$**, J = 5.7 Hz), 7.44 (d, 4H, Py**H$_m$**, J = 6.6 Hz), 7.12 (s, 2H, Ar**H**), 7.05 (s, 6H, Ar**H**), 5.94 (m, 8H, OCH_{in}**H$_{out}$**O), 4.80 (m, 8H, Ar**CH**), 4.46 (d, 4H, OC**H$_{in}$**H_{out}O, **J_2 = 8.1 Hz**), 4.27 (d, 4H, OC**H$_{in}$**H_{out}O, J_2 = 8.2 Hz), 2.21 (m, 8H, $ArCHCH_2$), 1.28 (m, 32H, CH_2**$CH_2CH_2CH_2CH_2$**CH_3), 0.88 (t, 12H, CH_2C**H$_3$**, J = 7.2 Hz). **ESI MS** not obtained.

Re-4-4'bypyridine monoethynylpyridine cavitand hemicage (12): 0.045 g of **11** (1.4×10^{-5} mol) were dissolved in 5 mL of dry $CHCl_3$ in a dry flask, 0.001 g of 4,4' bypyridine (7.2×10^{-6}mol) were added. The solution was stirred under vacuum at 65°C for 2 days. After cooling to room temperature hexane was added and the resulting solution was collected, leaving apart the remaining precipitate. **^{1}H NMR** ($CDCl_3$, 300 MHz): δ = 8.58 (d, 8H, Py**H$_o$**, J = 5.7 Hz), 8.45 (d, 4H, ByPy**H$_o$**), 7.37 (d, 4H, ByPy**H$_m$**, J = 6.6 Hz), 7.28 (d, 8H, Py**H$_o$**), 7.08 (s, 4H, Ar**H**), 7.04 (s, 12H, Ar**H**), 5.95 (m, 16H, OCH_{in}**H$_{out}$**O), 4.82 (m, 16H, Ar**CH**), 4.44 (d, 8H, OC**H$_{in}$**H_{out}O, J_2 = 8.1 Hz), 4.25 (d, 8H, OC**H$_{in}$**H_{out}O, J_2 = 8.2 Hz), 2.21 (m, 32H, ArCH**CH$_2$**), 1.28 (m, 128H, CH_2**$CH_2CH_2CH_2CH_2$**CH_3), 0.88 (t, 48H, CH_2C**H$_3$**, J = 7.2 Hz). **ESI MS** not obtained.

Re-mono-ethynylpyridine-three-benzonitriles cavitand cage (13): 0.030 g of cavitand **1** (2.34×10^{-5} mol) were dissolved in 20 mL of dry $CHCl_3$, 0.0047 g of $Re(CO)_5Br$ were added and the solution was stirred at 65°C overnight. After cooling to room temperature the mixture was concentrated under vacuum. the pure product was obtained by purification with silica gel chromatography using CH_2Cl_2 and ethyl acetate as eluant (9:1). Yield 80% **^{1}H NMR** ($CDCl_3$, 300

MHz)**:** δ = 8.72 (d, 4H, Py**H$_o$**, J = 5.7 Hz), 7.70 – 7.65 (d, 12H, NCArH$_o$), 7.40 (s, 2H, Ar**H**), 7.36 (s, 6H, Ar**H**), 7.31 (d, 4H, Py**H$_m$**), 5.95 (d, 4H, OCH$_{in}$**H$_{out}$**O), 5.14 (d, 4H, OCH$_{in}$**H$_{out}$**O) 4.83 (m, 8H, Ar**CH**), 4.32 (d, 4H, OC**H$_{in}$**H$_{out}$O, J$_2$ = 8.1 Hz), 4.13 (d, 4H, OC**H$_{in}$**H$_{out}$O, J$_2$ = 8.2 Hz), 2.33 (m, 16H, ArCH**CH$_2$**), 1.28 (m, 64H, CH$_2$**CH$_2$CH$_2$CH$_2$CH$_2$**CH$_3$), 0.88 (t, 24H, CH$_2$C**H$_3$**, J = 7.2 Hz); **ESI MS** *m/z*= 2878.2 [M – CO]$^+$.

Re-Pt-single heteronuclear cage (14): to a solution of 0.003 g of hemicage **13** (1.03 × 10^{-6} mol), in the NMR tube, we added 0.0014 g of Pt(dppp)OTf$_2$ (1.54 × 10^{-6} mol) and we recorded both ^{1}H and ^{31}P NMR spectra. **^{1}H NMR** (CDCl$_3$, 300 MHz) δ = 8.46 (d, 4H, Py**H$_o$**, J = 6.3 Hz), 7.76 – 7.03 (m, 84H, NCArH$_o$ + Ar**H** + Py**H$_m$** + PPh$_2$), 5.56 – 5.53 (m, 4H, OCH$_{in}$**H$_{out}$**O), 5.15 – 5.10 (m, 4H, OCH$_{in}$**H$_{out}$**O) 4.81 – 4.68 (m, 8H, Ar**CH**), 4.22 – 4.19 (m, 4H, OC**H$_{in}$**H$_{out}$O, partially under residual solvent peak), 2.33 (m, 16H, ArCH**CH$_2$**), 1.28 (m, 64H, CH$_2$**CH$_2$CH$_2$CH$_2$CH$_2$**CH$_3$), 0.88 (t, 24H, CH$_2$C**H$_3$**, J = 7.2 Hz); **^{31}P NMR** δ = – 5.1 ppm **ESI MS** not obtained

Mono-ethynylpyridine mono-benzonitrile cavitand (15): to a solution of 0.200 g of cavitand **2** (1.47 × 10^{-4} mol); in 35 mL of dioxane, 0.043 g of 4-(cyanophenyl)boronic acid pinacol ester (1.91 × 10^{-4} mol); 0.0061 g of Pd(PPh$_3$)$_2$Cl$_2$ (8.82 × 10^{-6} mol), 0.0022 of AsPh$_3$ (7.35 × 10^{-6} mol), and 0.047 g of Cs$_2$CO$_3$ (2.8× 10^{-4} mol) previously dissolved in 0.25 ml of water, were added. The mixture was stirred under Argon for 40 hours at 110°C. The solution was cooled at room temperature and concentrated under vacuum. The pure product was obtained by purification with silica gel chromatography using as eluant CH$_2$Cl$_2$ and Ethyl Acetate (95:5) followed by a purification with preparative TLC using CH$_2$Cl$_2$ and Ethanol (100:2). Yield 25% **^{1}H NMR** (CDCl$_3$, 300 MHz) δ = 8.58 (d, 2H, Py**H$_o$**, J = 6.6 Hz), 7.67 (d, 2H, Py**H$_m$**, J = 6.6 Hz), 7.18 – 7.08 (m, 6H, Ar**H**, NCAr**H$_m$**, NCAr**H$_o$**), 6.05 – 6.01 (m, 2H, OCH$_{in}$**H$_{out}$**O), 5.53 (m, 2H, OCH$_{in}$**H$_{out}$**O), 4.86 – 4.79 (m, 4H, Ar**CH**), 4.42 (m, 2H, OC**H$_{in}$**H$_{out}$O), 4.26 (m, 2H, OC**H$_{in}$**H$_{out}$O), 2.29 (m, 8H, ArCH**CH$_2$**), 1.28 (m, 32H, CH$_2$**CH$_2$CH$_2$CH$_2$CH$_2$**CH$_3$), 0.88 (t, 12H, CH$_2$C**H$_3$**, J = 7.2 Hz); **ESI MS (***m/z*): 1327.7 [MH]$^+$, [M = C$_{70}$H$_{76}$I$_2$N$_2$O$_8$].

Re-Mono-ethynylpyridine mono-benzonitrile hemicage (17a and 17b): 0.016 g of **15** (1.13 × 10^{-5} mol) were dissolved in 10 mL of dry CHCl$_3$, 0.0024 g of Re(CO)$_5$Br (5.65 × 10^{-6} mol) were added and the solution was stirred under argon at 65°C overnight. After warming to room temperature the solution was concentrated under vacuum. The pure product was obtained by silica gel

chromatography using CH_2Cl_2 and Hexane (95:5). Yield 77%. **^{1}H NMR** ($CDCl_3$, 300 MHz) δ = 8.77 – 8.69 (m, 4H, Py**H_o**), 7.67 – 7.63 (m, 4H, Py**H_m**), 7.17 – 7.07 (m, 16H, Ar**H**, NCAr**H_m**, NCAr**H_o**), 5.98 – 5.93 (m, 4H, OCH_{in}**H_{out}**O), 5.49 – 5.40 (m, 4H, OCH_{in}**H_{out}**O), 4.84 – 4.74 (m, 8H, Ar**CH**), 4.41 – 4.39 (m, 4H, O**CH_{in}**H_{out}O), 4.21 – 4.19 (m, 4H, O**CH_{in}**H_{out}O), 2.29 (m, 16H, ArCH**CH_2**), 1.28 (m, 64H, CH_2**$CH_2CH_2CH_2CH_2$**CH_3), 0.88 (t, 24H, CH_2C**H_3**, J = 7.2 Hz). **ESI MS** not obtained.

Pt-Re-Mono-ethynylpyridine mono-benzonitrile cage (18): To a solution of 0.0035 g of **17** (1.15×10^{-6} mol) were added 0.00056 g of Pt(dppp)OTf_2 (5.78×10^{-7} mol)in the NMR tube. ^{1}HNM and ^{31}P NMR were recorded **^{1}H NMR** ($CDCl_3$, 300 MHz) δ = 8.48 – 8.43 (m, 4H, Py**H_o**), 7.82 – 7.06 (m, 36H, Py**H_m** + Ar**H**, NCAr**H_m** + NCAr**H_o** + PPh_2), 5.99 – 5.89 (m, 4H, OCH_{in}**H_{out}**O), 5.54 – 5.51 (m, 4H, OCH_{in}**H_{out}**O), 4.84 – 4.70(m, 8H, Ar**CH**), 4.51 – 4.07 (m, 8H, O**CH_{in}**H_{out}O), 2.25 (m, 16H, ArCH**CH_2**), 1.28 (m, 64H, CH_2**$CH_2CH_2CH_2CH_2$**CH_3), 0.88 (t, 24H, CH_2C**H_3**). **^{31}P NMR** δ = – 5.1 ppm

5.5 References

1. D. L. Caulder and K. N. Raymond, *Acc. Chem. Res.*, 1999, **32**, 975-982.
2. B. Olenyuk, M. D. Levin, J. A. Whiteford, J. E. Shield and P. J. Stang, *J. Am. Chem. Soc.*, 1999, **121**, 10434-10435.
3. T. Yamamoto, A. M. Arif and P. J. Stang, *J. Am. Chem. Soc*, 2003, **125**, 12309-12317.
4. J. Klein, C. W. Lehmann, H. W. Schmidt and W. F. Maier, *Angew. Chem.-Int. Edit.*, 1998, **37**, 3369-3372.
5. M. Fujita, M. Tominaga, A. Hori and B. Therrien, *Acc. Chem.Res.*, 2005, **38**, 369-378.
6. T. Schroder, R. Brodbeck, M. C. Letzel, A. Mix, B. Schnatwinkel, M. Tonigold, D. Volkmer and J. Mattay, *Tetr. Lett.*, 2008, **49**, 5939-5942.
7. E. Menozzi, M. Busi, R. Ramingo, M. Campagnolo, S. Geremia and E. Dalcanale, *Chem.-Eur. J.*, 2005, **11**, 3136-3148.
8. A. Macchioni, G. Ciancaleoni, C. Zuccaccia and D. Zuccaccia, *Chem. Soc. Rev.*, 2008, **37**, 479-489.
9. D. Zuccaccia, S. Sabatini, G. Bellachioma, G. Cardaci, E. Clot and A. Macchioni, *Inorg. Chem.*, 2003, **42**, 5465-5467.
10. D. Zuccaccia, L. Pirondini, R. Pinalli, E. Dalcanale and A. Macchioni, *J. Am. Chem. Soc.*, 2005, **127**, 7025-7032.

11. G. Bellachioma, G. Ciancaleoni, C. Zuccaccia, D. Zuccaccia and A. Macchioni, *Coord. Chem. Rev.* 2008, **252**, 2224-2238.
12. K. D. Benkstein, J. T. Hupp and C. L. Stern, *Angew. Chem.-Int. Edit.*, 2000, **39**, 2891-2893.

Fluorescent Probes for Intracellular Manganese(II)

6

6.1 Introduction

6.1.1 Manganese in biological processes

All microorganisms require trace levels of manganese for survival; the list of enzymes that rely on manganese for their activity is numerous. Manganese is utilized as a cofactor by various aerobic organism for defensive antioxidant enzyme catalase and superoxide dismutase. Photosynthetic bacteria employ manganese in oxygen producing pathways, and manganese-dependent enzymes have been implicated in diverse metabolic processes including DNA synthesis, sugar metabolism, and protein glycosylation. Because manganese plays a role in so many vital cellular functions, virtually all organisms have evolved specialized systems devoted to the uptake and acquisition of this trace metal. Accumulation of manganese must also be tightly controlled , since the metal is potentially toxic. For instance, in many cases the uptake of manganese is often regulated by its bioavailability.

In human body manganese (Mn) is both essential for regulating neurological and skeletal functions but it is also toxic at excessive levels of exposure. Excessive inhalation, as a result of exposure to industrial and environmental emissions, can cause neurological damage, which may manifest as memory deficit, loss of motor control. A number of clinical studies have demonstrated that traditional methods of monitoring Mn exposure in body fluids, for instance blood, plasma/serum and urine are limited use and reflect only the recent exposure[1-3].

Disease States Related to Manganese Deficiency or Excess

Acromegaly (human growth hormone deficiency)[398]
Alcoholism[399-401]
Amyotrophic lateral sclerosis[402]
Atherosclerosis[403]
Arthritis (rheumatoid)[404,405]
Cancer[406]
Catabolic disease[407]
Diabetes[408-412]
Down's syndrome[413]
Epilepsy[414]
Eye disorders[415]
Iminodipeptiduria (prolidase deficiency)[416-418]
Manganese rickets[419]
Morvan's fibrillary chorea[420]
Motor neuron disease[421,422]
Osteoporosis[423]
Otolith defects[424]
Perthe's disease[425]
Phenylketonuria[426]
Thyroid disease[427]
Viral hepatitis[428]
Viral meningitis[429]
Wilson's disease[430]

Figure 1 Table of disease caused by lack or excess of Manganese reported by Dorothy J. Klimis-Tavantzis,[4, 5]

Manganese is essential for the normal functioning of mammalian tissues and organs. Without exception, all human tissues contain manganese in concentrations that are remarkably constant throughout most of life [6]. A lower concentration of Mn is typically is found in the brain relative to other organs (i.e. liver, pancreas, and kidney). However, chronic manganese poisoning is often characterized clinically mainly by neurological and psychiatric symptoms. In fact, the brain has the tendency to retain manganese for longer periods than other organs; this could be due to its basic inability to eliminate the excess of the metal. Various pathologies are associated with a lack or excess of manganese; such as Parkinson's disease, tremor, ataxia and hallucinations (Figure 1). Chronic excess of manganese causes damage to both grey and white matter of the brain as well as motor neurons. Maternal exposure to manganese, either preconceptions or during pregnancy, can lead to fetal developmental defects, especially involving nervous system.

Regions	Mn Concentration (μg/g dry tissue weight)
Frontal Lobe	
1 Frontal Pole	1.41 ± 0.11
2 Precentral gyrus (Superior 1/3)	1.68 ± 0.45
3 Precentral gyrus (Medial 1/3)	1.39 ± 0.14
4 Precentral gyrus (Inferior 1/3)	1.69 ± 0.28
Occipital Lobe	
5 Occipital Pole	1.60 ± 0.18
6 Calcarine cortex (cuneus)	1.55 ± 0.15
Parietal Lobe	
7 Postcentral gyrus (Superior 1/3)	1.98 ± 0.33
8 Postcentral gyrus (Medial 1/3)	1.49 ± 0.22
9 Postcentral gyrus (Inferior 1/3)	1.52 ± 0.24
10 Supramarginal gyrus	1.17 ± 0.07
Temporal Lobe	
11 Uncus	1.13 ± 0.15
12 Cingulate gyrus (Anterior 1/3)	1.29 ± 0.15
13 Cingulate gyrus (Medial 1/3)	1.30 ± 0.19
14 Cingulate gyrus (Posterior 1/3)	1.15 ± 0.13
15 Mammilay bodies	1.89 ± 0.19
16 Superior colliculus	1.21 ± 0.12
17 Inferior colliculus	1.38 ± 0.17

Regions	Mn Concentration (μg/g dry tissue weigh
18 Olfactory bulb	3.36 ± 0.69
19 Optic nerve	1.08 ± 0.14
20 Optic chiasm	1.30 ± 0.20
21 Caudate nucleus (head)	1.29 ± 0.12
22 Caudate nucleus (body)	1.41 ± 0.14
23 Caudate nucleus (tail)	1.89 ± 0.14
24 Putamen	1.67 ± 0.11
25 Globus pallidus	1.40 ± 0.09
26 Thalamus	0.94 ± 0.12
27 Frontal lobe, white matter	0.72 ± 0.09
28 Occipital lobe, white matter	0.88 ± 0.11
29 Parietal lobe, white matter	0.81 ± 0.13
30 Temporal lobe, white matter	0.74 ± 0.07
31 Red nucleus	1.08 ± 0.12
32 Substantia nigra	1.02 ± 0.13
33 Inferior olivary nucleus	1.02 ± 0.09
34 Superior olivary nucleus	0.92 ± 0.14
35 Pineal gland	4.20 ± 1.03
36 Cerebellum (vermal cortex, superior half)	1.14 ± 0.08
37 Cerebellum (vermal cortex, inferior half)	1.35 ± 0.18
38 Cerebellar hemisphere (cortex)	1.37 ± 0.15
39 Tuber cinereum	2.19 ± 0.33

Figura 2 Manganese distribution in human body

6.1.2 Manganese in MRI

Magnetic resonance imaging (MRI), or nuclear magnetic resonance imaging (NMRI), is primarily used in the specialty of radiology/physiology to visualize human body and its pathology. MRI provides significantly higher contrast among different soft tissues types than computer tomography (CT) does, as result it is especially useful in neurological, musculoskeletal, cardiovascular, and oncological imaging. Rather than using ionizing radiation, it employs a magnetic field to align the nuclear magnetization of (usually) hydrogen atoms of tissue water. Radiofrequency fields are used to systematically alter the alignment of this magnetization, causing the hydrogen nuclei to produce a detectable magnetic field. This signal can be manipulated by additional magnetic fields to acquire sufficient information to construct an image of the body. The contrast between different tissues in MRI is generally due to three parameters: the volumetric protons density, and their two magnetic relaxations times T_1 and T_2. T_1 is called *longitudinal* or *spin-lattice* relaxation time, and it refers to the time that magnetization vectors need to reach the equilibrium after perturbation. T_2 is called *transverse* or *spin-spin* relaxation time and it is due to the decay of magnetisation along x and y axis; in fact, different spins experience a slightly different magnetic field due to random fluctuation of the field itself. As it is difficult and dangerous to modify the amount of water or fat in vivo, the agents used to increase tissue contrast act by modifying the relaxation times.

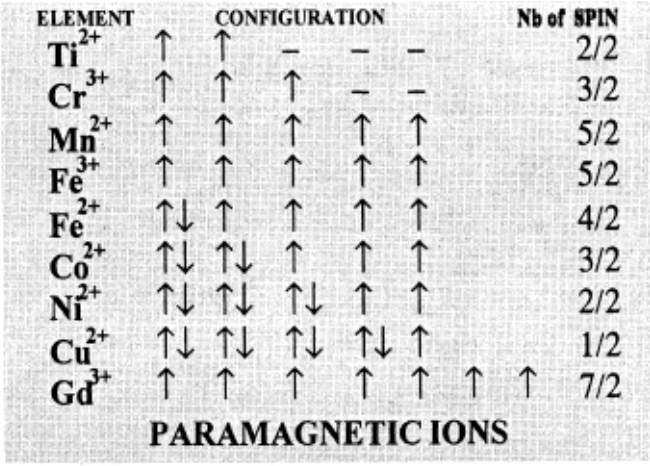

Figure 3 Table of metals used as contrast agent for their unpaired electrons

It can be demonstrated that the strength of dipolar interaction between unpaired electrons and water molecules induces a dramatic change in T_1 and T_2. The compounds that provide such dipolar interactions are referred as "contrast agent" (Figure 3). The most commonly used, due to its seven unpaired electrons, is Gd^{3+}; whereas Mn^{2+} is still under clinical investigation.
With five unpaired electrons, manganese serve as a highly efficient contrast agent. An interesting study was carried out by Turnbull's laboratory at NYU Medical School in wich $MnCl_2$ was used to increase T_1 in a technique referred to as MEMRI (Manganese Enhanced MRI). In this study systemically-administered manganese (Mn) helped to reveal fine anatomical details in T_1-weighted MR images of neonatal mouse brains (Figure 4). [7, 8]

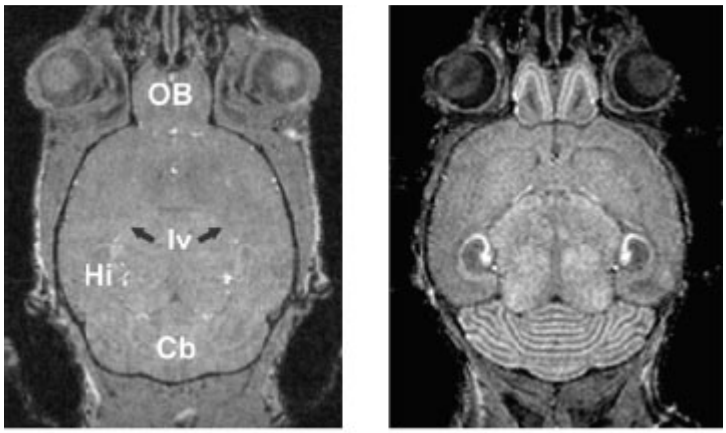

Figure 4 Mouse brain images: after addition of $MnCl_2$(right image) and without addition of $MnCl_2$ (left image)

Advantages of MEMRI technique include its non-invasive nature and the fact that can be monitored; at the same time however is not well-suited for monitoring lower physiological level of manganese. For this reason we have developed a new manganese monitoring approach together with Turnbull laboratory.
In this Chapter we report the innovative use of "ratiometric displacement for detection of intracellular manganese(II)."

6.2 Results and discussion

Recently Canary reported a sensor system to monitor ratiometrically the paramagnetic Cu^{2+} ion (Figure 5) in aqueous solution.[9] Two commercially available dyes were employed, Calcein blue (CB) (ligand 1) and Fluozin-1 (FZ1) (ligand 2). An equimolar Cd^{2+} was employed as the reporter ion. At the beginning, Cd^{2+} was bound to ligand 1 and the formed complex was strongly fluorescent ("on"), while ligand 2 kept "free" and had weak fluorescence ("off"). When adding Cu^{2+}, ligand 1 preferred to bind Cu^{2+}, releasing Cd^{2+}. This caused the effect of quenching the fluorescence and switching ligand 1 "off". The liberated Cd^{2+} was caught by ligand 2 whose fluorescence was then turned "on". This Cu^{2+} sensing system has a μM scale sensitivity and works well in the presence of biologically abundant Na^{+}, K^{+}, Mg^{2+}, Ca^{2+}

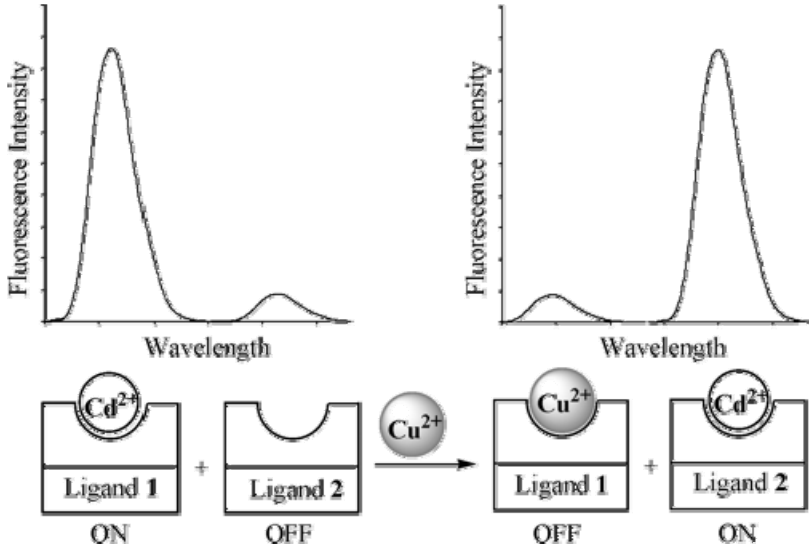

Figure 5 Ratiometric displacement reported by Canary's group for determination of Cu2+

The same approach was used for determination of manganese(II) (Figure 6). Solution experiments showed that the metal-swap displacement assay worked effectively for Mn(II) but with reduced sensitivity. With an equimolar solution

of Cd(II), CB, and Fz1, strong blue and weak green fluorescence is observed with excitation at 350 and 493 nm, respectively. As the concentration of Mn(II) is added, the blue fluorescence diminishes and the green fluorescence increases intensity proportionally. Overall, the 435 nm fluorescence is quenched by a factor of 12, while that at 518 increases by a factor of 7 (Figure 7). Since complexation of Mn(II) quenches CB and Cd(II) causes Fz1 to show increased fluorescence quantum yield, the observed behavior is consistent with the expectation that Mn(II) competes with Cd(II) for complexation of the stronger chelator (CB), liberating Cd(II) to form a complex with Fz1.

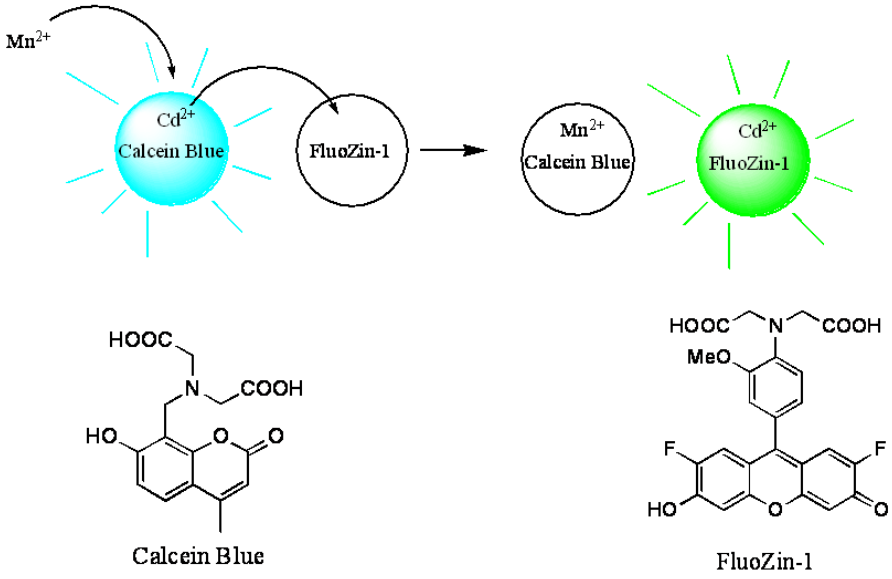

Figure 6 .Metal displacement assay reported by Canary's group for Manganese (II) in solution

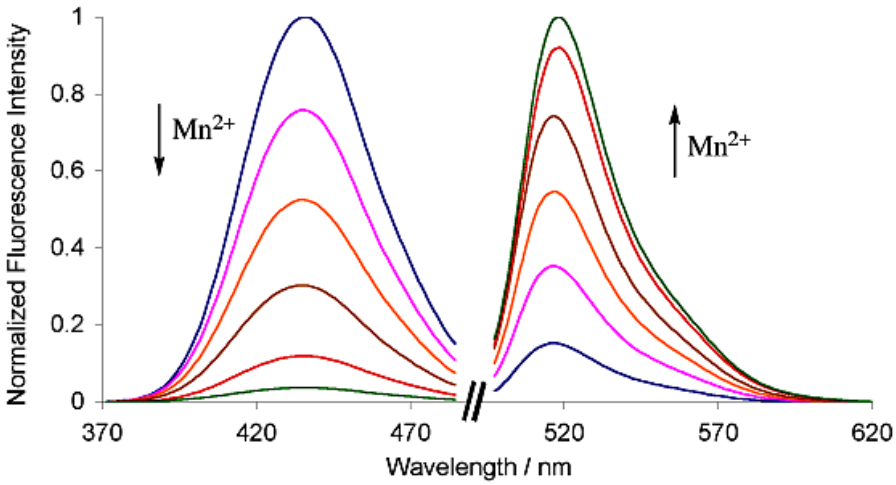

Figure 7.Normalized fluorescence response for the titration of aqueous solution (pH=7.2) containing 10 µM calcein blue, 10 µM fluozin-1, 10 µM $Cd(ClO_4)_2$, 50 mM HEPES and 100 mM KNO_3 with $MnCl_2$. Shown spectra contain 0, 5, 10, 20, 40, 60, 80, 100 and 1000 µM $MnCl_2$.

The basis for the reduced sensitivity of the system to Mn(II) than to Cu(II) can be rationalized on the basis of relative binding constants.

Lower association of Mn(II) compared with Cu(II) would be expected as predicted by the classic Irving-Williams series. Association constants of Mn(II) and Cd(II) were determined by direct titration and by competition. Mn(II) is less competitive for complexation with CB as indicated by the relative association constants for Mn(II) (1.7×10^7 M^{-1}) vs. Cd(II) (1.4×10^8 M^{-1}). A direct competition experiment for Mn(II) and Cd(II) for CB indicated a 7.5-fold preference for Cd(II). Our association constant for Cd(II) differs slightly from that in the literature. (Phillips, D.; Brignac, P., Jr. Anal Lett 1971, 4, 867) This contrasts to the very strong association of Cu(II) with CB (1.9×10^{14} M^{-1}). Fortunately, addition of excess Mn(II) still resulted in ratiometric behavior as shown in Figure 7. With 10 µM concentrations of the two dyes and Cd(II),

ratiometric behavior was observed over a range from 5-1000 µM. Addition of excess Mn(II) results in effective competition for CB. It is fortunate that the excess Mn(II) does not interfere with the binding of Cd(II) to Fz1. This contrasts the case with Cu(II), where addition of an excess of Cu(II) above the concentration of the dyes resulted in quenching of fluorescence of Fz1.

The further step was to apply this approach *in vitro;* in order to see if we could detect manganese also in biological environment. We utilized at first A549 cell line

6.2.1 A549 cell line experiments

Human lung carcinoma cell line A549 was examined as it was known to take up transition metal ions from media containing millimolar concentrations of metal salt [10] and because the cells were known to be reasonably tolerant to $CdCl_2$[11]. The dyes used in solution are not cell permeable due to their hydrophilicity that results from the negative charges of the carboxylate groups at physiological pH. Therefore, acetoxymethyl (AM) esters of calcein blue and fluozin-1 were used (Figure 8), as these neutral derivatives cross the cell membrane and are then hydrolysed by intracellular esterases within one hour.[12]

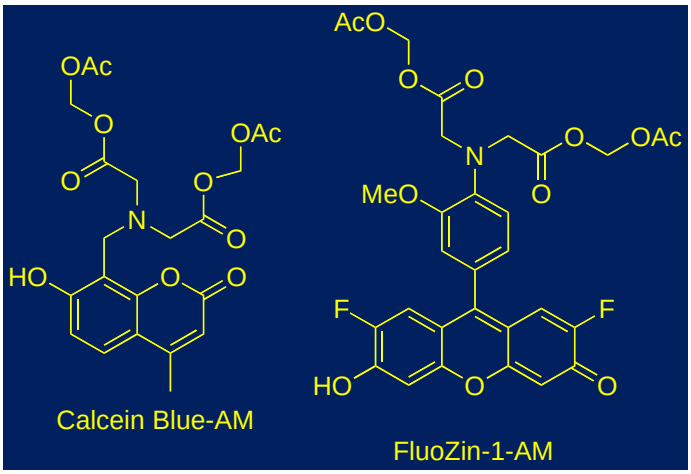

Figure 8. Structure of Calcein Blue AM and Fluozin 1 AM.

We carried out the experiment when cells reached 70% of confluence(concentration in the dish). The process involved three steps: a) addition of the $MnCl_2$ water solution to the cell medium and incubation for three hours, b)after washing, addition of the two dyes' solution and incubation for one hour, c)addition of $CdCl_2$ solution to the medium and incubation for another hour; we took pictures after washing carefully. For the initial experiments, measurable responses to Mn(II) were observed by incubating the cells in F12 medium containing 10 mM $MnCl_2$ and 1 mM $CdCl_2$.

The Mn(II) assay is illustrated in Figure 9. The A549 cells lacking manganese (top row) showed strong blue fluorescence due to [Cd(CB)] formation. Meanwhile, the FITC channel reported weak fluorescence of the uncomplexed fluozin-1. The DPAI signal was considerably quenched in the cells containing manganese because of the displacement of Cd(II) by Mn(II) and formation of Mn(CB). The displaced Cd(II) was bound by fluozin-1, enhancing its fluorescence, as reported by the FITC channel.

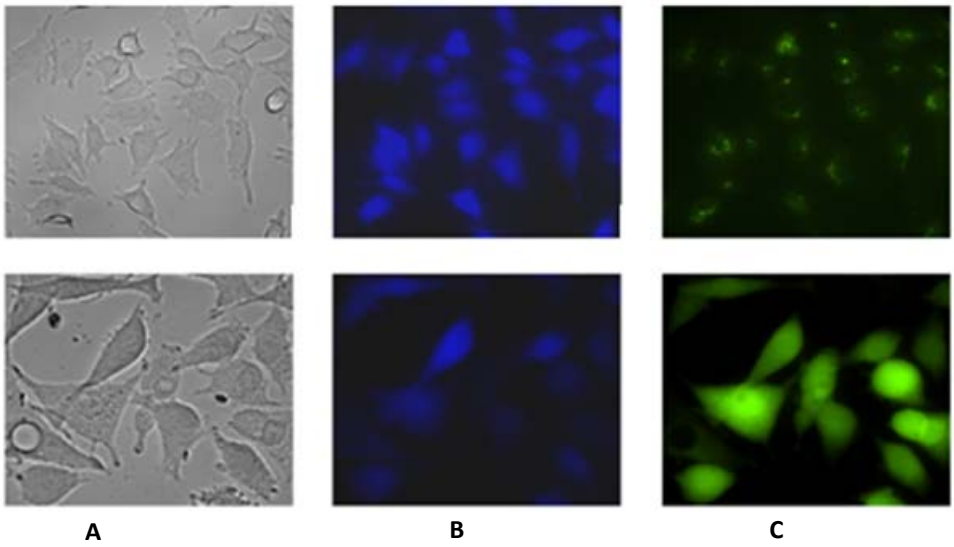

Figure 9 Assay of Mn(II) in A549 cells. Images were obtained upon treating A549 cells containing Mn^{2+} (bottom row) and lacking Mn^{2+} (top row) with the displacement assay ingredients, calcein blue-AM, fluozin-1-AM and $CdCl_2$. **A** top and bottom row: Brightfield transmission images; (**B** top and bottom): In the absence of Mn^{2+}, DAPI channel showed strong fluorescence, and FITC channel showed weak staining (**C**) In the presence of Mn^{2+}, DAPI channel reported the quenching of calcein blue and enhancement of fluozin-1 fluorescence in the FITC channel (**C** bottom row).

In this assay, the presence of Mn(II) in A549 cells can be detected when external 10 mM $MnCl_2$ was present in the cell medium (exactly how much Mn(II) in the cells was unknown). However, this concentration of Mn(II) was on the cusp of tolerance for these cells. Lower concentrations of Mn(II) could not be detected, and it was not clear whether the sensitivity was due to the method or due to the impermeability of the cells to Mn(II) at sub-mM concentrations.

6.2.2 Transfection

Transfection is the process of introducing nucleic acids into eukaryotic cells by non-viral methods. There are two classes of cellular transfection. In the *transient transfection* the introduced DNA does not insert in the into the host genome, therefore genes producted are only transiently expressed. In *stable transfection,* by contrast*,* DNA is incorporated into a host chromosome, and it is therefore replicated in daughter cells.

In order to test the method at lower Mn(II) concentrations, the cells were transfected with DMT-1 (divalent metal transporter 1). DMT1 is a divalent metal transporter conserved from prokaryotes to higher eukaryotes that exhibits an unusually broad substrate range, including Fe^{2+}, Zn^{2+}, Mn^{2+}, Cu^{2+}, Cd^{2+}, Co^{2+}, N^{i2+}, and Pb^{2+}, and mediates active proton-coupled transport.

Transient transfection protocol gave a transfection efficiency of approximately 30%.

We carried out the experiment with transfected cells using the same protocol as before for not transfected ones.; we were able to detect 10 μM concentration as shown in Figure 10.

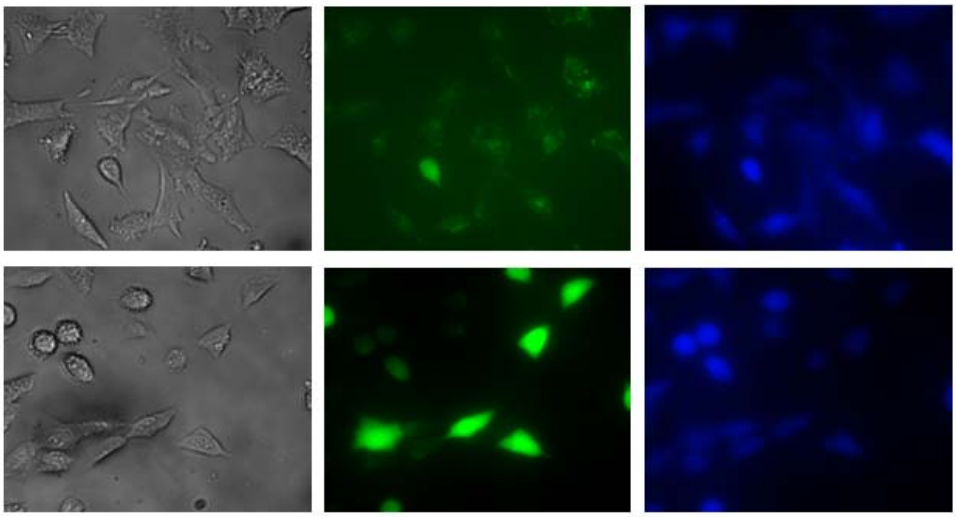

Figure 10 Assay of Mn(II) in transfected A549 cells. Images were obtained upon treating transfected A549 cells containing Mn^{2+} (bottom row) and lacking Mn^{2+} (top row) with the displacement assay ingredients, calcein blue-AM, fluozin-1-AM and $CdCl_2$. In the absence of Mn^{2+}, DAPI channel showed strong fluorescence (**C** top row), and FITC channel showed weak staining (**B** top row) In the presence of Mn^{2+}, DAPI channel reported a slight quenching of calcein blue (C bottom row) and enhancement of fluozin-1 fluorescence (**B** bottom row).

As shown in Figure 10 the green field experienced an enhancement of fluorescence due to presence of manganese(II) whereas the blue field showed a slightly less fluorescence due to the quenching. In order to validate the this result, negative control experiment was conducted. Non-transfected A549 cell were analyzed under the same conditions as the previous experiment. We observed that there was no difference in fluorescence between cells with added manganese and cells without manganese (Figure 11). That suggested that for this kind of experiment in vitro we need transfection to decrease the amount of manganese detectable.

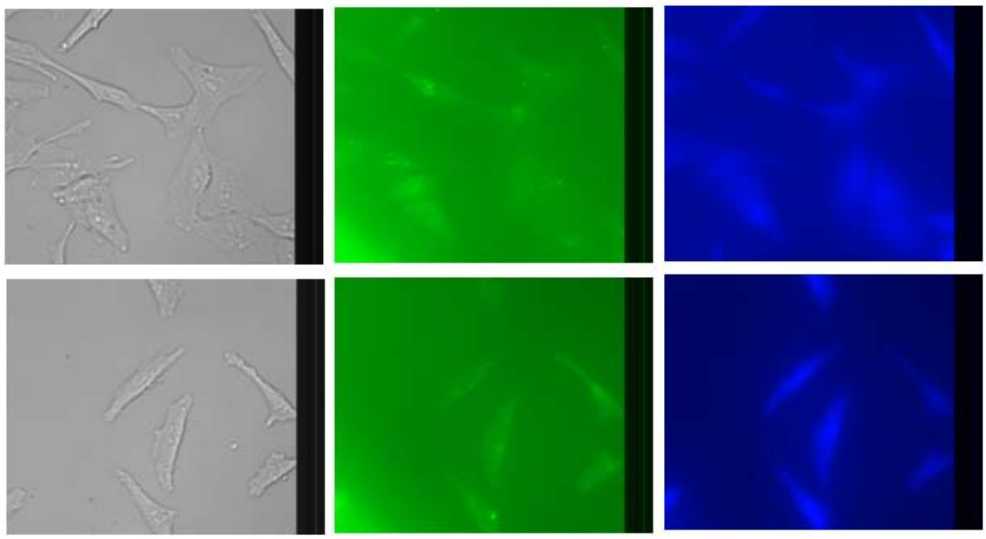

Figure 11 Assay of Mn(II) in non-trasnfected A549 cells. Images were obtained upon treating A549 cells containing 5μM of Mn^{2+} (bottom row) and lacking Mn^{2+} (top row) with the displacement assay ingredients, calcein blue-AM, fluozin-1-AM and $CdCl_2$. Without transfection there is no difference between the two rows (with or without Manganese)

The fact that transient transfection protocol gave a yield that was around 30%, made our sample to be not homogeneus; this is the reason why we decided to perform experiments using stable transfected cells. We utilized HEK 293 cell lines that were provided by Buffalo University.

6.2.3 HEK 293 Cell line experiments

HEK 293 are a specific cell line originally derived from human embryonic kidney cells grown in tissue culture. Those cells were stable transfected with DMT1. DMT1 has at least four isoforms (different forms of the same protein due the plomorphysm of peptides): two are derived from N-terminal alternatives and two are from C-terminal alternatives. Alternative promoters, presumably, allow transcription to start at exon (a sequence of nucleic acid) 1A or exon 1B;. The alternative isoforms of DMT1 are 1A/+IRE, 1A/−IRE, 2/+IRE and 2/−IRE (where 1A and 2 refer to the exon that carries the translation start site and ± IRE refers to the presence or absence of the IRE)[13] where IRE is iron responsive element. We worked with 1A(+) and 2(-) HEK cells.

The cells were first incubated with $MnCl_2$ for 3 hours. A mixture of fluorescent dyes was administered with 1 hour incubation time. Finally, the cells were treated with a solution of the medium containing $CdCl_2$ for one hour. The cells were imaged immediately after the cadmium treatment. Intracellular fluorescence was visualized using a Leica DMIRE2 fluorescence microscope equipped with DAPI LP (excitation filter 340-380 nm) and FITC BP (excitation filter 480/40) filters whose parameters were optimal for calcin blue and fluozin-1 fluorophores, respectively.

In each experiment, cells were grown with or without 5 µM $MnCl_2$. All cells were treated with mM concentrations of Fz1AM, CBAM, and 10 µM $CdCl_2$. The cell variants containing transfected DMT-1 (HEK 293 1A(+) and HEK 293 2(-)) showed strong enhancement of fluorescence with the FITC channel, and somewhat diminished fluorescence in the DAPI channel. Cells without DMT-1 transfection (HEK 293 (-)) or cells that were transfected but without the DMT-1 gene showed no difference in either channel with or without Mn(II). These results indicate that only cells with a Mn(II) transporter give a positive response with the fluorescence assay.

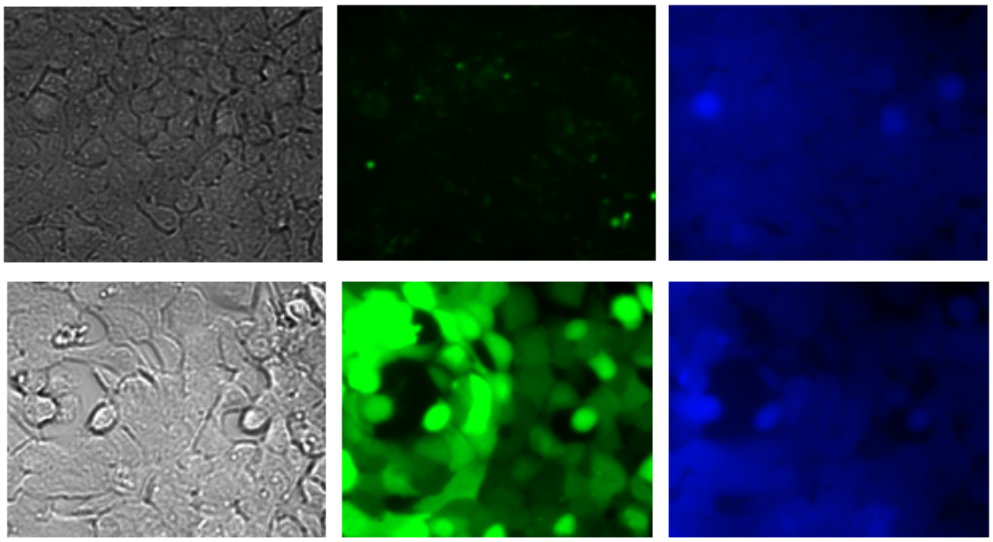

Figure 12 Assay of Mn(II) HEK 1A+ 293 cells. in the top row no manganese added awhereas in the bottom row 5Um Manganese were added. Images taken with a 40X magnification for the

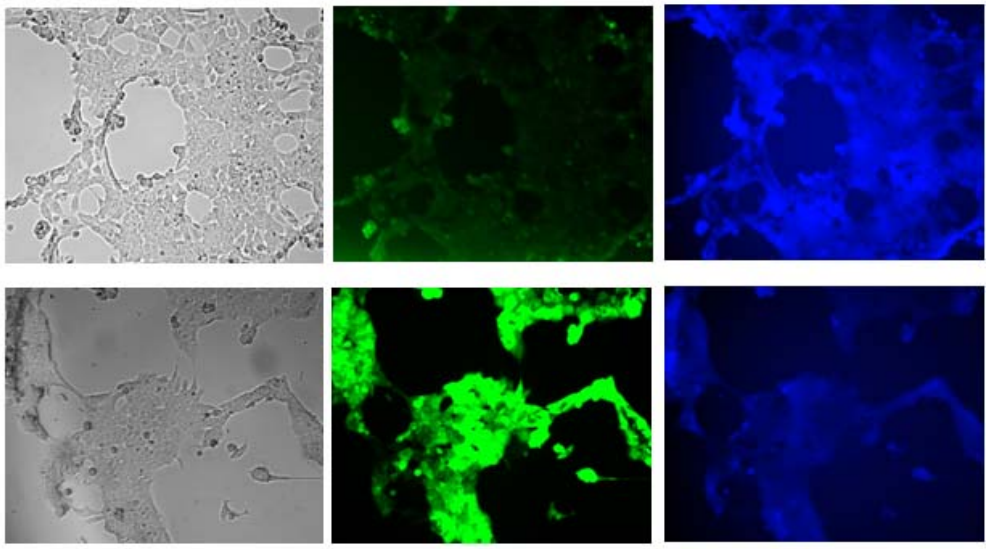

Figure 13 Assay of Mn(II) HEK 1A+ 293 cells. Images taken with a 10X magnification for the same experiment as in Figure 12

All the negative controls were conducted; HEK 1A(+) cells were treated with only CB AM, with CB AM and Cd^{2+}, and with CB AM and Mn^{2+}. Cells treated with only CB gave enhancement with Cd(II) but no with Mn(II). (Figure14)

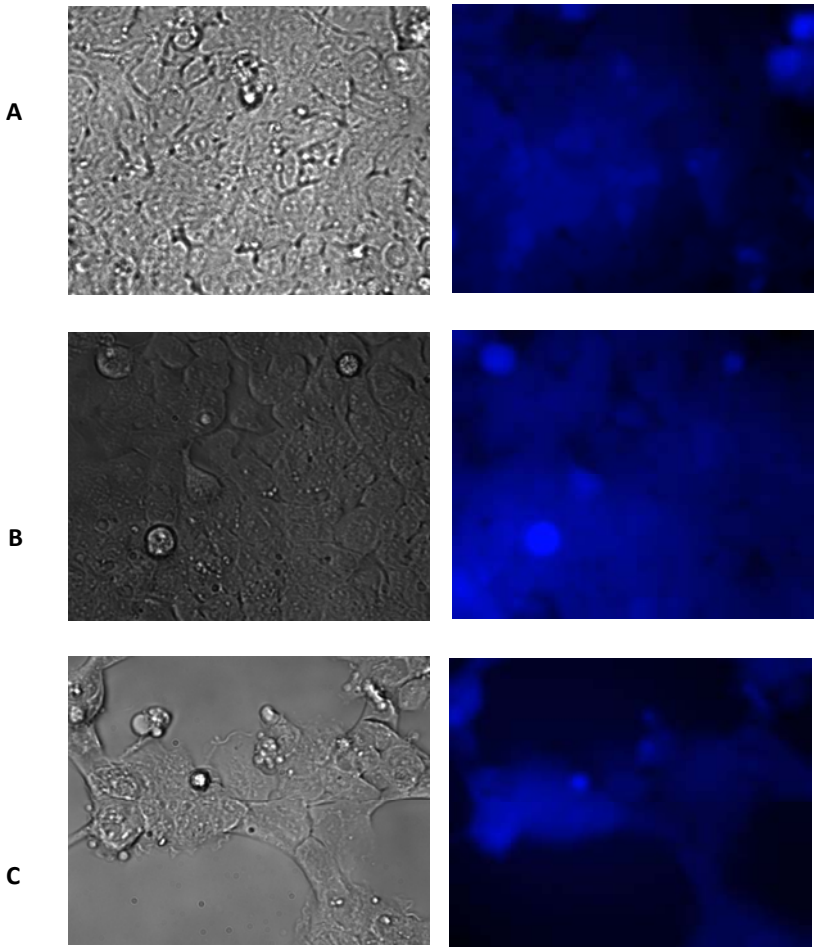

Figure 14 a) HEK 1A(+) CB-AM 26.6 µM; b)HEK 1A(+) CB-AM 26.6 µM, Cd^{2+} 10 µM; c) HEK 1A(+) CBAM 26.6 µM**,** Mn^{2+} 5uM

Then cells were treated with Fz1AM, Fz1AM and Cd^{2+}, and Fz1AM and Mn^{2+}. Fz1AM gave signal only if also presented with Cd(II). (Figure 15 B) whereas the presence of Mn(II) eliminated the fluorescent response (Figure 15 C).

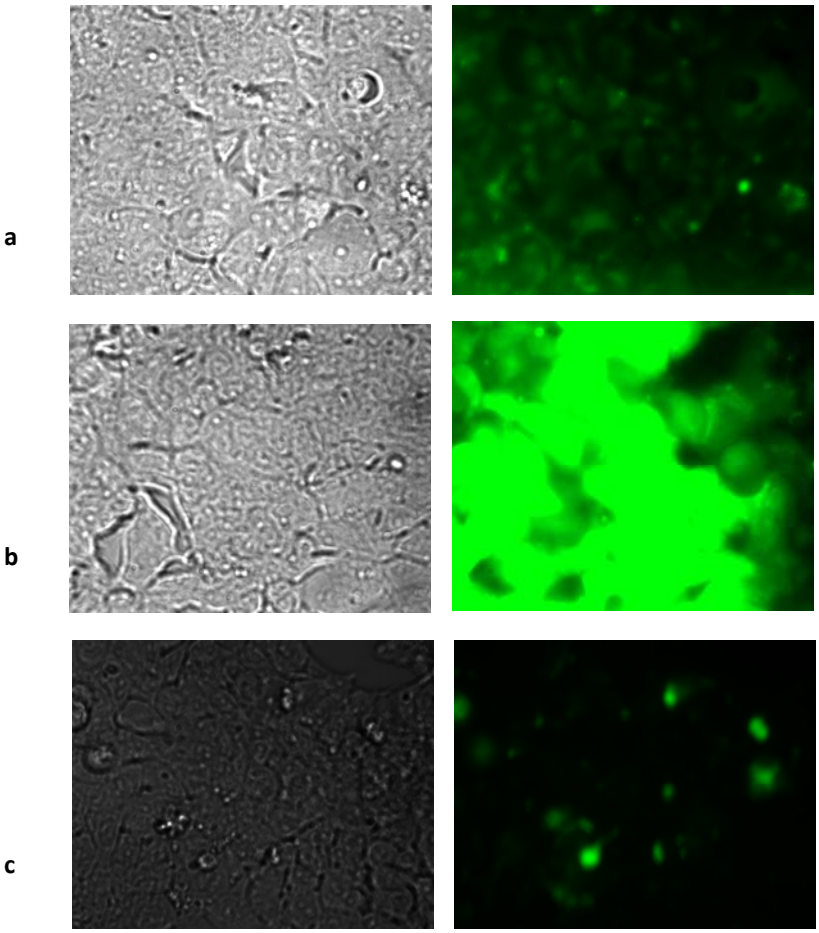

Figure 15 a) HEK 1A(+) Fz1AM 3.6 µM; b) HEK 1A(+) Fz1AM 3.6 µM, Cd^{2+} 10 µM; c) HEK 1A(+) Fz1AM 3.6 µM, Mn^{2+} 5µM

Cells were treated with both dyes and no metals and both dyes and Cd^{2+}. Treatment with CBAM and Fz1AM gave quenching of CB with Mn(II) and enhancement of CB with Cd(II) (Figure16).

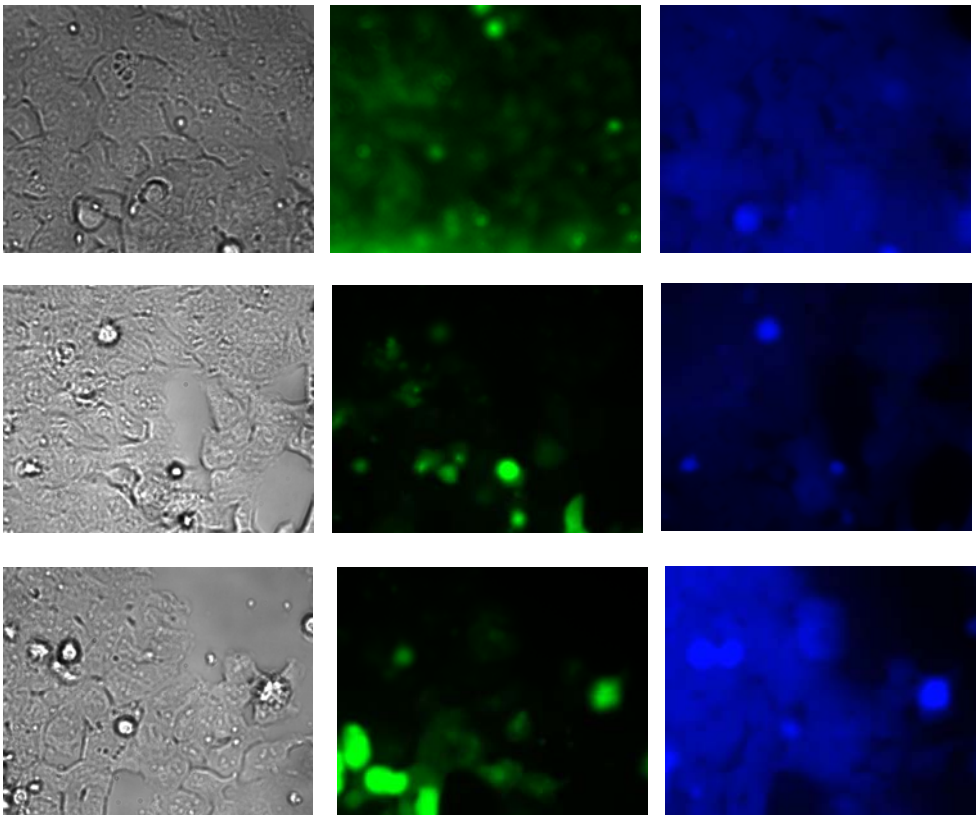

Figure 16 HEK 1A(+) CBAM 26.6 uM, Fz1AM 3,6uM, Second row: HEK 1A(+) CBAM 26.6 uM, Fz1 3,6uM Mn^{2+} 5 uM Bottom row: HEK 1A(+) CBAM 26.6 uM, Fz1AM 3,6uM, Cd^{2+} 10uM

The other important controls were conducted using HEK 293(-), cells that were transfected but not with DMT1 (Figure 17), and HEK 293T (Figure 18), not transfected at all. The two experiments were carried out in the same condition as previously shown, with the same f dyes and metals concentrations. It is possible to observe that in both cases there is no difference in fluorescence intensity for green channel as well as blue one. This is a further proof that transfection helps cells to uptake manganese from solution.

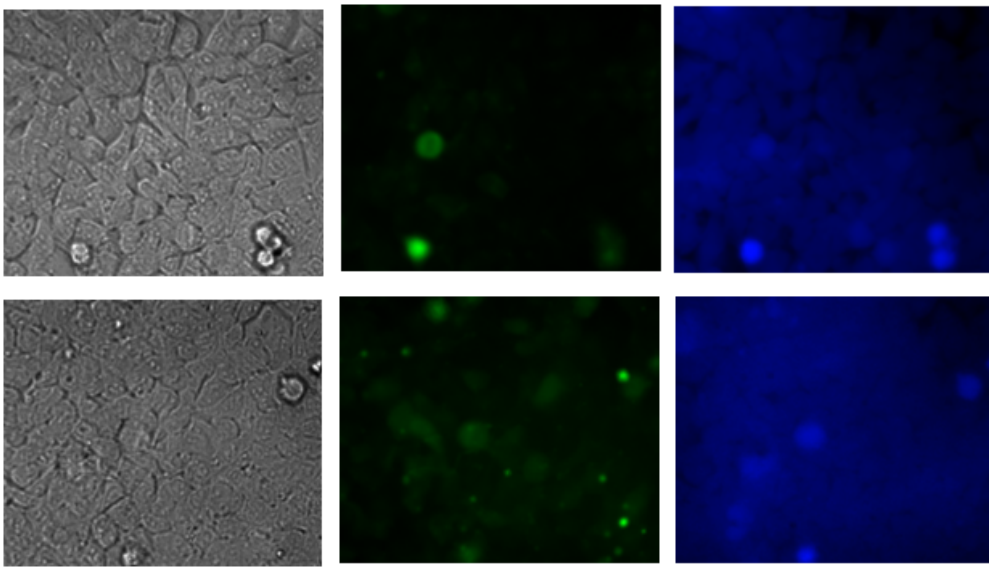

Figure 17 HEK 293 (-) 0µM of Mn^{2+}, 3.6µM Fz1AM, 26.6 µM CB-AM, 10 µM Cd^{2+} Bottom row: HEK 293 (-) 5µM Mn^{2+}, 3.6uM Fz1AM, 26.6 µM CB-AM, 10 µM Cd^{2+}

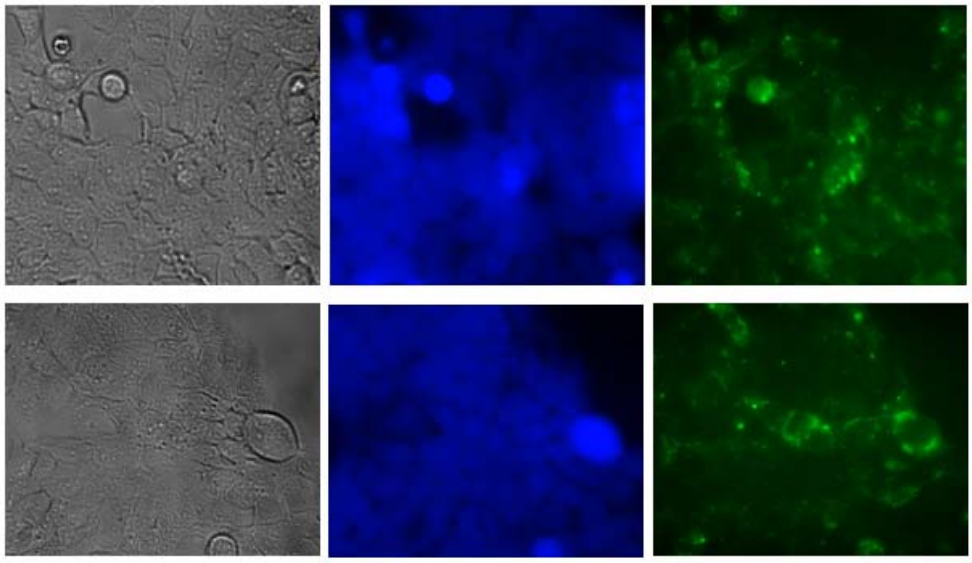

Figure 18 HEK T 0µM of Mn^{2+}, 3.6µM Fz1AM, 26.6 µM CBAM, 10 µM Cd^{2+} Bottom row: HEK T 5µM Mn2+, 3.6µM Fz1AM, 26.6 µM CB-AM, 10 µM Cd2

6.2.4 Quantitative approach

We then developed a quantitative approach in order to detect the Manganese concentration by measuring the fluorescence intensity. We carried out the experiments with several concentrations of manganese leaving constant the amount of dyes and Cd^{2+}. We analyzed eight vials for each concentration in one day. In Figure19 we report the pictures corresponding to different 50, 10, 5, 1 and 0 µM of Manganese for both blue and green channel.(Figure 19)

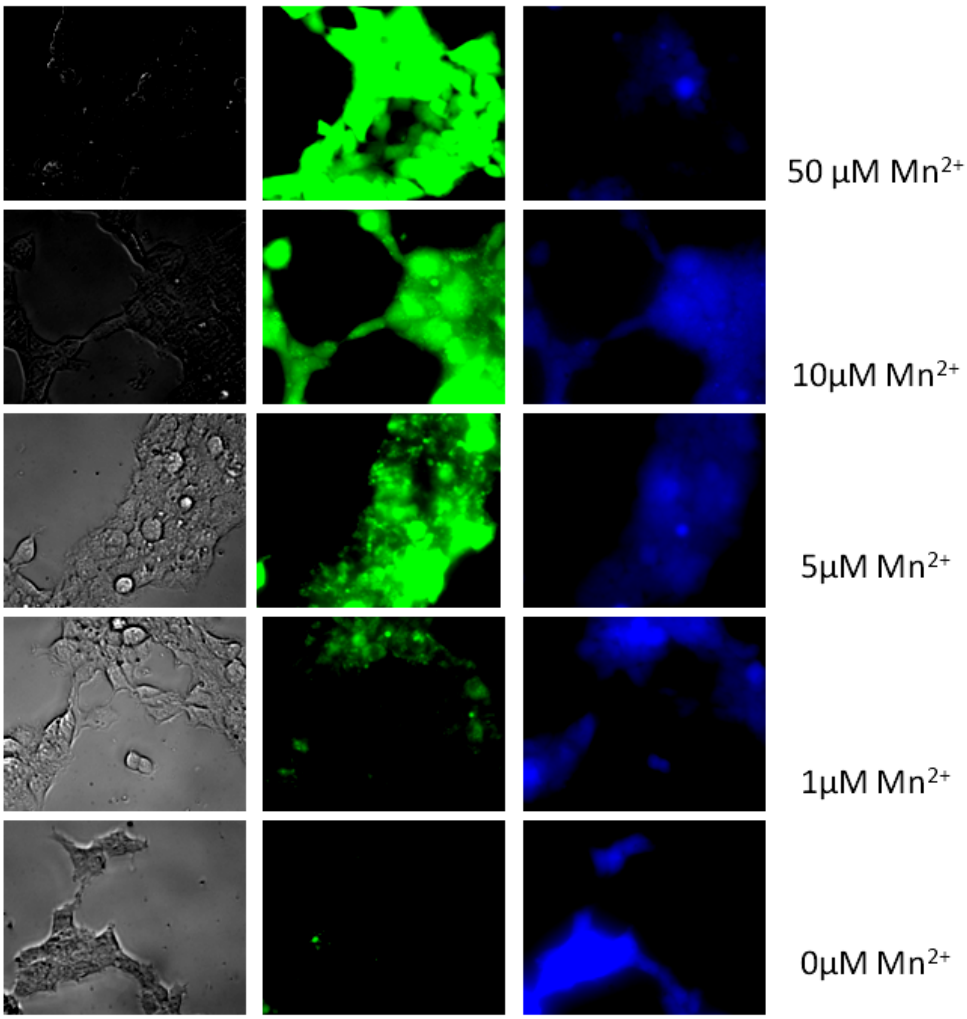

Figure 19 Quantitative approach experiment at several concentrations of $MnCl_2$

We can observe that there is an enhancement of the green fluorescence, going from 0 µM Mn to 50 µM, of about 11 times, whereas for the blue fluorescence a decrement of about 3 times.

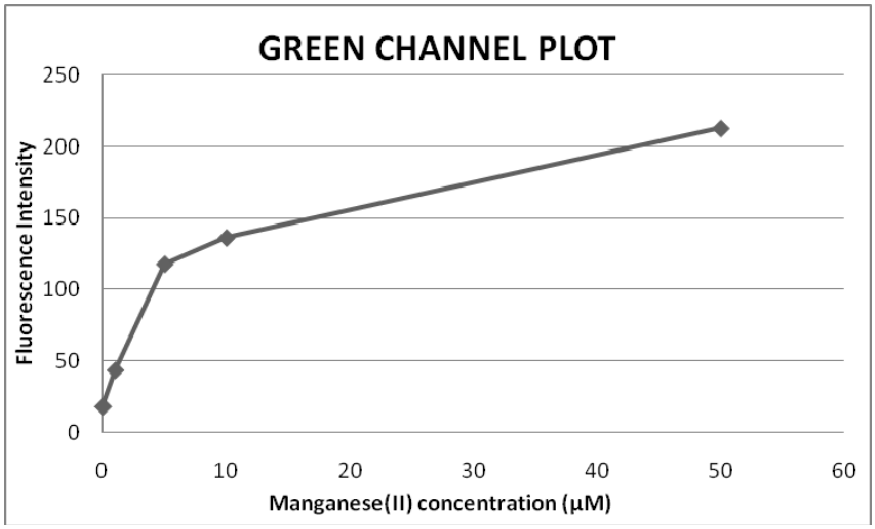

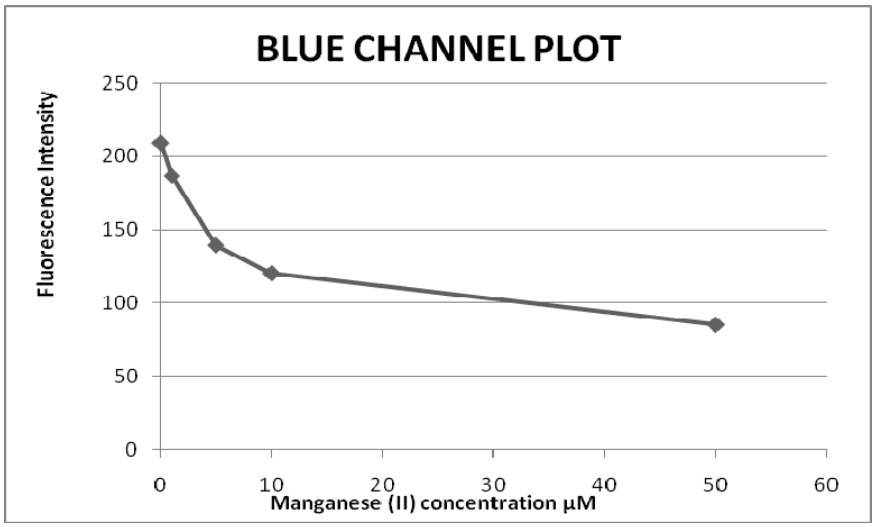

Figure 20 Plot of fluorescence intensity over manganese concentration, showing a logarithmic behavior

We plot the fluorescence intensity over the concentration for both channels and we obtained two logarithmic plots as expected.

We then corrected both intensities for intensity of cells with zero Mn(II). And we obtained, through a simple regression, a double reciprocal plot (see supporting information). This is the typical Michaelis-Menten kinetics, where reactions are catalyzed by enzymes. (Figure 21)

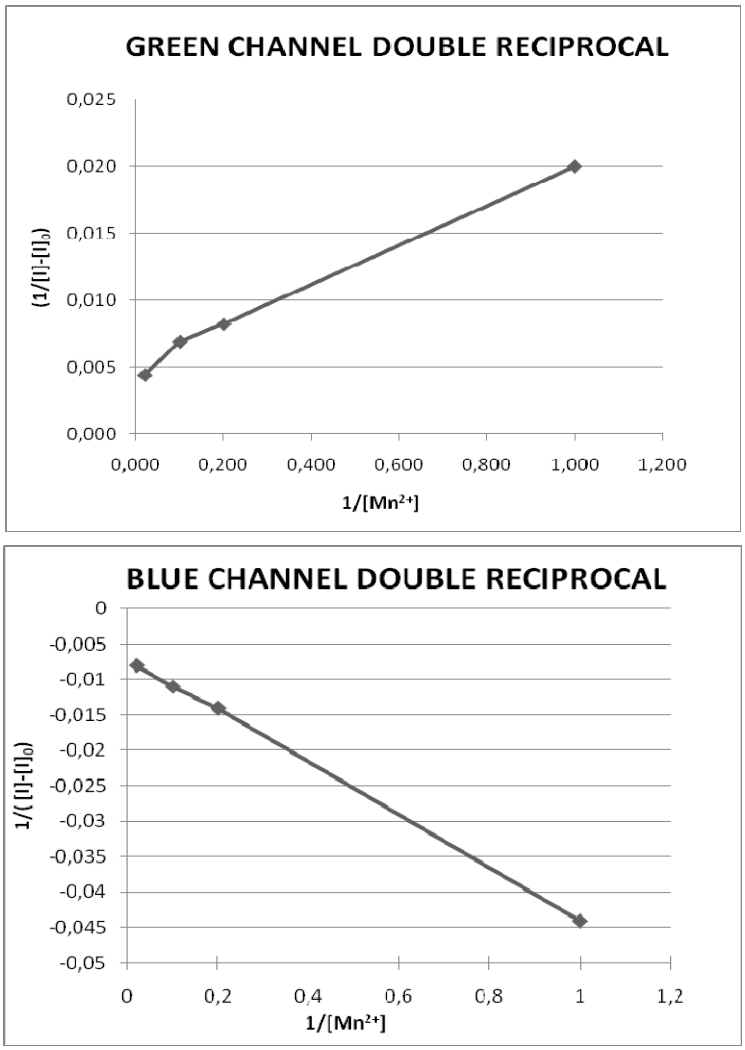

Figure 21 Double reciprocal plot for green channel and blue channel. **I** is the measured fluorescence intensity for each concentration and $\mathbf{I_0}$ is the fluorescence intensity for 0 μM of manganese.

6.2.5 Synthesis of a new dye

Although the approach previously shown, gave good results both qualitatively and quantitatively , it admittedly has some limitations. We are not able to know the exact the concentration of the two dyes inside the cells, even if we know their concentration in the extra cells' medium. This is due to the fact that cells' plasma membrane could have different permeability toward the two different molecules; moreover, as the ester chains are cleaved immediately after transversing membranes pass the cells membrane and we do not know if the efficiency of this process is the same for the two dyes. This, of course, could affect the effective concentration of the dyes inside the cells.

To address this issue we designed a new dye combining the properties of the previous dyes: specifically we linked Fz1AM and CBAM through an ester moiety. (Figure22).

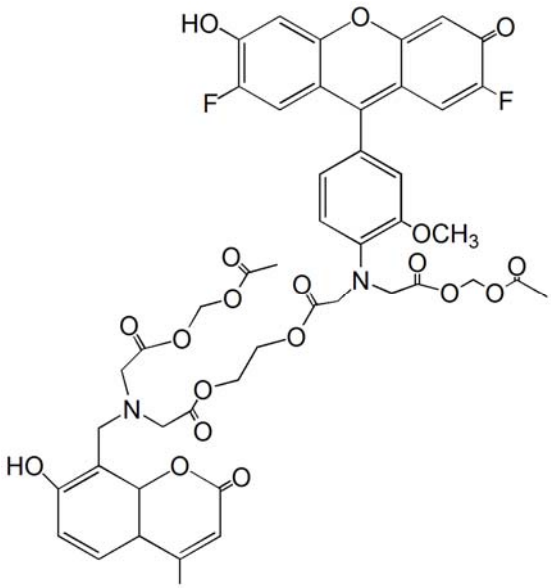

Figure22 Target molecule **1**: CB and Fz1 are link through an ester chain.

Our rational for this approachwas that by linking the two molecules, it was ensured that they passed the cells membrane in a ratio that was 1 to 1; moreover, the efficiency of the cleavage was now the same for all molecules. The permeability of the membrane toward this molecule is due to the AM

chain as previously shown. The link between Fz1 and CB moieties was still an ester to make sure that it could be cleaved by enzymes inside cells.

The first step in this approach was the synthesis of Fz1 (**7**) as reported by Bacci.[14]

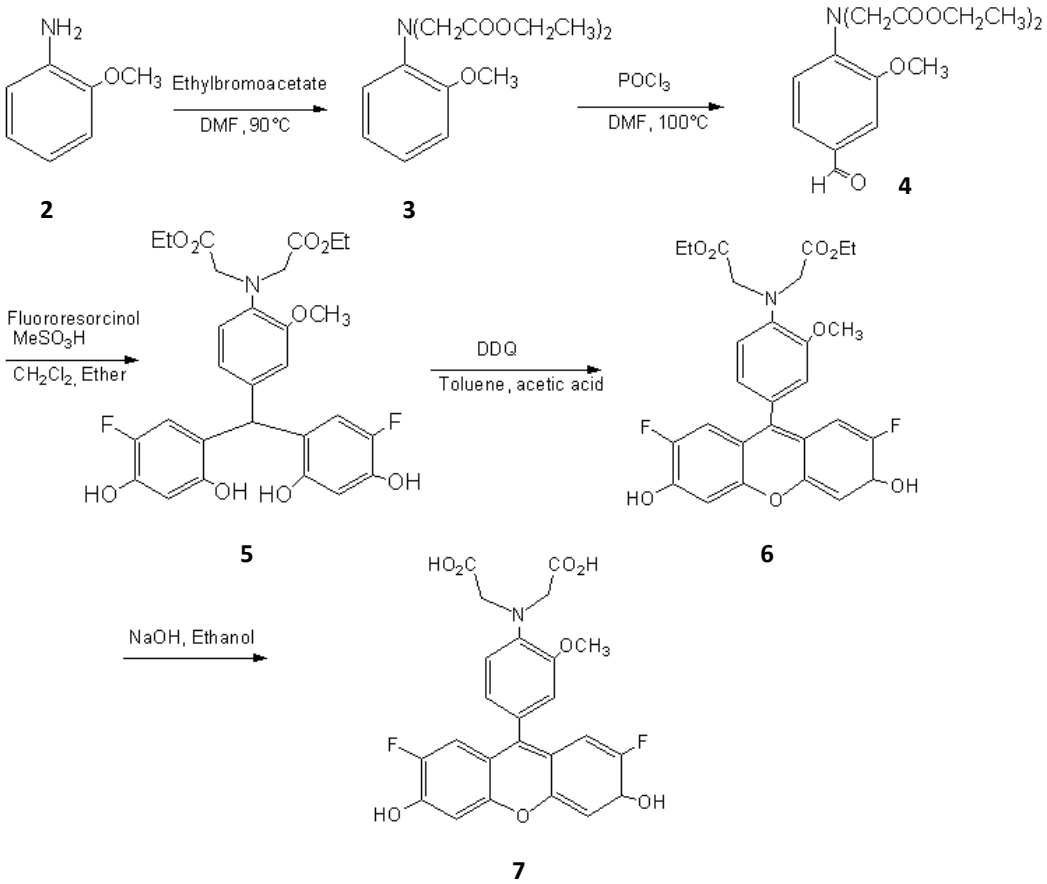

Scheme 1 Synthesis of Fz1

The further step was to insert one link on CB carboxylic acid in order to obtain **8**. The reaction was performed in methanol and acetonitrile using 1.2 equivalents of bromomethylacetate. The reaction mixture was stirred at 60°C for three hours. Unfortunately, the reaction gave the di-subsituted product

and several byproducts; also chancing reaction conditions such as temperature, base and solvent, it was not possible to separate the desired product **8.**

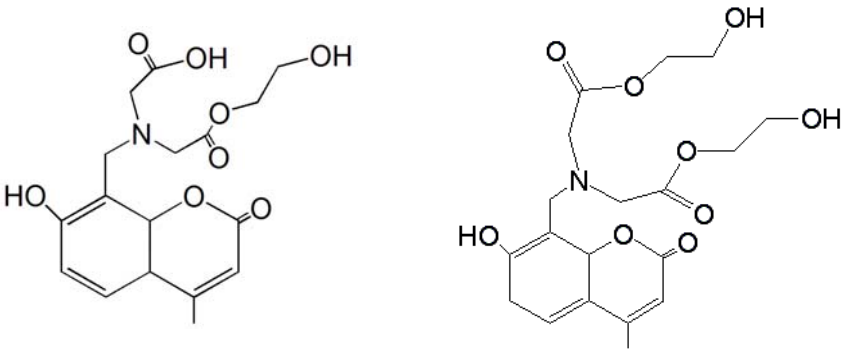

8 **9**

Figure 23 CB with one link **8** useful for the synthesis of the target molecule **1** and the di-substituted product **9**

As it was easy to obtain the product having two links **9**; we designed a new target molecule **10** (Figure 24): this posses two Fluozin1 units linked through ester links to one CB moiety. The only change respect to **1** is the ratio between the two days, but both chemical and biological properties remained

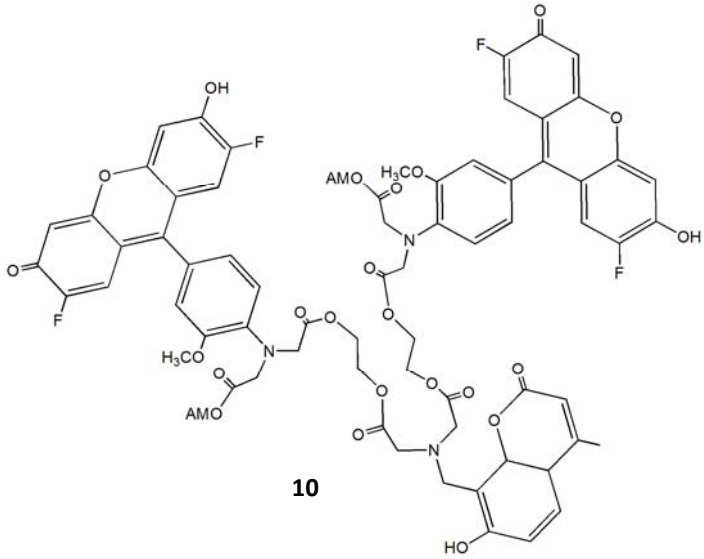

10

Figure 24 New target dye **10** possessing a 2:1 ratio between Fz1 and CB

unchanged.

As a confirm, we conducted a titration to ensure that the ratiometric behavior in solution was the desired one. In the presence of two equivalents of Fz1 with respect to CB. (Figure 25). As the concentration of Mn(II) was added, the blue fluorescence diminished and the green fluorescence increased intensity proportionately as we expected.

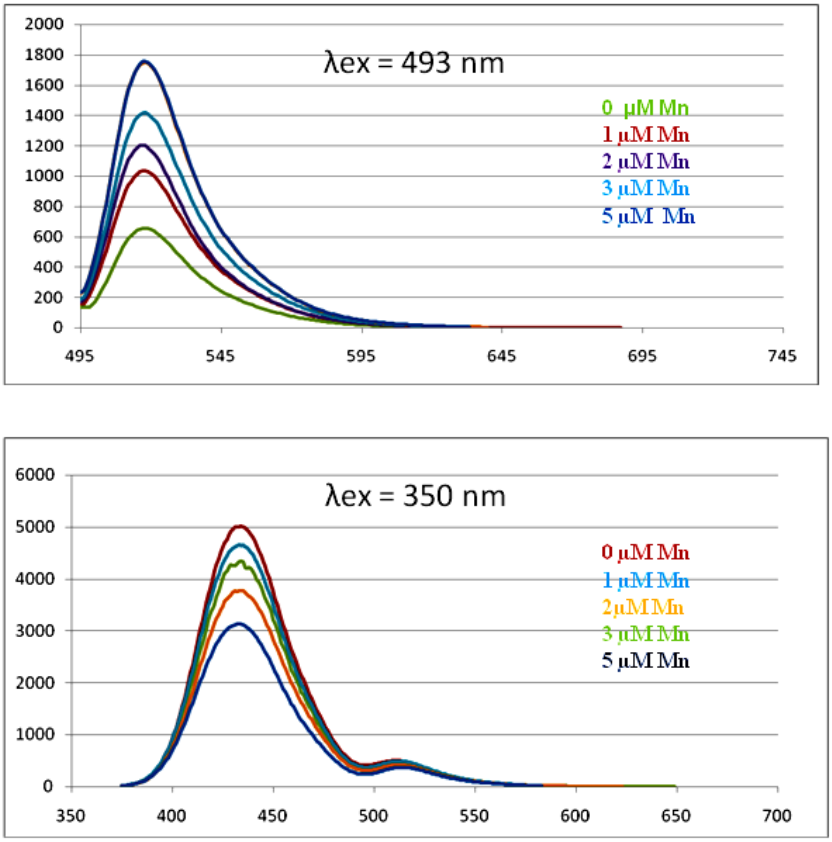

Figure 25 Response for the titration of aqueous solution (pH=7.2) containing 5 µM calcein blue, 10 µM fluozin-1, 5 µM Cd^{2+}, 50 mM HEPES and 100 mM KNO_3 with $MnCl_2$. Shown spectra contain 0, 1, 2, 3, 5, µM $MnCl_2$.

In order to connect the two Fz1 units with CB moiety we had to make more reactive compound **10**; in order to do that we wanted to synthesize **11** possessing bromide instead of an alcoholic group on the links. At first we performed the reaction in dry DMF and using CBr_4 as brominating agent both at room temperature and 50° C but we did not succeed. We then used NBS that is a commonly used for this kind of reaction but also in this case, also changing solvents and temperature, we did not obtain our product.

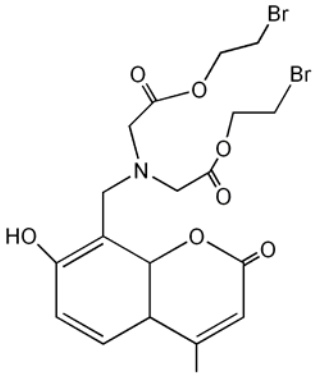

11

We then reacted directly CB with bromoethane in dry DMF and DIPEA and we obtained our product in high yield. (Scheme 2)

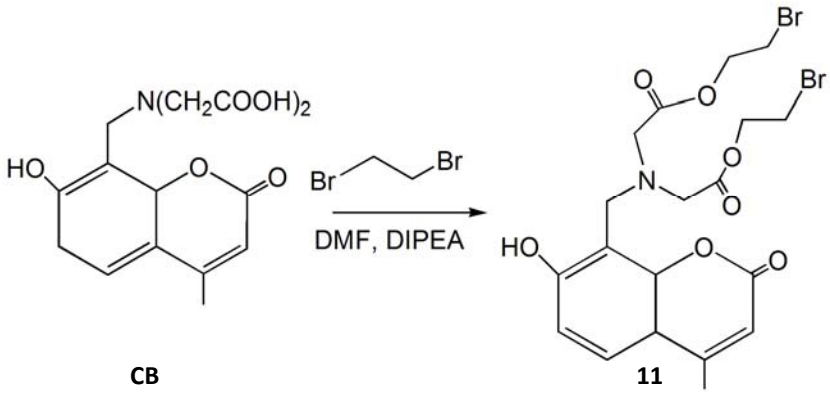

CB **11**

Scheme 2 Successful synthesis of compound **11** starting from CB and bromoethane

We performed the last step of the synthesis of our target molecule **11**; in dry DMF we added Fz1 (**7**) and compound **11** in a 2:1 ratio with DIPEA as a base; the solution was stirred for 24 hours and then, using LC-MS we were able to detect the peak corresponding to **11**. The esterification of **11** to give the final AM ester for biological application is in progress.

6.3 Experimental: cell culture.

6.3.1 Materials.

The cell culture medium Dulbecco's modified Eagle's medium (DMEM-F12) with L glutamine, FBS (fetal bovine serum), F12 and F12K medium, Fluozin-1 acetoxymethylester (Fz1AM), and Pluronic acid F127 were obtained from Invitrogen. Calcein Blue acetoxymethylester (CBAM) was obtained from Sigma. and TransIT-LT1 transfection reagent was obtained from Mirus.

Cell culture.

Cells were kept at 37°C in a humidified atmosphere of 5% CO_2. For imaging experiments, the cells were grown in 96 wells plates for 2 days, reaching 60-70% confluence. HEK 293 cells were cultured in DMEM F-12 medium supplemented with 10% of FBS medium. A549 cells were cultured in F12-K medium supplemented with 10% of FBS medium.

A549 transient transfection.

For transient transfection A549 were grown to a confluence of 40-50%. A solution was prepared as follows: 9 ml of free FBS F12-K medium, 0.28 ntrans lt1, 0.1 mL of DNA (DMT1, IRE, GFP, 1 mg/mL). The solution was left for 40 minutes at room temp and then added to 92 mL of regular medium. The cells were incubated for 36/48 hours and then washed with regular medium. The yield of transfection was around 25%.

6.3.2 HEK 293 stable transfection

Cell lines HEK 1A(+), HEK 2(-) and HEK(-) were provided by professor Jaime J. Smith in Buffalo

6.3.3 A549 Mn^{2+} measurements.

Transient transfected cells were washed with F12 medium supplemented with 10% of FBS and a solution of $MnCl_2$ (0.0001M) was added to reach a concentration of 5 µM. The cells were incubated for three hours at 37°C. A solution of dyes was prepared in HBSS with 6.6 µM of Fluozin1 AM (from a stock solution that was 0.005 M in DMSO), 26.6 µM of Calcein Blue AM (from a stock 0.005 M in DMSO), and 6.6 µM of Pluronic Acid F127. The cells were carefully washed and a solution of the two dyes was added. The cells were incubated for one hour, washed carefully and a solution of $CdCl_2$ (0.0001 M) was added to reach a concentration of 10 mM. The cells were incubated for one additional hour and washed.

6.3.4 HEK 293 Mn^{2+} measurements

Mn^{2+} was detected using both fluozin1 AM and Calcein Blue AM.

The experiment was run in a 96 wells plates with a confluence of 60-70%. The cells were washed and a solution of $MnCl_2$ (0.0001M) was added to reach a concentration of 5 µM. The cells were incubated for three hours at 37°C and 5% CO_2. The cells were washed carefully and an aliquot of the solution of the two dyes was added. A solution of dyes was prepared in HBSS with 3.6 µM for fluozin1 AM, 25µM of Calcein Blue AM, 3.6µM of Pluronic Acid F127. The cells were incubated for one hour, washed carefully and a solution of $CdCl_2$ (0.0001 M) was added to reach a concentration of 10 µM. The cells were incubated for one additional hour and washed.

For all the experiments pictures were taken with bright field, green field and blue field

6.4 Experimental: synthesis

Diethyl 2,2'-(2-methoxyphenylazanediyl)diacetate (3) To a solution of , 0.137 mL o-anisidine in DMF dry (1.2×10^{-3} mol) were added 0.362 g of K_2CO_3 (2.64×10^{-3} mol), 0,435 g of KI (2.64×10^{-3} mol); the solution was stirred for 10 minutes and 0.395 mL of ethylbromoacetate were added dropwise (2.64×10^{-3} mol); the solution was stirred under nitrogen at 90°C overnight. The reaction mixture was cooled to room temperature and washed with HCl 1M, water, and NaCl, and extracted with dichloromethane. The product was purified by silica gel chromatography using as eluant Hexane and Ethyl acetate (9:1).
The pure product was a yellowish oil. Rf= 0.34 in 9:1 Hexane: Ethylacetate. Yield ws 85%.
^{1}H NMR (CDCl3) δ: 6.97 – 6.91 (m, 1H, Ar**H**); 6.85-6.80 (m, 3H, Ar**H**); 4.20 (q, 4H C**H$_2$**CH3); 4.11 (s, 4H, N**CH$_2$**); 3.82 (s,3H, O**CH$_3$**), 1.25 (t,6H CH_2**CH_3**)
^{13}C NMR: δ 171; 15; 138; 124; 122; 119; 112; 60; 55; 53.
ESI MS 295.9 $[M]^+$, 317.9 $[M+Na]^+$

Diethyl 2,2'-(4-formyl-2-methoxyphenylazanediyl)diacetate (4) To a solution of 0.366 mL $POCl_3$ (4×10^{-3} mol) in dry DMF were 0.12 g of **3** (0.4mmol) were added dropwise. The solution was heated at 100°C for 5 hours.
After reaching room temperature, iced water was added and the pH was adjusted by adding a $NaHCO_3$ to reach pH = 7. The organic phase was extracted with Ethylacetate.
The pure product was obtained by purification with silica gel chromatography using as eluant hexane:ethyl acetate (7:3)
The pure product was obtained as a yellow oil in a 80% of yield ^{1}H **^{1}H NMR ($CDCl_3$):** δ: 9.73 (s, 1H, CO**H**); 7.33 (m, 2H, Ar**H**); 6.75 (d, 1H, Ar**H,** J = 3.4 Hz); 4.17 (q, 4H, OC**H$_2$**CH_3); 4.11 (s, 4H, NC**H$_2$**); 3.87 (s, 3H, OC**H$_3$**); 1.20 (t, 6H, , OCH_2C**H$_3$**)
^{13}C NMR ($CDCl_3$): 189.94, 170.11, 149.7, 144.4, 129.5, 125.6, 115.78,110.2, 60.3, 60.17, 55.3, 53.8, 20.4, 13.7
ESI MS *m/z* = 323.9 $[M]^+$, 345.9 $[M+Na]^+$

Diethyl 2,2'-(4-(bis(5-fluoro-2,4-dihydroxyphenyl)methyl)-2-methoxyphenylazanediyl)diacetate(5) 0.031 g of **4** (0.095mmol) were dissolved in dry CH_2Cl_2 and Ether (0.75+0.75 ml), 0.025 g of fluororesorcinol (0.19 mmol) and $MeSO_3H$ (13% in volume) were added and the solution was

stirred for 4 hours at room temperature. It was then washed with water and the crude product was extracted with ethyl acetate.
The pure product was obtained by purification with silica gel chromatography using as eluant hexane:acetone (6:4) The yield was 50%.
^{1}H NMR (DMSO) δ: 9.32 (s, 2H,O**H**); 8.80(s, 2H, O**H**); 6.35(d, 1H, Ar**H**); 6.30(s,1H, Ar**H**); 6.25 (d,2H, Ar**H**); 6.23(d,1H, Ar**H**), 6.12(d,2H, Ar**H**); 3.91 (q, 4H, OC**H$_2$**CH$_3$); 3.8 (s, 4H, NC**H$_2$**); 3.51 (s,3H, OC**H$_3$**), 0.98 (t, 6H, OCH$_2$C**H$_3$**)
^{13}C NMR (DMSO) δ: 173.6, 155, 152.4, 152.0, 144.1, 139.5, 138.1,123.4, 122, 119.2, 117.5, 116.7, 116.7, 61.5, 56.13, 55.3, 14.58
ESI MS *m/z* = 562 $[M]^+$, 583 $[M+Na]^+$

Diethyl 2,2'-(4-(2,7-difluoro-3,6-dihydroxy-9H-xanthen-9-yl)-2-methoxyphenylazanediyl)diacetate (6) 0.050 g **5** (9×10^{-5} mol) was dissolved in 1 mL of acetic acid and diluted with toluene, a solution of 0.044 g of DDQ (1.9×10^{-4}) in toluene and acetic acid (1 mL+1 mL) was added dropwise. The solution was stirred for 4 hours until the colour of the mixture turned to dark red.
The reaction mixture was dried over vacuum and purified by silica gel chromatography using CH_2Cl_2: MeOH (1:1).
The pure product is a bright red-orange solid.
^{1}H NMR (DMF) δ: 7.22 (d, 1H, Ar**H**); 7.15 – 7.0 (m, 4H, Ar**H**); 4.35 (s, 4H, N**CH$_2$**); 4.25 (q ,4H, O**CH$_2$**CH$_3$); 3.91 (s,3H, OC**H$_3$**); 1.32 (s, 6H, OCH$_2$**CH$_3$**).
^{13}C NMR (DMF) δ: 171.2; 151.4; 150.8; 143.7; 137.7; 137.1; 121.7; 121.2; 117.8; 116.5; 116.27; 113.8; 104; 60.5; 60.1; 55.5; 53.8; 20.24; 14.
ESI MS *m/z* = 541 $[M]^+$.

2,2'-(4-(2,7-difluoro-3,6-dihydroxy-9H-xanthen-9-yl)-2-methoxyphenylazanediyl)diacetic acid (7) Compound **6** was dissolved in ethanol (suspension) and a solution of NaOH 1M was added dropwise. The solution was stirred overnight at room temperature.
A solution of HCl in water was added dropwise and the pure product was extracted with ethylacetate.
^{1}H NMR (MeOD) δ: 8,4 (s, 1H, Ph**OH**), 7,2 (m, 1H, Ar**H**) 7-6.8 (m, 4H, Ar**H**), 6,4 (d, 2H, Ar**H**), 4,0 (s, 4H, NC**H$_2$**), 3.8 (s, 3H, OC**H$_3$**)
^{13}C NMR (MeOD) 189.8; 171.2; 151.4; 150.8; 143.7; 137.7; 137.1; 121.7; 121.2; 117.8; 116.5; 116.27; 113.8; 104; 60.5; 60.1; 55.5; 53.8; 20.24; 14.
ESI MS: 484 $[M]^+$
Bis(2-hydroxyethyl) 2,2'-((7-hydroxy-4-methyl-2-oxo-4a,8a-dihydro-2H-chromen-8-yl)methylazanediyl)diacetate (9): 0.030 g of calcein blue (9.3×10^{-5})

were dissolved in dry DMF (20 ml) and 174 µL DIPEA were added dropwise (5 $\times 10^{-4}$); the mixture was stirred for 30 minutes at 70°C and then 37 µL of iodoethanol were added dropwise (5 $\times 10^{-4}$). The reaction mixture was stirred at 70°C for 5 hours and checked by TLC. After reaching room temperature, the crude was washed with water and extracted with ethylacetate. The product was purified by silica gel chromatography using as eluant CH_2Cl_2 : MeOH (9:1) Yield was 85%

^{1}H NMR (DMSO) δ: 7.6 (s, 1H, Ar**H**), 6.85 (s, 1H, Ar**H**), 6.11(s, 1H, CH_3=C**H**), 4.13(s, 2H, C$\mathbf{H_2}$N), 4.02 (t, 4H, C$\mathbf{H_2}$OH), 3.63 (s,4H, N($\mathbf{CH_2}$)$_2$, 3.58 (t, 4H, $CO_2C\mathbf{H_2}$) 2.50 (s, 3H, C$\mathbf{H_3}$=CH)

^{13}C NMR (DMSO): 171.51, 161.5, 160.3, 154.1; 153.51; 125.8; 113.1; 112.55; 110.5; 109.6; 66.7; 63.35; 59.8; 47; 18.13; 9.14.

ESI MS: *m/z* = 408.1 $[M]^+$

Bis(2-bromoethyl) 2,2'-((7-hydroxy-4-methyl-2-oxo-4a,8a-dihydro-2H-chromen-8-yl)methylazanediyl)diacetate (11) 0.030 g of calcein blue (9.3 $\times 10^{-5}$) was dissolved in dry DMF (20 ml) and 20µL DIPEA were added dropwise (3.7 $\times 10^{-5}$) and the mixture was stirred for 30 minutes at 70°C; 43.5 µl dibromoethane were added dropwise (3.7 $\times 10^{-4}$), the reaction was stirred at 60°C for 6 hours and checked by TLC. After cooling to room temperature and the crude was washed with water and exctracted with ethylacetate. The product was purified by silica gel chromatography using Hexane:ethylacetate (6:4) as eluant.

The pure product was obtained with a 65% of yield.

^{1}H NMR (MeOD) δ: 7.65 (s, 1H, Ar**H**); 6.92 (s, 1H, Ar**H**); 6.15 (s, 1H, CH_3=**CH**), 4.50 (t, 2H, **CH$_2$**OH); 4.25 (s, 2H, **CH$_2$**N); 3.74 (s, 4H, N(C$\mathbf{H_2}$)$_2$); 3.62 (t,2H, $CO_2C\mathbf{H_2}$); 2.61 (s,3H, C$\mathbf{H_3}$=CH).

^{13}C NMR (MeOD): 171.51; 161.5; 160.3; 154.1; 153.51,125.8; 113.1; 112.55; 110.5; 109.6; 66.7; 63.35; 59.8; 47; 18.13; 9.14.

ESI MS: 532.4 $[M]^+$

3,21-bis(4-(2,7-difluoro-3-hydroxy-6-oxo-6H-xanthen-9-yl)-2-methoxyphenyl)-12-((7-hydroxy-4-methyl-2-oxo-4a,8a-dihydro-2H-chromen-8-yl)methyl)-5,10,14,19-tetraoxo-6,9,15,18-tetraoxa-3,12,21-triazatricosane-1,23-dioic acid (10) 0.025 g of **11** (5.2×10^{-5}) were dissolved in dry DMF (2mL), 21 µL of DIPEA were added dropwise and the mixture was stirred for 1 hour at 80°C; compound 0.050 g of **7** (1.4×10^{-4} mol)were dissolved in 1 ml of DMF dry and add dropwise. The mixture was stirred for 24 hours at 90°C, cooled to r.t. and washed with water and a solution of HCl.

LC – MS showed the peak corresponding to the product at R_t 31 minutes using the following method:
-0-2 min 100% water
-2-22 minutes from 100% water to 100% ACN
-22-45 100% ACN
The product was purified by silica gel TLC preparative using hexane and acetate (5:5)
^{1}H NMR (MeOD): 8.54 (s, 3H,Ph**OH**); 8.0 – 7.30 (m,14H, Ar**H**); 6.03 (s, 1H, CH3=C**H**), 4.27 (s, 2H CBC**H_2**N), 4.21 (s, 4H,FZ1C**H_2**N), 4.1 (s,4H,FZ1C**H_2**NH), 3.65-3.53 (s, 20H, CO2**CH_2CH_2**CO_2). 2.41 (s, 3H, C**H3**=CH).
ESI MS *m/z* = 1346.6 $[M]^+$

6.5 References

1. Aslam, D. R. Chettle, A. Pejovic-Milic and A. J. Waker, *Phys. Med. Biol.*, 2009, **54**, 17-28.
2. Aslam, A. Pejovic-Milic, D. R. Chettle and F. E. McNeill, *Phys. Med. Biol.*, 2008**, 53**, 4081-4092.
3. Aslam, A. Pejovic-Milic, D. R. Chettle, F. E. McNeill, M. W. Pysklywec and J. Oudyk, *Phys. Med. Biol.*, 2008, **53**, N371-N376.
4. P. Y. Yang and D. J. Klimis-Tavantzis, *Biol. Trac. El.t Res.* 1998, **64**, 275-288.
5. P. Y. Yang and D. J. Klimis-Tavantzis, *J. Nutr. Bioch.*, 1998, **9**, 324-331.
6. E. J. Talavera, J. L. Arcaya, D. Giraldoth, J. Suarez and E. Bonilla, *Neuroch. Res.*, 1999, 24, 705-708.
7. Y. Z. Wadghiri, J. A. Blind, X. H. Duan, C. Moreno, X. Yu, A. L. Joyner and D. H. Turnbull, *Nmr in Biom.e*, 2004, **17**, 613-619.
8. X. Yu, Y. Z. Wadghiri, D. H. Sanes and D. H. Turnbull, *Nat. Neurosci.* 2005, **8**, 961-968.
9. M. Royzen, Z. H. Dai and J. W. Canary, *J. Am. Chem. Soc.*, **2005**, 127, 1612-1613.
10. J. H. Zhao, H. B. Chen, T. Davidson, T. Kluz, Q. W. Zhang and M. Costa, *Toxicol. App. Pharm.*, **2004**, 196, 404-409.
11. Y. J. Kang, S. T. Nuutero, J. A. Clapper, P. Jenkins and M. D. Enger, *Toxicol.*, **1990**, 61, 195-203.
12. M. W. Roe, J. J. Lemasters and B. Herman, *Cell Calcium.*, 1990, **11**, 63-66.

13. M. D. Garrick, H. C. Kuo, F. Vargas, S. Singleton, L. Zhao, J. J. Smith, P. Paradkar, J. A. Roth and L. M. Garrick, *Biochem. J.*, 2006, **398**, 539-546.
14. J. P. Bacci, A. M. Kearney and D. L. Van Vranken, *J. Org. Chem.*, 2005, **70**, 9051-9053.